UNITED STATES DEPARTMENT OF THE INTERIOR

GEOLOGICAL SURVEY

TEST AND EVALUATION

of the

GURALP SYSTEMS CMG-3S BROADBAND

BOREHOLE DEPLOYABLE SEISMOMETER SYSTEM

by

L. Gary Holcomb

Charles R. Hutt

Open-File Report 91-282

Albuquerque, New Mexico

1991

Table of Contents

Table of Figures

1 INTRODUCTION

This report summarizes a series of tests designed to evaluate the performance characteristics of the Guralp Systems CMG-3S broad band borehole deployable seismometer system conducted by the United States Geological Survey's (USGS) Albuquerque Seismological Laboratory (ASL). This evaluation program was conducted in conjunction with and under contract from the Department of Energy's (DOE) Sandia National Laboratories (SNL). The experimental data was gathered during the months of October, November, and December of 1989. This report contains a chronological history of the study, presents the detailed results of the analysis of the data and draws conclusions concerning the performance of this seismic sensor system.

Although the CMG-3S sensor system is borehole deployable, it was not possible to evaluate the system in a borehole configuration at ASL because all of the ASL boreholes are too small to accommodate this sensor system. Therefore, it was necessary to conduct all the measurements in the ASL surface vault facility. This was not a major restriction because the ASL surface vault is essentially as quiet as a borehole at long periods under no-wind night time conditions. However, the borehole environment is unique because the mechanical coupling between the sensor system and the earth in a borehole is quite different than it is in a typical vault installation. In addition, boreholes are frequently rather dirty environments and frequently the humidity is quite high. These conditions were not evaluated by this study because they could not be realistically duplicated in the ASL vault.

Various aspects of the sensor's performance in several environments were investigated to determine the effects of operation under different conditions. An experiment was conducted to determine whether or not the sensor was sensitive to atmospheric pressure changes. The characteristics of a new installation technique, which consisted of bonding the sensor to the vault floor partially encased in a block of plaster of Paris, were tested to determine its effects on instrument performance. The effects of a partial vacuum within the sensor cases was evaluated by pumping the cases down with a roughing pump, sealing the cases, and monitoring their operation. Finally, the CMG-3S performance was monitored when installed on three point leveling plates in a protected environment. Of the four test configurations, this configuration most closely approximates the probable conditions of a borehole installation.

All of the data presented herein has been analyzed with the direct model for processing data from side-by-side seismometer tests (see Holcomb, 1989). This represents the first real world application of this method to analyze test results. The major advantage of this method of analysis lies in the fact that the model yields unique estimates of the system noise levels for both sensors even if the two sensors under test have significantly different levels of system noise. In contrast, noise estimates derived from the coherence function yield only one common noise estimate for both sensors; if the true system noise levels for the two sensors are really quite different, this coherence derived noise estimate is truly representative of neither sensor.

Since this is the first application of the direct method to the analysis of real sensor data the derivation of a direct method for calculating the noise levels of two sensors in a side-by-side evaluation is repeated here. This will provide a complete documentation of the derivation of the method and its application in one volume. The bulk of this derivation was presented previously (see Holcomb 1989); it was slightly extended later (see Holcomb 1990).

2 MODEL MATHEMATICAL RELATIONSHIPS

The system to be evaluated is modeled in Figure 2.1 where X is assumed to be the coherent ground motion power spectral density (PSD) input to both systems. All quantities in the figure are assumed to be functions of frequency. Experimentally, the observer does not know X, N_1, and N_2; the signals appearing at ports 1 and 2 are the only two time functions whose PSD functions (P_{11} and P_{22}) are available for measurement and analysis. In addition, the system transfer functions (H_1 and H_2) are assumed to be known. The circle containing "S" denotes a summing junction.

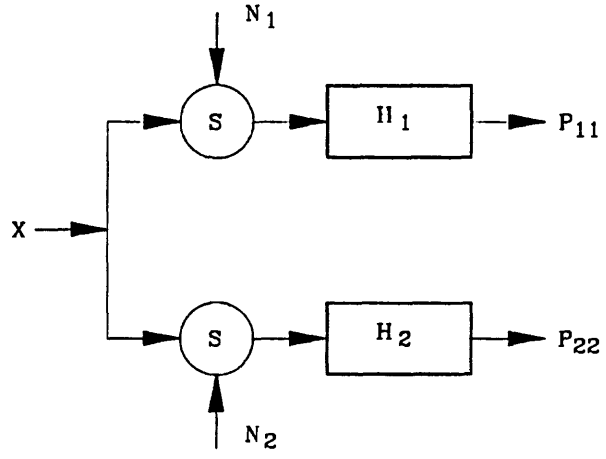

Figure 2.1 Linear system model of side-by-side evaluation of two seismometer systems.

2.1 BASIC MODEL EQUATIONS

Figure 2.1 contains a block diagram depicting the configuration of two seismometer systems operating in close enough proximity to one another that the seismic signal input power X may be assumed to be at the same level and coherent between the sensors. The two systems are assumed to have system transfer functions H_1 and H_2 which are not necessarily equal. In addition the sensors are assumed to be generating incoherent self noise powers N_1 and N_2 referred to the input, not necessarily equal.

The relationships between power at various points in the block diagram in Figure 2.1 can be written in terms of system equations which relate the power outputs from the systems to the power appearing at the inputs of the systems. The power spectral density of the output of system 1 is given by

$$P_{11} = |H_1|^2 [X + N_1] \qquad \textit{Equation} \quad 2.1$$

and the same quantity for system 2 is

$$P_{22} = |H_2|^2 [X + N_2] \qquad \textit{Equation} \quad 2.2$$

The cross spectral density between the outputs of the two systems may be written as

$$P_{12} = H_1 H_2^* X \qquad \textit{Equation} \quad 2.3$$

where H_2^* represents the complex conjugate of H_2.

2.2 SOLUTION OF MODEL EQUATIONS

The solution of these three equations depends on the desired information one needs to acquire. In the case of test and evaluation of two seismometers operating side-by-side, one frequently needs estimates of the noise levels associated with the subject instruments. This information can easily be obtained directly from the three equations without resorting to intermediate definitions of additional quantities such as the coherence function or the signal-to-noise ratio (SNR) as follows. Simply solve Equation 2.1 for N_1 to yield

$$N_1 = \frac{P_{11}}{|H_1|^2} - X \qquad \textit{Equation} \quad 2.4$$

Substituting for X from Equation 2.3 yields

$$N_1 = \frac{P_{11}}{|H_1|^2} - \frac{P_{12}}{H_1 H_2^*} \qquad \textit{Equation} \quad 2.5$$

Similarly, solving Equation 2.2 for N_2 and substituting for X from Equation 2.3 yields

$$N_2 = \frac{P_{22}}{|H_2|^2} - \frac{P_{12}}{H_1 H_2^*} \qquad \textit{Equation} \quad 2.6$$

The two system noise power spectra in Equations 2.5 and 2.6 are expressed in terms of directly measurable quantities at the outputs of the two test systems and the system transfer functions. It is important to observe that both noise estimates are evaluated independently from one another. This means that it is possible to directly obtain noise estimates from two sensors whose noise characteristics are significantly different from one another.

3 COHERENCE

Since the system noise spectra can be derived directly, as has been demonstrated above, the question arises as to the utility of the coherence function. The coherence function can be used to make preliminary estimates of the systems SNR's and to place lower limits on the SNR's as will now be shown.

The coherence function is defined as (see Bendat and Piersol, 1971 p 32)

$$\gamma^2 = \frac{|P_{12}|^2}{P_{11}P_{22}} \qquad \textit{Equation} \quad 3.1$$

Substituting for P_{11}, P_{22}, and P_{12} from equations 2.1, 2.2, and 2.3 respectively yields

$$\gamma^2 = \frac{|H_1 H_2^* X|^2}{|H_1|^2 [X+N_1]\,|H_2|^2 [X+N_2]} \qquad \textit{Equation} \quad 3.2$$

The response functions divide out of the expression leaving

$$\gamma^2 = \frac{X^2}{X^2 + X(N_1+N_2) + N_1N_2} \qquad \textit{Equation} \quad 3.3$$

Inverting, multiplying both sides by X^2, and dividing both sides by N_1N_2 yields

$$\frac{1}{\gamma^2}\frac{X^2}{N_1N_2} = \frac{X^2}{N_1N_2} + \frac{X}{N_2} + \frac{X}{N_1} + 1 \qquad \textit{Equation} \quad 3.4$$

Rearranging we have

$$\frac{X}{N_1}\frac{X}{N_2}\left(1 - \frac{1}{\gamma^2}\right) + \frac{X}{N_1} + \frac{X}{N_2} + 1 = 0 \qquad \textit{Equation} \quad 3.5$$

This expression relates the power SNR's of the two channels to the coherence and it is in the form of the general equation of an equilateral hyperbola. Figure 3.1 presents the interrelationship of the two channel SNR's for 9 values of coherence spaced 0.1 apart and Figure 3.2 extends the plot to high values of coherence extending from 0.90 to 0.99.

The asymptotes to these hyperbolas are given by

$$\frac{X}{N_1} = \frac{X}{N_2} = \frac{\gamma^2}{1-\gamma^2} \qquad \textit{Equation} \quad 3.6$$

Therefore, given a value of the coherence between the output signals of a side-by-side test of two instruments, the power SNR's in both instruments must be at least as high as the value given by Equation 3.6. Since it is unlikely that, under low background conditions, the SNR on one instrument will greatly exceed that in the other if the PSD's are somewhat equal, the plots in Figures 3.1 and 3.2 can be used to obtain quick estimates of the system SNR's.

The special case of equal SNR's in both channels can be analyzed by letting $N_1 = N_2$ ($\frac{X}{N_1} = \frac{X}{N_2}$) in Equation 3.5 and solving for the quadratic for the SNR. The root is found to be

$$\frac{X}{N_1} = \frac{X}{N_2} = \frac{\gamma}{1-\gamma} \qquad \textit{Equation} \quad 3.7$$

This condition is the special case of equal noise in both sensors which was modeled at ASL earlier (see Peterson *et al.* 1980).

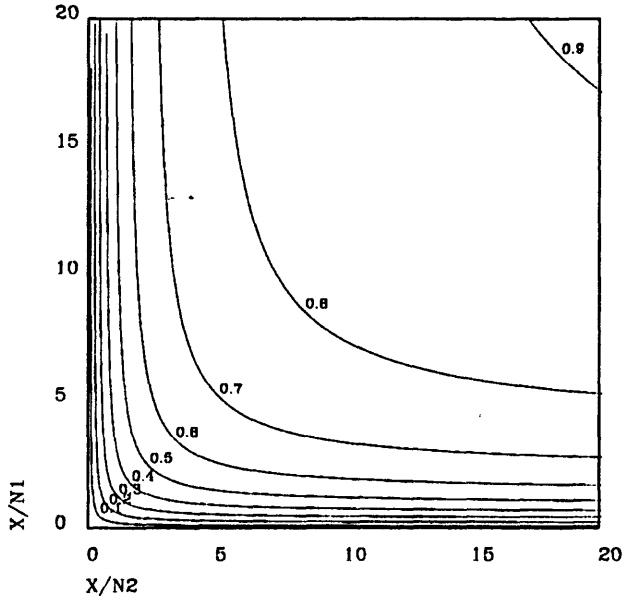

Figure 3.1 The interrelationship of the channel power SNR's and coherence at low levels of coherence.

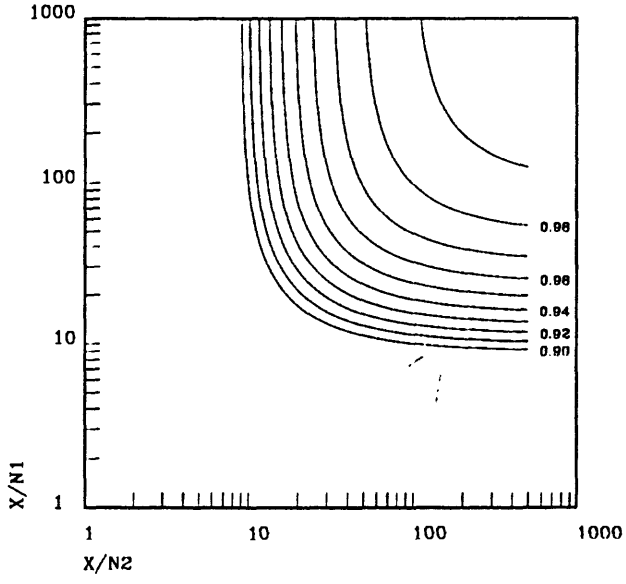

Figure 3.2 The interrelationship of the channel power SNR's and coherence at high levels of coherence.

Equation 3.6 can be solved for $N_1 = N_2 = N$ to yield

$$N = X\left(\frac{1}{\gamma^2} - 1\right) \qquad \textit{Equation} \quad 3.8$$

and substituting for X from equation 2.3

$$N = \frac{P_{12}}{H_1 H_2^*}\left(\frac{1}{\gamma^2} - 1\right) \qquad \textit{Equation} \quad 3.9$$

Equation 3.9 can be used to calculate absolute upper limits based on the coherence (the asymptotic limits) for the noise in both sensors involved in a test. The noise estimates calculated from equations 2.5 and 2.6 should both lie below that indicated by equation 3.9 throughout the sensor passband.

4 DATA PROCESSING

The analysis of the data acquired by the ASL Harvard type experimental (ALQX) digital recording system was conducted on the ASL Microvax II cluster using algorithms and software written at ASL. A brief summary of the data collection system and highlights of the processing algorithms will be outlined here.

4.1 Raw Data Preprocessing

The ALQX digital data recording system recorded all of the long period data from the CMG-3S sensors and the STS-1 sensors. The ALQX digital data system is a combination 16 bit and 24 bit recording system which produces four bands of data for each channel. It is capable of recording three channels of 16 bit data; the data flow in a typical 16 bit channel is shown in Figure 4.1. It is also capable of recording three channels of 24 bit data; the data flow in a typical 24 bit channel is shown in Figure 4.2. In addition, there are three more 16 bit channels, but since they were not utilized in recording the data for this report, they will not be described herein.

The data is recorded on 150 megabyte 1/4 inch data cartridges after data compression using a first difference compression algorithm developed at Harvard by Joe Steim (see Halbert et al. 1988, Appendix A).

The data from the tapes produced by the recording system are first reformatted, decompressed, and time aligned while being dumped on disk. Then the data is low pass filtered at a period appropriate to prevent aliasing due to the decimation which follows. Next, the time series is decimated by a factor of 2, divided into segments which are arbitrarily positioned in time, and a 50% overlap between time segments is generated. Then a Hanning window is applied to each segment. Finally, the Fast Fourier Transform (FFT) of each segment is calculated (see Stearns, 1975, p 265 for the algorithm used) and stored in a disk file to serve as the processed data base. Each processed data base normally contains several days of time continuous FFT data.

4.2 Final Data Processing

The object of the data analysis of side-by-side test data is to resolve the internal system noise in the two sensors under evaluation. Seismic instrument noise is most easily resolved during time periods when the system input is at its lowest levels; that is, when the seismic input due to earthquakes, explosions, wind etc. is at its minimum (see Holcomb, 1990 for an analysis of noise analysis errors arising from sensor misalignment in the presence of high levels of seismic background). The selection of time periods during which the seismic background is low is frequently quite laborious because it is usually done by visual inspection of analog records. Therefore, a rather simple algorithm has been derived at ASL to perform this function automatically thereby freeing the analyst from the visual drudgery, and freeing the results from the analyst's bias.

First, the total system output power levels (P_{11} and P_{22} in Figure 2.1) were evaluated by calculating the power contained in the FFT's of their respective output time series; then the PSD bins between 10 and 100 seconds are summed for each PSD segment and the sums stored. Assuming that instrument self noise is relatively constant with time, the PSD segments for which these sums are small represent time periods during which seismic input to the sensors was low. The algorithm then assumes that the seismic input will be free of "event" data 10% of the time and selects the quietest 10% of the PSD segments to be included in the final analysis.

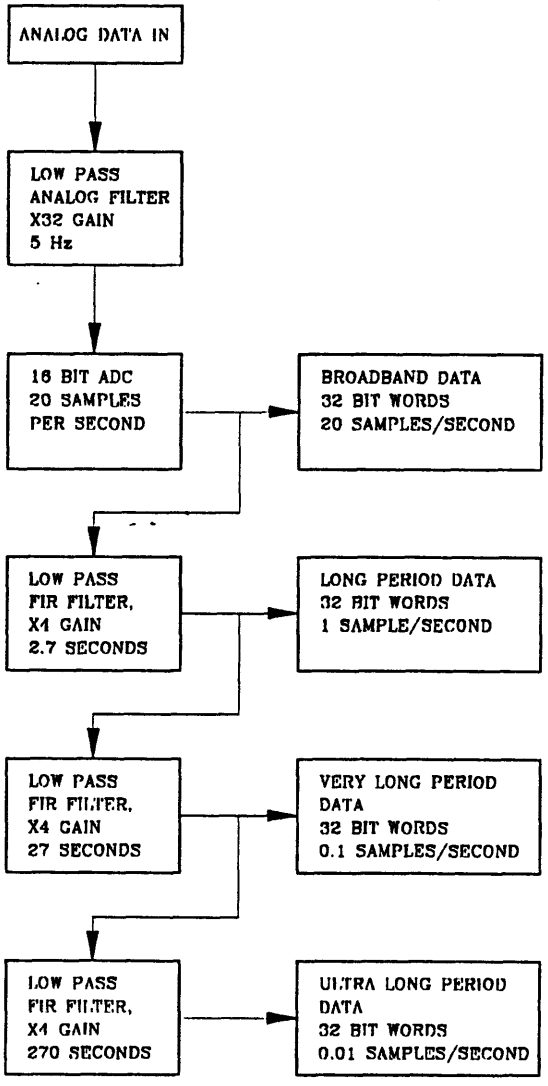

Figure 4.1 Data processing algorithm and the four types of data produced by a typical 16 bit recording channel in the ALQX digital data recording system.

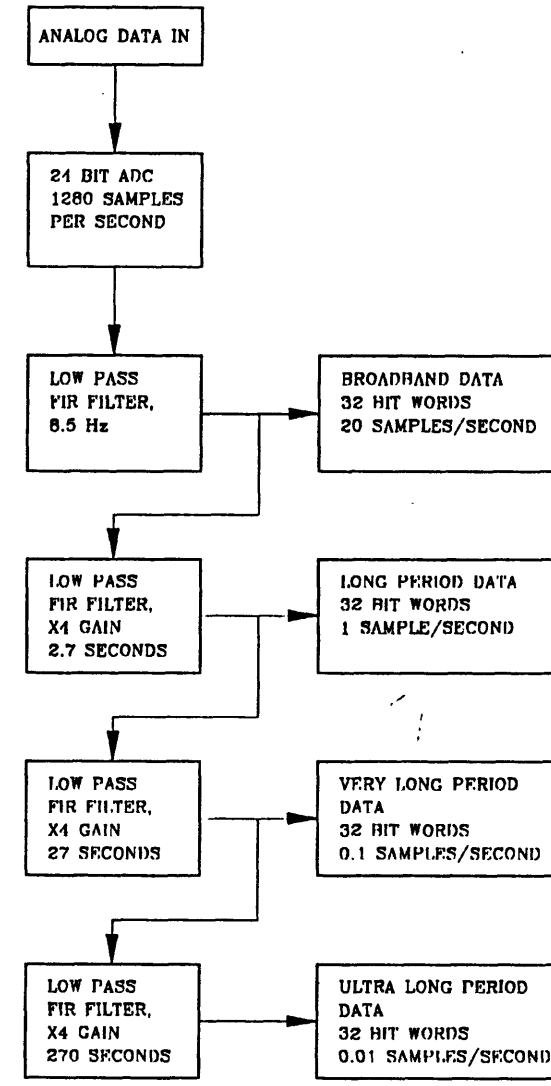

Figure 4.2 Data processing algorithm and the four types of data produced by a typical 24 bit recording channel in the ALQX digital data recording system.

There is a major assumption involved in this process; both sensors are assumed to be equally noisy and the noise is assumed to be evenly distributed over time. This assures that variations in the PSD sums are due to variations in seismic input. Unfortunately, this assumption does not strictly hold because seismic sensor systems frequently contain noise sources which generate noise in bursts and bursts are not necessarily time coincident between channels. This means that quiet segment sums on one channel do not necessarily correspond in time to quiet

segment sums on other channels. Since system noise level calculations must be made on time coincident segments from two channels, one of the channels may contain noise bursts not discriminated against by the quiet segment selection algorithm operating on data from the other channel. Since the noise sources associated with burst noise normally die out with time the assumptions made in the algorithm become more realistic the longer the instrument has been installed.

Investigations conducted during the study contained herein indicated that the algorithm described above performed better if the PSD bins were summed between 30 and 100 seconds instead of between 10 and 100 seconds. This change eliminated the effects of variations in the 18 second microseism peak as criteria in selecting the segments. It enhanced the effects of instrument noise on the segment selection process in the 30 to 100 second portion of the spectrum; long period instruments tend to be noisy in this band.

Once the 10% quietest PSD segments are identified by this algorithm, they were smoothed using a combination of ensemble averaging and frequency smoothing (see Bendat & Piersol pp. 329-330). The number of segments included in each ensemble average is not constant since it is dependent on the total length of the input time series. The frequency smoothing algorithm, which is used to smooth in the frequency domain, was the one developed earlier by one of the authors (see Holcomb, 1989, pp. 6-2 through 6-5).

5 PRELIMINARY HIGH FREQUENCY TESTS

Initial measurements at high frequencies were made to assure that the instruments were functioning properly and to become familiar with their operation. The initial high frequency measurements were also intended to be a cross check with high frequency measurements conducted in the shotgun boreholes at SNL's FACT site. The initial installation technique consisted of super glueing 3 small (approximately 1/4" in diameter) steel ball bearings to the bottom of each sensor package approximately 120° apart and setting the packages on the concrete floor of the ASL extemal vault. In addition, a new installation technique, which consisted of potting the two CMG-3S sensors in a block of plaster of paris, was evaluated. In both installations, the packages were located within approximately 5" of each other and were visually oriented parallel with each other.

A Hewlett Packard 3562A spectrum analyzer was used to conduct the high frequency measurements. This instrument is a modem 14 bit digital spectrum analyzer which is capable of simultaneously digitizing data from two input channels and performing complex spectral analysis of the accumulated data. It is preprogramed to calculate and display on screen and on plotter output all of the usual spectral quantities of interest such as histogram, power spectral density, coherence, auto correlation, and transfer function magnitude and phase. In addition it can be programmed to perform additional calculations as desired. Therefore, it is a powerful tool for use in measurements such as those being made in this study.

5.1 TYPICAL VAULT INSTALLATION

As supplied from the factory, the CMG-3S sensors were not equipped with the usual adjustable vault installation feet because they were intended solely for borehole installation. The possibility of simply placing the flat bottomed sensor cases directly on the concrete floor of the vault was investigated, but this procedure did not result in a stable installation because the vault floor was not flat to the degree necessary to provide simultaneous contact with the entire sensor base. Therefore, it was necessary to adapt the sensors to provide a three point installation capability. Three ball bearings whose diameter was approximately 1/4" were glued to the base of the sensor cases with super glue. The balls were evenly spaced at approximately 120° apart and were positioned near the edges of the base.

Figures A.1, A.2, and A.3 contain the uncorrected PSD estimates for the vertical, north, and east components respectively when the two CMG-3S sensors were installed on ball bearing feet. A comparison of the uncorrected PSD estimates (power spec1 and power spec2 for each component) in Figures A.1, A.2, and A.3 reveals that there are significant differences in the PSD estimates obtained from the two sensors particularly in the portion of the spectrum centered about 50 Hz. All three components of the PSD for the first sensor (power spec1) contains a large "hump" near 50 Hz whereas this hump is significantly reduced in the PSD of the second sensor horizontal sensors and completely absent in the PSD of the second sensor vertical component. Careful study will reveal other differences in the spectra of the two sensors individual components. These "humps" are believed to be installation dependent because experience has shown that they frequently move around in frequency from installation to installation.

Figures A.4, A.5, and A.6 contain the uncorrected instrument noise PSD estimates and coherence functions for the vertical, north, and east components respectively. The Lajitas low noise model lies at -80 db in all three of these figures. The vertical component noise level (Figure A.4) lies below the Lajitas noise out to about 12 Hz, the north component noise level (Figure A.5) lies below the Lajitas noise out to about 15 Hz (if we ignore the abnormally high levels below 4 Hz), and the east component noise level (Figure A.6) lies below the Lajitas noise out to about 8 Hz. These values are significantly less than the corresponding values as measured in the shotgun boreholes at the SNL FACT site. All three component's estimated noise levels at FACT were below the low noise model out to beyond 20 Hz.

5.2 POTTED IN PLASTER OF PARIS

For years, the authors have toyed with the idea of using a potting medium as a means of installing seismometers in both boreholes and vaults. This type of installation procedure should result in a very rigid coupling of the sensors to the earth thereby producing an improved reproduction of the motion of the ground. Since the CMG-3S sensors had no factory supplied legs, it was decided that this would be an excellent opportunity to evaluate this installation procedure.

The existing surface of the concrete floor in the ASL vault had a shiny smooth finish. Therefore, the area in which the CMG-3S sensors were to be installed was roughed up with a hammer and chisel to create a rough surface for the potting medium to bond to. Plaster of paris was chosen as the potting material because it was readily available, was easy to work with, and it would be fairly easy to remove after the experiment was completed. The two sensors were potted in a 50 cm by 50 cm by 25 cm high block of plaster of paris poured directly on the newly roughed floor of the vault. The top inch or two of the sensor projected above the plaster of paris block and the two sensors were positioned about 1 inch apart. The were visually positioned parallel to one another prior to pouring the plaster of paris in the potting form.

Figures A.7, A.8, and A.9 contain the uncorrected PSD estimates for the vertical, north, and east components respectively when the two CMG-3S sensors were potted in plaster of paris. A comparison of the uncorrected PSD estimates (power spec1 and power spec2 for each component) in Figures A.7, A.8, and A.9 indicates that the individual component power spectra were much more similar when the two sensors were potted than they were when they were installed on ball bearing feet. In fact, differences in the power spectra obtained from different instruments are difficult to visually identify. Note that there are no obvious "humps" in the uncorrected PSD estimates in Figures A.7, A.8, and A.9.

Figures A.10, A.11, and A.12 contain the uncorrected instrument noise PSD estimates (noncoh) and coherence functions (coherence) for the vertical, north, and east components respectively. Here again, the Lajitas low noise model lies at -80 db in all three figures. Potting in plaster of paris significantly extends the frequency at which the estimated noise levels reach the low noise model for all components. Under potted conditions, the vertical estimated PSD noise level reaches the low noise model at about 13 Hz, the north estimate reaches the model at about 23 Hz, and the east estimate reaches the model at about 20 Hz. These numbers very closely approximate the same data as measured in the shotgun boreholes at the SNL FACT site. For some reason, the vertical component was the noisiest channel in both sets of measurements.

It is evident that potting the two sensors significantly improved their noise level performance over that shown when installed on ball bearing legs. The most probable explanation for the improvement is that the sensors were held more rigidly to the ground when they were potted. This improved the coupling of ground motion into the sensors. It is important to emphasize the change in the overall character of both the uncorrected PSD estimates and the instrument noise PSD estimates when the installation method was changed from ball bearing legs to potting in plaster of paris. All of the PSD estimates obtained from the potted installation are much smoother than those obtained from the ball bearing leg installation. The authors believe that the "bumps" or roughness which are usually observed at high frequencies in the PSD estimates for the unpotted installation, and for that matter in most other commonly used methods of installation, are caused by mechanical resonances within the sensor package. Potting the sensor in a dense medium (at least plaster of paris is denser than air) effectively damps any resonances in the sensor.

In the past 20 years or so, modern sensor design has advanced to the point that the typical internal sensor system noise is below input signal levels at most quiet sites. As a result, developing new and improved installation methods is rapidly becoming the name of the game in both long and short period seismology because the noise contributed by the installation frequently dominates noise arising from the sensor itself. Quieter installation techniques are badly needed and greater effort should be devoted to devising improvements in this area in the future.

6 PRESSURE SENSITIVITY

Experience with long period sensors in the past has shown that operating horizontal sensors in sealed cases can lead to excessive noise at long periods due to tilt motions induced by bending of the sealed case, which in turn is caused by external atmospheric pressure variations. Since the CMG-3S cases are sealed, it was decided to check for pressure sensitivity in these sensors by isolating the CMG-3S sensors from atmospheric pressure changes.

Both CMG-3S sensors were installed side-by-side inside a bottomless high gain long period (HGLP) pressure tank in the external ASL vault room. This tank was bottomless in the sense that the original 0.5 inch thick steel bottom of the tank had been removed to leave an approximately 3 inch wide rim round the outside edge of the bottom. This rim had then been bonded to the concrete floor of the vault to yield an air tight seal between the tank and the floor; at least the seal was air tight at the periods of interest. The same experimental setup had been used in the past to conduct pressure sensitivity evaluations of other long period sensors. The sensors were installed on leveling plates by placing their flat bottoms directly the plates. The plates were three point screw adjustable leveling plates which facilitate independent rough preliminary leveling of each unit to level them to within the range of the internal CMG-3S leveling process. The adjusting feet in the leveling plates rested directly on the epoxy paint coated concrete floor in the bottom of the tanks. Previous experience with sensors containing active devices had revealed that air convection within the tank can be a problem because of the heat given off by such sensors. Therefore, a lighted 60 watt light bulb was placed outside the tank resting on top of the tank lid to provide heat to stratify the air inside the HGLP tank to subdue air convection. A capped pipe fitting plumbed into the side of the tank provided a means whereby the tank could be easily vented or sealed.

6.1 SEALED IN HGLP TANK

The first tests were conducted with the HGLP tank sealed. One parallel horizontal component from each of the CMG-3S sensors and one parallel component from an STS-1 horizontal were recorded on the ALQX data system. The two CMG-3S sensors were visually aligned with one another by observing them from above and positioning them as parallel as possible with the markings provided. They were both aligned with the STS-1 sensor in the cross tunnel by visually extrapolating the STS-1 alignment from the cross tunnel into the external vault room. Therefore, there may be an error in the alignment between the STS-1 sensor and the two CMG-3S sensors. The two CMG-3S sensors were positioned approximately 12 cm apart; the STS-1 sensor was located approximately 10 meters from the CMG-3S sensors. This distance should be insignificant at the periods of interest.

Figures 6.1 and 6.2 contain comparative noise estimates as calculated with the direct model of a side-by-side test of the CMG-3S (A) horizontal and STS-1 horizontal respectively. This data was obtained while the two instruments were operated in a sealed HGLP tank for a little over 3 days. As noted in the figure captions, the CMG-3S (A) horizontal data was used as the basis for selecting the quiet time segments to be included in the data presented in both figures. The segments actually selected by the automatic segment selection algorithm are depicted in Figures 6.3 through 6.6, which contain time plots of most of the data actually collected. Each selected segment is approximately one hour and eight minutes long; the selected segments are enclosed

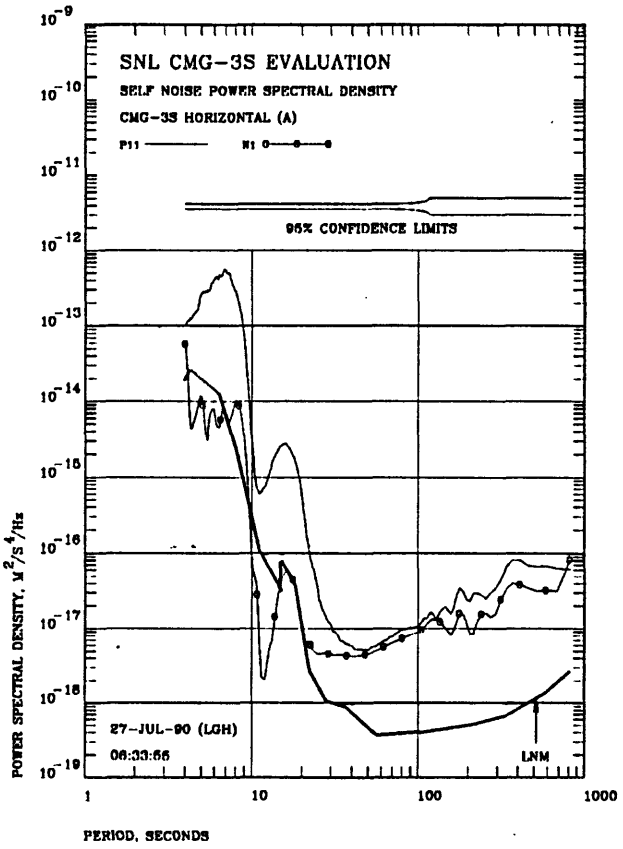

Figure 6.1 Estimated total PSD and self noise PSD of the CMG-3S (A) horizontal when installed in a sealed HGLP tank. The CMG-3S (A) horizontal selected the segments.

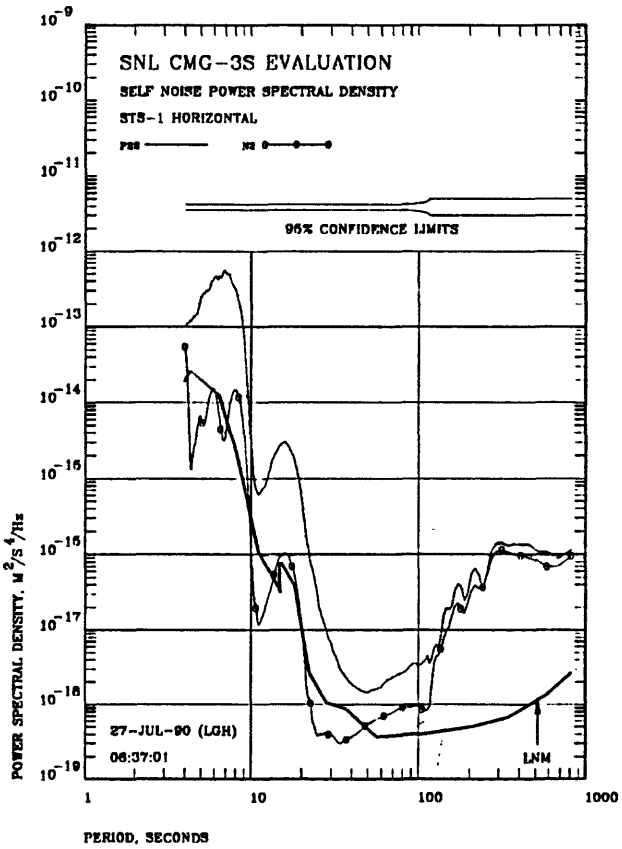

Figure 6.2 Estimated total PSD and self noise PSD of the STS-1 horizontal. The CMG-3S (A) horizontal selected the segments.

by square brackets in the figures. No segments were selected from day 349; therefore the data collected on that day has not been plotted. All of the time domain data presented in this report has been low-pass filtered with a 15 second cutoff and plotted with a magnification of approximately 10K at 25 seconds. Low-pass filtering the data at 15 seconds emphasizes the time plots in the part of the spectrum in which the sensors are likely to be noisy thereby making it easier to compare the time plots with the PSD estimates. The low pass filtering and high magnification plot also facilitate the visual identification of low level features in the time domain. The amplitude of the time domain data has been deliberately clipped by the plotting software to prevent the peaks of large amplitude signals from obscuring data in adjacent time traces.

Note that the two total PSD estimates in Figures 6.1 and 6.2 virtually overlay one another out to around 25 seconds. Above 25 seconds, the raw PSD estimate for the CMG-3S horizontal becomes larger than that for the STS-1 horizontal up to about 100 seconds. Above 100 seconds, the character of the STS-1 horizontal noise is quite abnormal. The noise level is much higher than is normally the case with these high quality instruments. Note also that the estimated noise PSD levels for both of the instruments are quite similar from 4 to approximately 25 seconds.

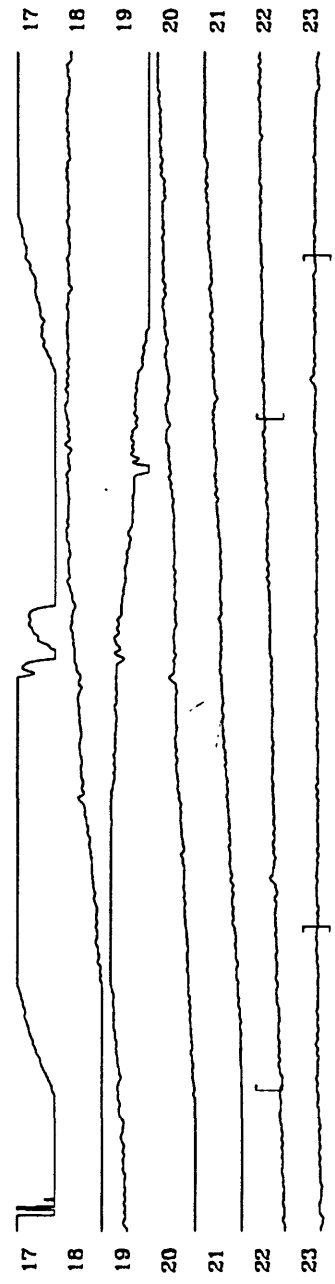

Figure 6.3 Time record for day 347 of the CMG-3S (A) horizontal when installed in a sealed HGLP tank.

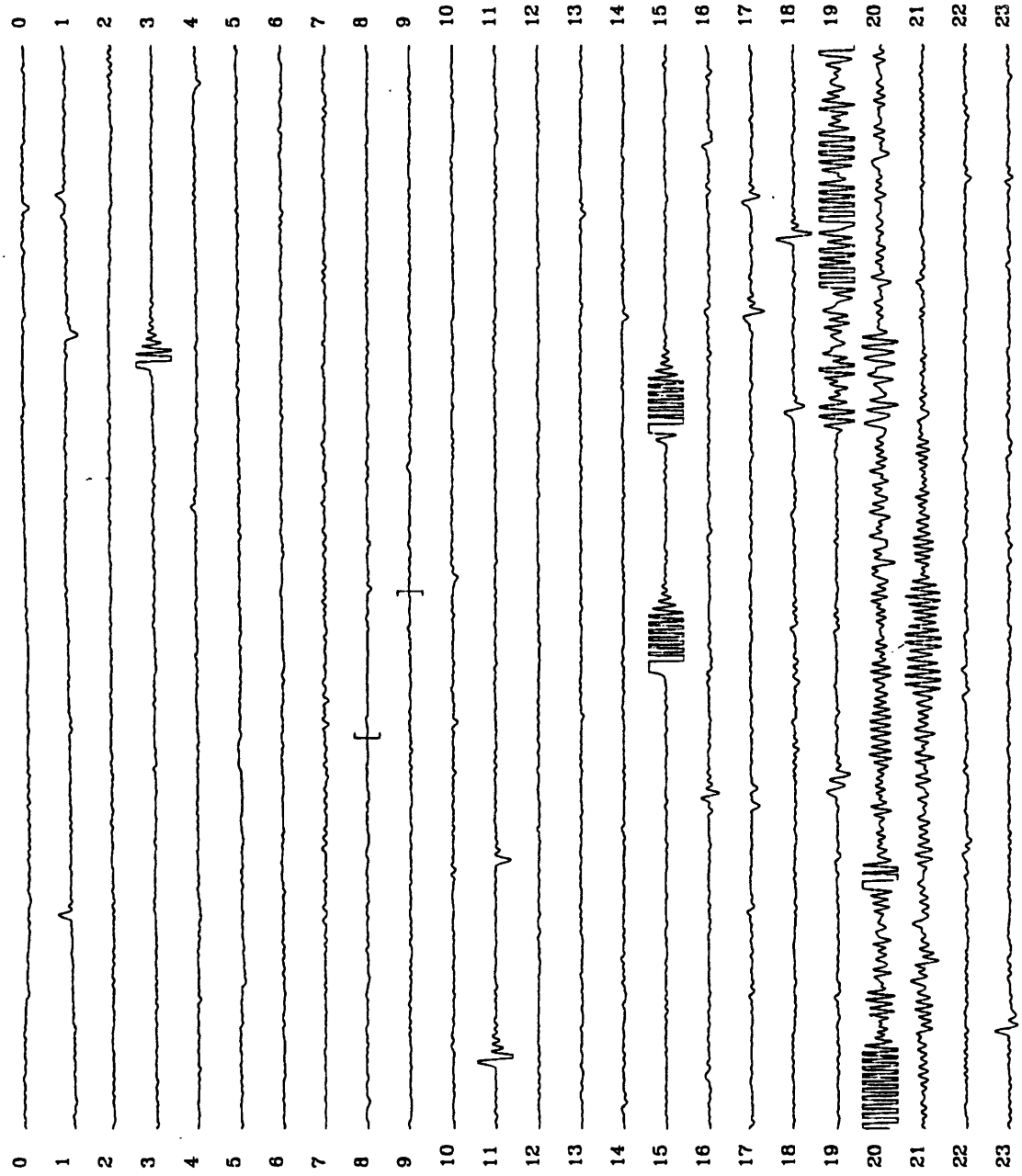

Figure 6.4 Time record for day 348 of the CMG-3S (A) horizontal when installed in a sealed HGLP tank.

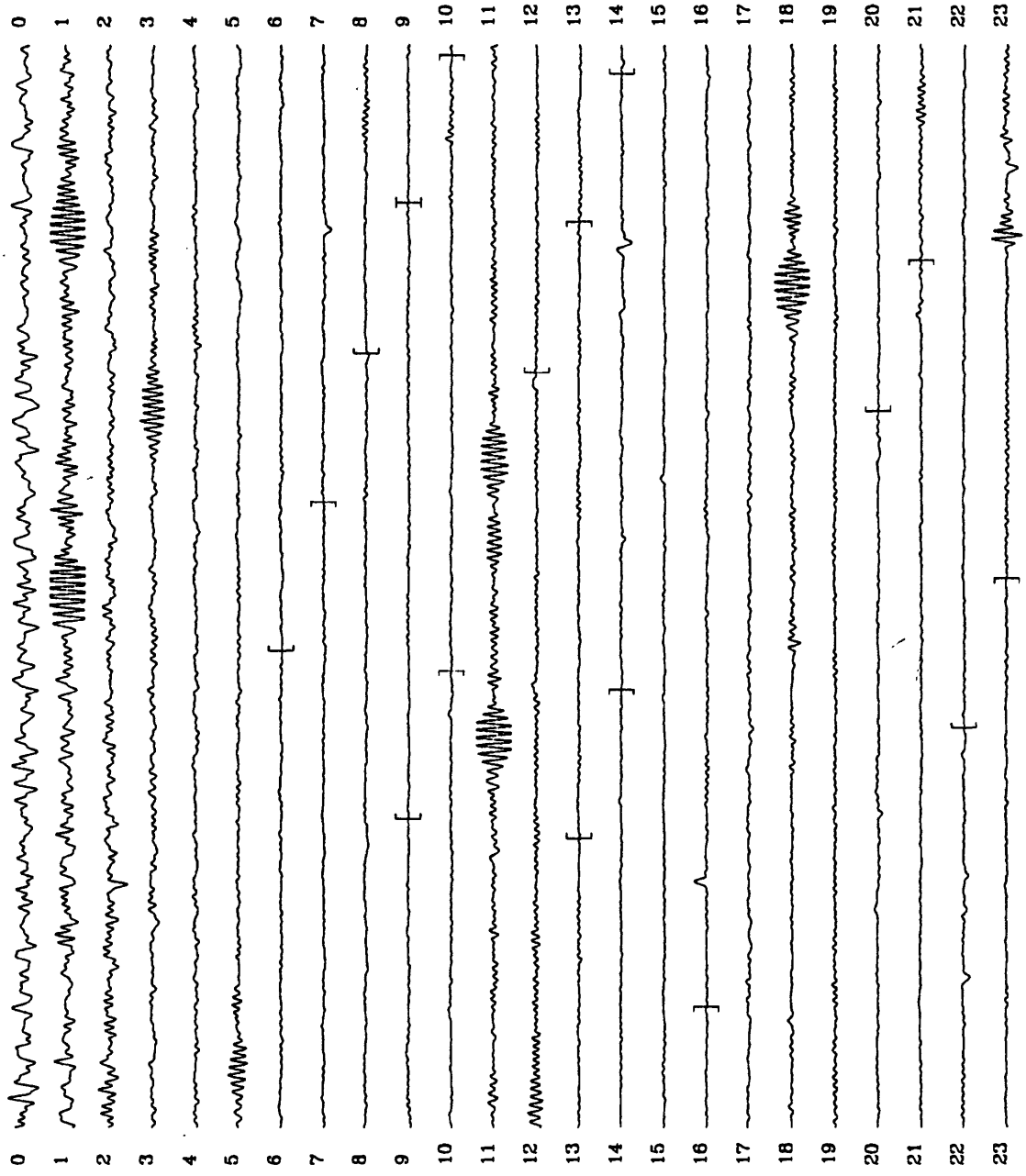

Figure 6.5 Time record for day 350 of the CMG-3S (A) horizontal when installed in a sealed HGLP tank.

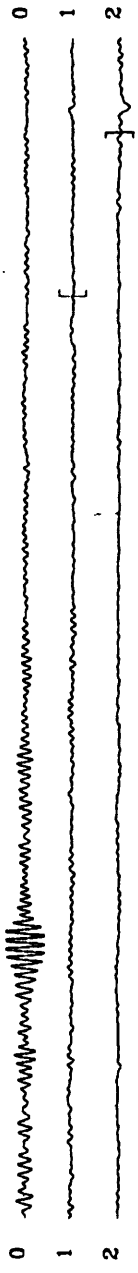

Figure 6.6 Time record for day 351 of the CMG-3S (A) horizontal when installed in a sealed HGLP tank.

The estimated noise PSD in this part of the band (4 to 25 seconds) is probably not representative of the true noise level in either instrument. Instead, it is probably due to alignment error between the two horizontal components. An earlier analysis (see Holcomb, 1990) demonstrated that errors in alignment in side-by-side tests results in apparent system noise, which is shaped more or less like the seismic background, and which lies at a fixed distance below the seismic background across the band. The PSD noise estimates in both Figures 6.1 and 6.2 from 4 to 25 seconds approximate these characteristics quite well. Both instrument noise estimates lie approximately a factor of 40 below their respective total power estimates (the total power estimates should be very close to the seismic background in this part of the spectrum because sensor noise is typically far below background signals in this band) and their shape approximates the total power estimate. A SNR ratio of 40 translates into a possible misalignment of approximately 11° (see Figures 6.20 and 6.21 of Holcomb, 1990). Therefore, the true instrument noise in the band extending from 4 to 25 seconds for both sensors probably lies somewhat below the levels shown in the two figures; it is probably well below the indicated levels at shorter periods.

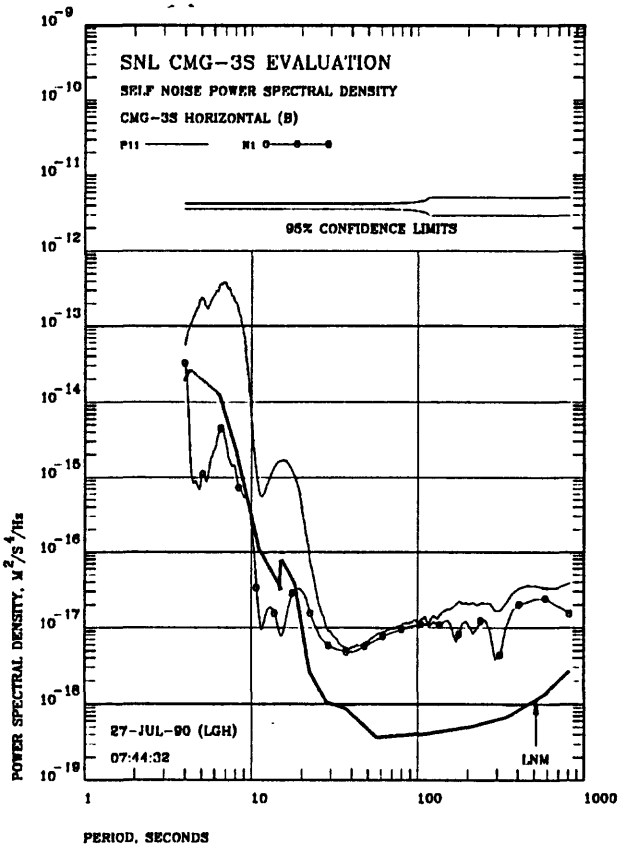

Figure 6.7 Estimated total PSD and self noise PSD of the CMG-3S (B) horizontal when installed in a sealed HGLP tank. The CMG-3S (B) horizontal selected the segments.

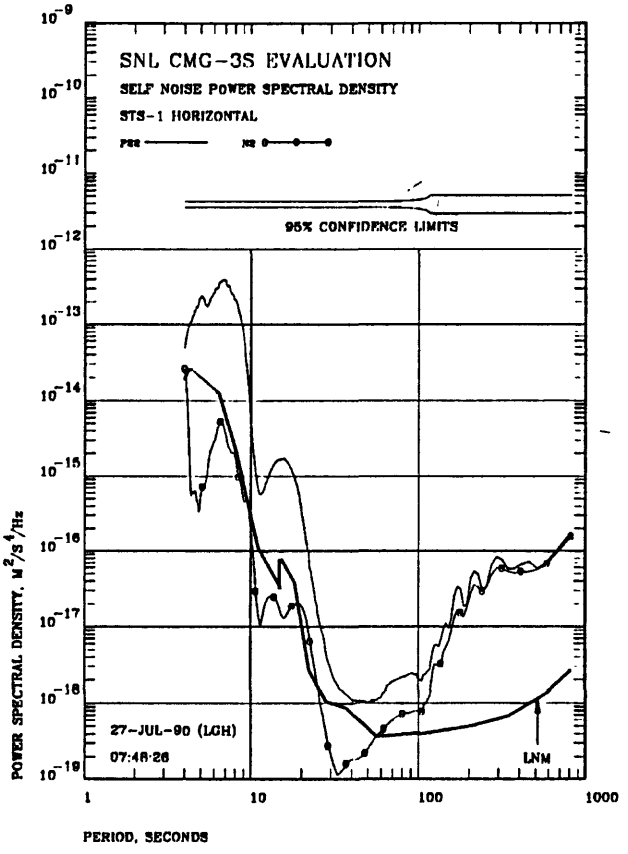

Figure 6.8 Estimated total PSD and self noise PSD of the STS-1 horizontal. The CMG-3S (B) horizontal selected the segments.

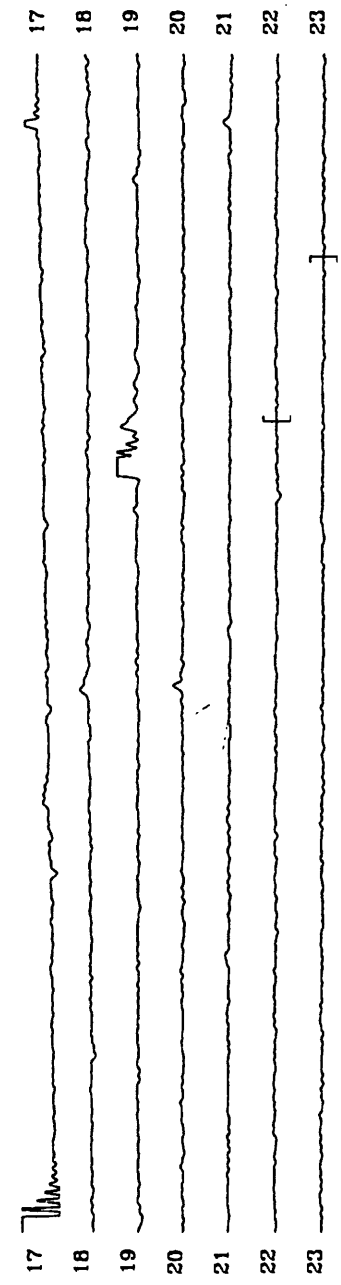

Figure 6.9 Time record for day 347 of the CMG-3S (B) horizontal when installed in a sealed HGLP tank.

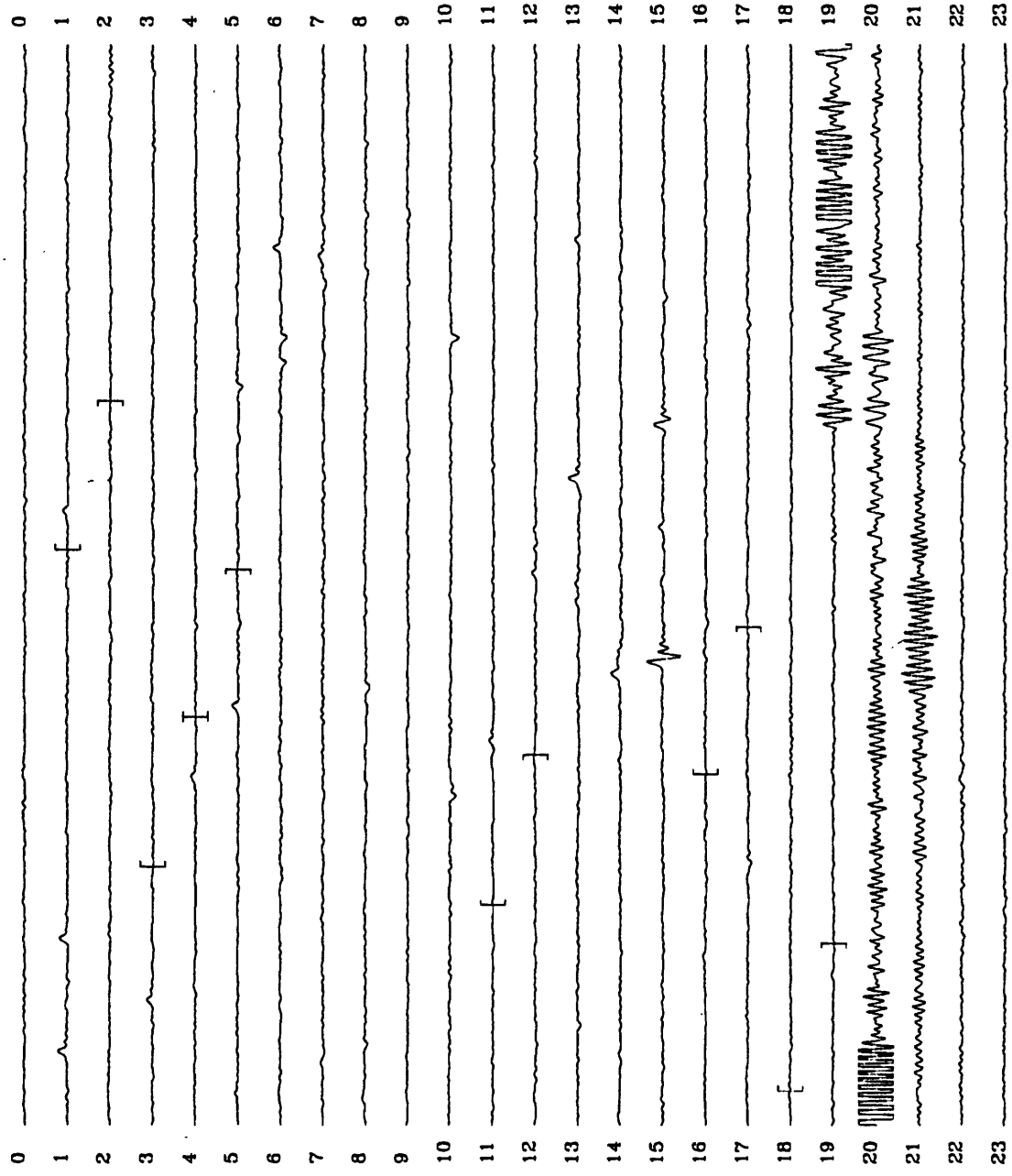

Figure 6.10 Time record for day 348 of the CMG-3S (B) horizontal when installed in a sealed HGLP tank.

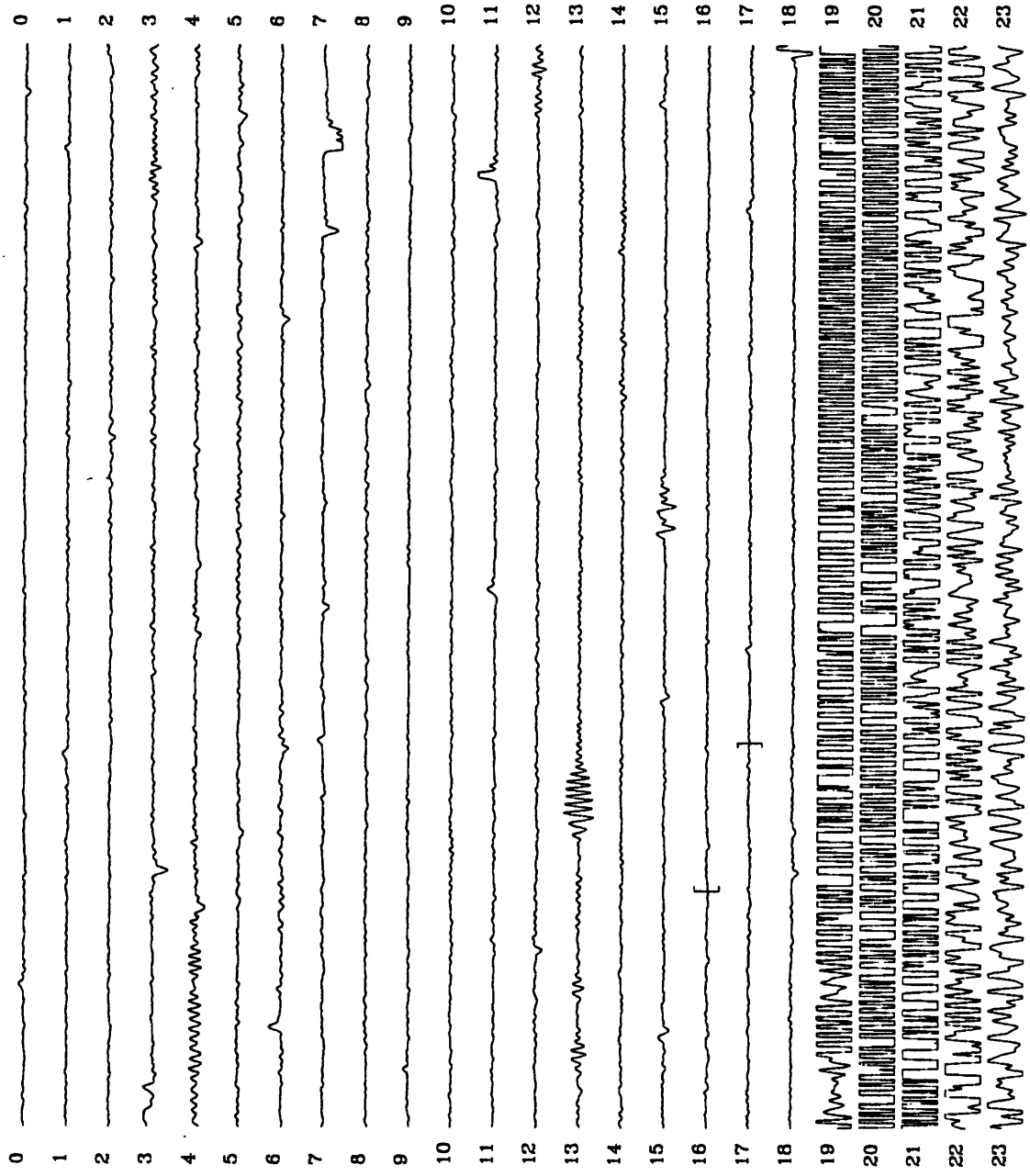

Figure 6.11 Time record for day 349 of the CMG-3S (B) horizontal when installed in a sealed HGLP tank.

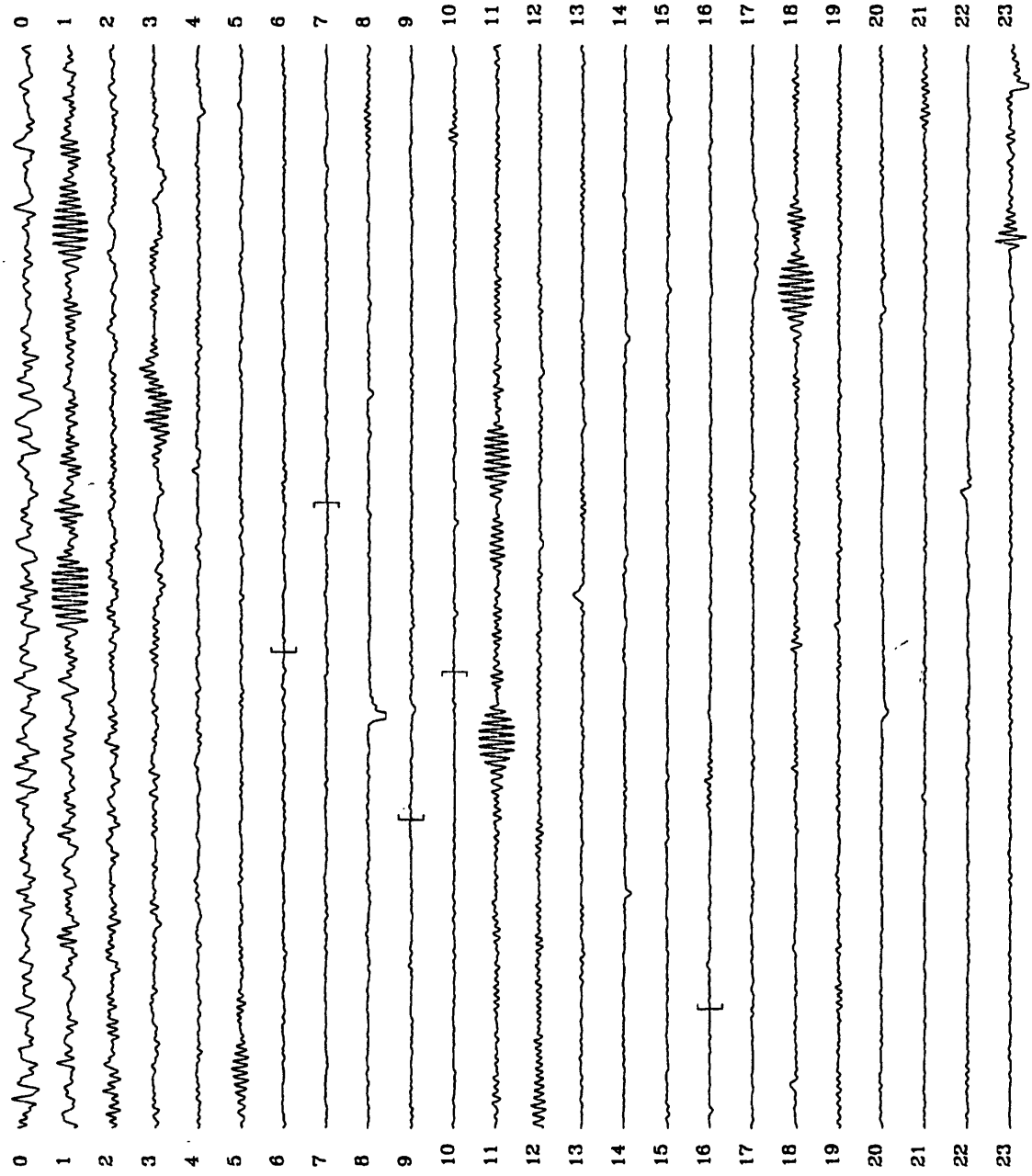

Figure 6.12 Time record for day 350 of the CMG-3S (B) horizontal when installed in a sealed HGLP tank.

As Figures 6.7 and 6.8 demonstrate, the general character of the noise estimates for the CMG-3S (B) horizontal are approximately the same as those obtained for the (A) horizontal above. Here again, the noise estimates for the CMG-3S (B) horizontal and the STS-1 horizontal are nearly the same from 4 to approximately 25 seconds thereby indicating that the calculated noise estimates in this band are due to instrument misalignment. The general level of the noise estimates in the band extending from 4 to 25 seconds for CMG-3S (B) and the STS-1 in Figures 6.7 and 6.8 are slightly lower (the noise PSD estimates are approximately a factor of 100 smaller than the total PSD estimates) than those in the same band for CMG-3S (A) and the STS-1 in Figures 6.1 and 6.2. Therefore, the degree of misalignment between the CMG-3S (B) and the STS-1 horizontal must be of the order of approximately 8°. Above 25 seconds, the noise estimates for the two instruments are unique and comparable to those obtained above. From 25 to 100 seconds, the noise estimates for sensors A and B are virtually identical; above 100 seconds sensor B may be slightly quieter.

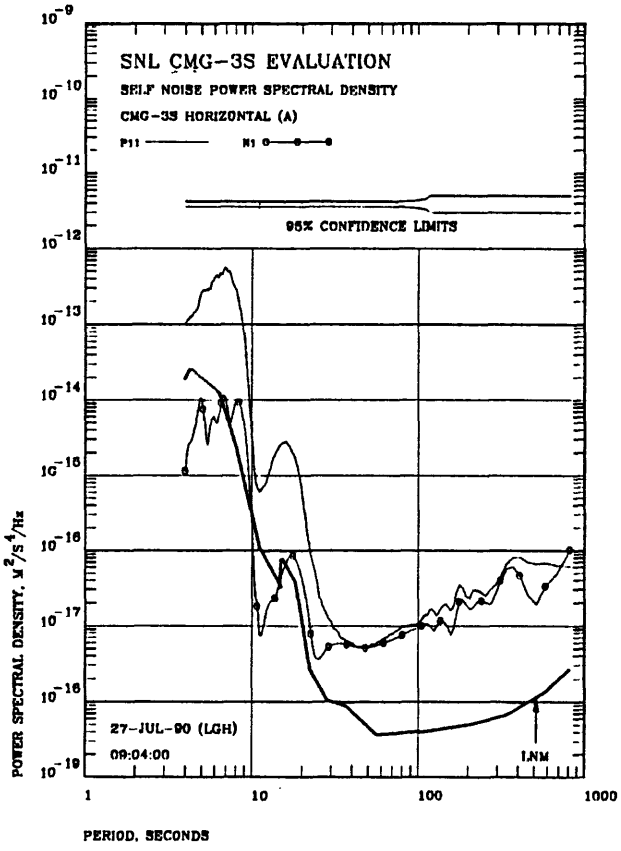

Figure 6.13 Estimated total PSD and self noise PSD of the CMG-3S (A) horizontal when installed in a sealed HGLP tank. The CMG-3S (A) horizontal selected the segments.

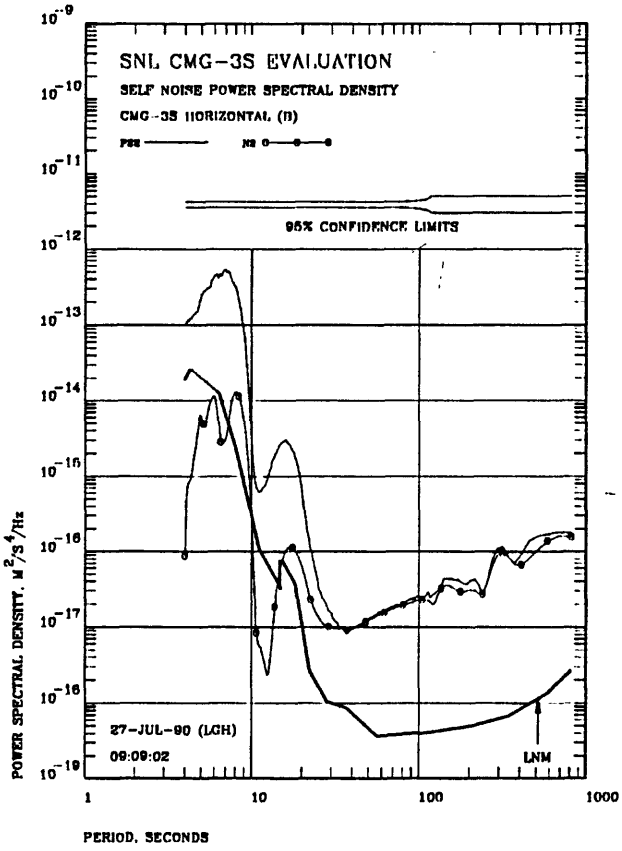

Figure 6.14 Estimated total PSD and self noise PSD of the CMG-3S (B) horizontal. The CMG-3S (A) horizontal selected the segments.

Above 25 seconds the estimated noise level for the CMG-3S horizontal is progressively larger than that for the STS-1 horizontal. In addition, both noise estimates lie less than a factor of 10 below their respective total power estimates. Since a given misalignment error creates a fixed separation between the seismic background and the alignment generated noise at all periods, and since the estimated noise levels above 25 seconds are unique, these estimates are probably representative of true instrument noise in this part of the spectrum.

Figures 6.7 and 6.8 contain direct model noise estimates for the side-by-side evaluation of the CMG-3S (B) horizontal and the STS-1 horizontal. In these two figures, the quite segments from the CMG-3S (B) horizontal data were used to select the data to be included in the two figures. The time domain segments selected by the segment selection algorithm are shown in Figures 6.9 through 6.12. The STS-1 horizontal used in this evaluation is the same horizontal used in the CMG-3S (A) evaluation above.

Figures 6.13, 6.14, 6.15, and 6.16 contain noise estimates obtained from a direct model analysis of the data from CMG-3S (A) and the CMG-3S (B) horizontals when compared with each other. Figures 6.13 and 6.14 contain the results of using the CMG-3S (A) horizontal as the basis for selecting the quiet segments whereas Figures 6.15 and 6.16 contain the results of using the CMG-3S (B) horizontal to select the quiet segments. The actual segments selected for the two sets of PSD estimates are the same as those shown in Figures 6.3 through 6.6 and 6.9 through 6.12 respectively.

Between 4 and 25 seconds, the noise estimates for the two CMG-3S horizontal components compared with one another, as shown in Figures 6.13, 6.14, 6.15, and 6.16, are approximately a factor of 60 below the level of the total power. This fact means that the two CMG-3S horizontals were misaligned by about 10°. A misalignment this large seems to be a bit excessive, but it is quite possible since the two sensors were visually aligned.

The reader may note that, since the STS-1 horizontal with which the two CMG-3S horizontals were compared with in Figures 6.1, 6.2, 6.7, and 6.8 was the same STS-1 horizontal, and that since the indicated degree of misalignment of the two CMG-3S sensors with this common STS-1 sensor were 8° and 11°, the misalignment between the two CMG-3S sensors should be either 3° or 19°. A possible explanation for this discrepancy lies in the difficulty in visually estimating the SNR between 4 and 25 seconds because, as an inspection of the figures will indicate, the SNR is not constant over the period interval. There may also be more than one process which is contributing to the apparent instrument noise level in this band. For instance, cross-axis coupling has been proven to be a contributor of apparent instrument noise which is shaped like the background spectrum (see Durham, 1982) The object herein is not to obtain a quantitative estimate of the degree of the possible misalignment; the object is to explain why the estimated noise levels are so high in this portion of the spectrum and why they resemble the earth's background in the shorter period end of the spectrum.

Above 25 seconds, the self noise PSD estimates for the CMG-3S (A) horizontal obtained by a direct model analysis of the CMG-3S (A) and CMG-3S (B) data as shown in Figure 6.13 are approximately the same as the self noise PSD estimates for the CMG-3S (A) horizontal obtained by a direct model analysis of the CMG-3S (A) and STS-1 data as shown in Figure 6.1. Similarly, above, 25 seconds, the self noise PSD estimates for the CMG-3S (B) horizontal obtained

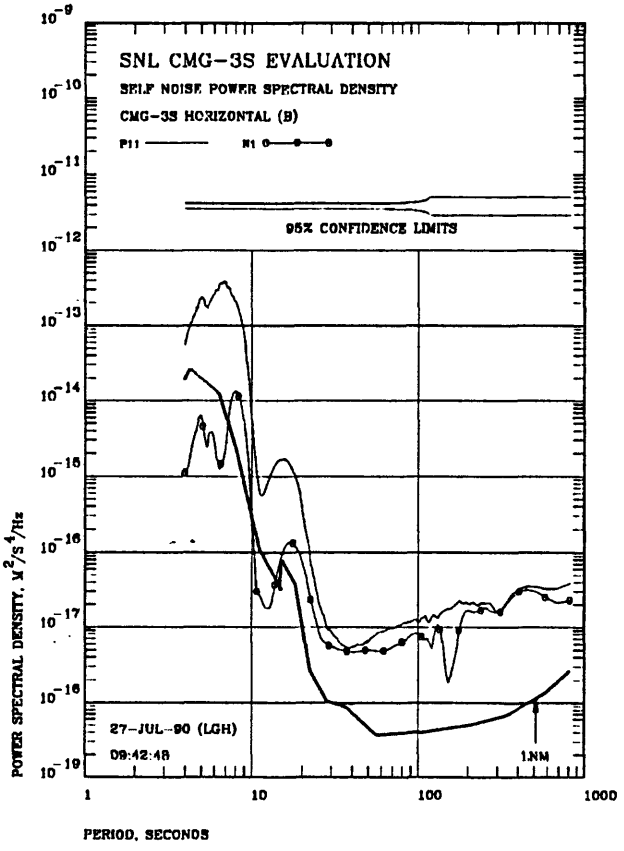

Figure 6.15 Estimated total PSD and self noise PSD of the CMG-3S (B) horizontal when installed in a sealed HGLP tank. The CMG-3S (B) horizontal selected the segments

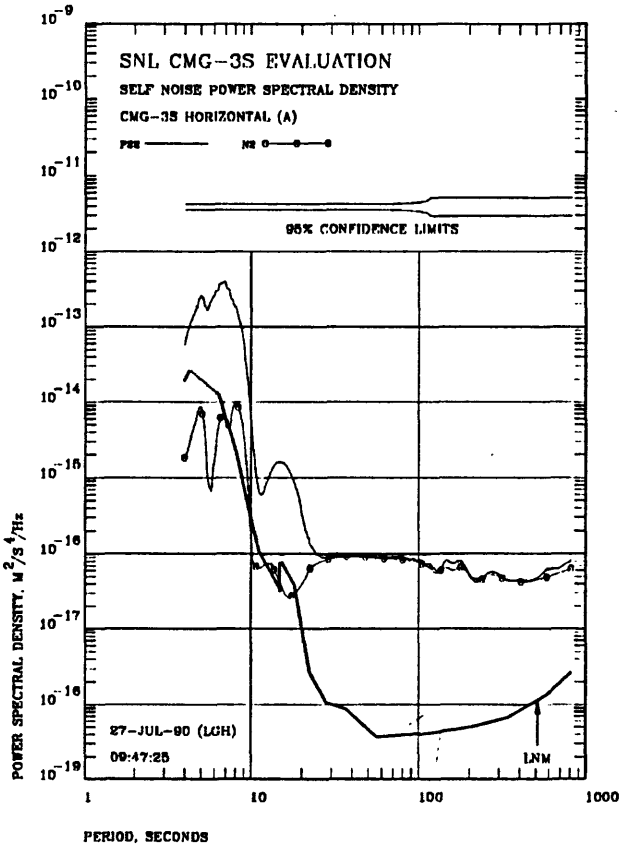

Figure 6.16 Estimated total PSD and self noise PSD of the CMG-3S (A) horizontal. The CMG-3S (B) horizontal selected the segments.

by a direct model analysis of the CMG-3S (B) and CMG-3S (A) data as shown in Figure 6.15 is approximately the same as the self noise PSD estimates for the CMG-3S (B) horizontal obtained by a direct model analysis of the CMG-3S (B) and STS-1 data as shown in Figure 6.7. The fact that the direct model calculated noise estimates obtained from a comparison of two moderately noisy sensors (CMG-3S (A) and CMG-3S (B)) are approximately the same as the same estimates obtained from a comparison of a moderately noisy sensor with a fairly quiet sensor (CMG-3S (A) and STS-1) is indicative of the power of the direct model analysis procedure.

However, the self noise PSD estimates for the CMG-3S (A) horizontal shown in Figure 6.16 are considerably higher than the self noise PSD estimates for the CMG-3S (A) horizontal shown in Figures 6.1 and 6.13. Likewise, the self noise PSD estimates for the CMG-3S (B) horizontal shown in Figure 6.14 are considerably higher than the self noise PSD estimates for the CMG-3S (B) horizontal shown in Figures 6.7 and 6.15. These higher noise estimates are due to the segment selection process and the fact that both of the CMG-3S horizontals were "burping" during the test period.

A "burp" is defined (by these authors at least) as a randomly distributed excursion in the time signal, which frequently appears in the time domain much like the linear impulse response of the system. They are readily evident in the time domain plots above; for instance, there are two burps near the end of hour 17 and two more slightly earlier in hour 18 of Figure 6.4. The two very large signals near the middle of hour 15 of Figure 6.4 are probably also burps; note that they are also evident in the time record for CMG-3S (B) (see Figure 6.10) but at a greatly reduced amplitude. A comparison of Figures 6.3 through 6.6 with Figures 6.9 through 6.12 shows that the burps on the CMG-3S (A) horizontal are not necessarily time coincident with the burps on the CMG-3S (B) horizontal. This indicates that these signals are not due to ground motion; instead, they are believed to be either generated within the seismic sensor itself or are somehow associated with the physical installation of the sensor. They are probably mechanical in origin; small mechanical movements are probably translated into mechanical tilts of the sensing mechanism. As a result, burps are usually larger in amplitude and more frequent on horizontal than on vertical sensors. Burps are a common phenomena on most long period seismic systems and both the amplitude and the frequency of occurrence usually decay out with time if the system is left undisturbed long enough.

The fact that the data selected to be analyzed to create Figures 6.13 and 6.14 was based on the data from CMG-3S (A) means that burps in the CMG-3S (A) output were edited out of the data used to create Figure 6.13 by the segment selection algorithm whereas burps in the CMG-3S (B) output were not necessarily edited out of the data used to create Figure 6.14. Therefore, the CMG-3S (B) PSD noise estimate of Figure 6.14 appears to be noisier than it does in Figures 6.7 and 6.15 in which the data from the CMG-3S (B) was used to select the segments. The same argument explains why the noise PSD estimate for CMG-3S (A) in Figure 6.16 is noisier than the corresponding noise estimates in Figures 6.1 and 6.13. All of the noise estimates should be nearly equal if the instruments were not burping.

6.2 VENTED IN HGLP TANK

Next, the same two sensors were operated in a "vented" HGLP tank. Venting was achieved by removing the cap from a 3/4 inch diameter pipe, which was plumbed into the tank base. This allowed air pressure to equalize between the inside and the outside of the HGLP tank. No other changes were made; the sensors were not physically moved, the tank was not opened, the recording system was not stopped, etc..

Figures 6.17 and 6.18 contain comparative noise estimates of the CMG-3S (A) horizontal and the STS-1 horizontal respectively during the time that the CMG-3S (A) sensor was operated in the vented tank for almost 3 days. The CMG-3S (A) horizontal selected the segments which were included in the analysis. The segments actually selected are enclosed in square brackets in Figures 6.19 and 6.20.

A visual time domain comparison of the CMG-3S (A) horizontal operation in a vented tank contained in Figures 6.19 and 6.20 with the CMG-3S (A) horizontal operation in a sealed tank contained in Figures 6.3 through 6.6 indicates that there is no detectable difference in the time records. Both the frequency and amplitude of the burping seems to be about the same under the two conditions.

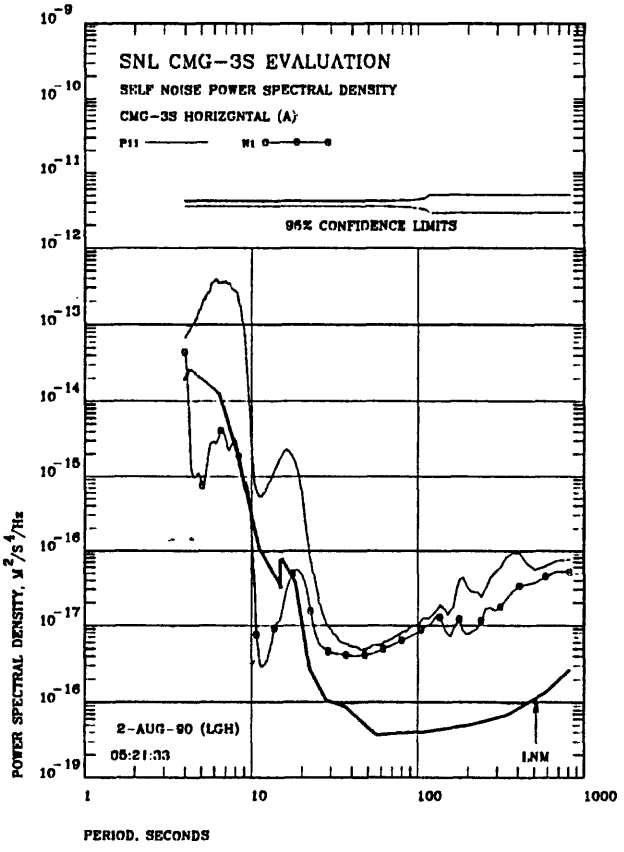

Figure 6.17 Estimated total PSD and self noise PSD of the CMG-3S (A) horizontal when installed in a vented HGLP tank. The CMG-3S (A) horizontal selected the segments.

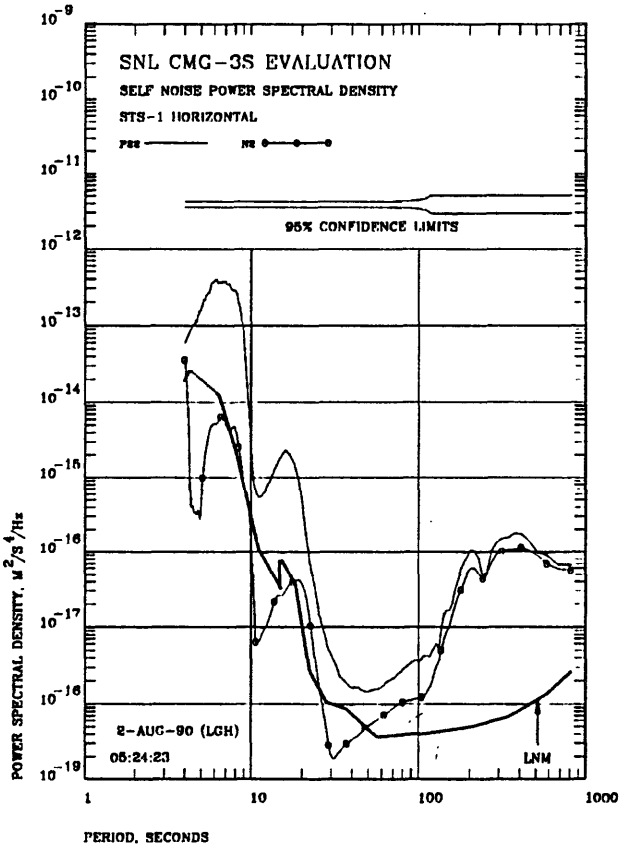

Figure 6.18 Estimated total PSD and self noise PSD of the STS-1 horizontal. The CMG-3S (A) horizontal selected the segments.

A comparison of the estimated instrument noise levels (N_1) for vented tank operation in Figure 6.17 with the estimated instrument noise levels (N_1) for sealed tank operation Figure 6.1 reveals that there was no detectable change in the performance of CMG-3S (A) in a vented versus a sealed tank. From 4 to 25 seconds, the calculated noise levels lie at approximately the same distance below the total noise curves thereby indicating approximately the same degree of misalignment. Above 25 seconds the calculated noise levels in the two figures are virtually identical. This indicates that the noise levels indicated in Figure 6.17 for operation in a vented tank are not significantly contaminated by pressure induced bending of the CMG-3S case. If bending of the sensor case were a problem, the vented noise levels in Figure 6.17 should be greater than the sealed noise levels in Figure 6.1.

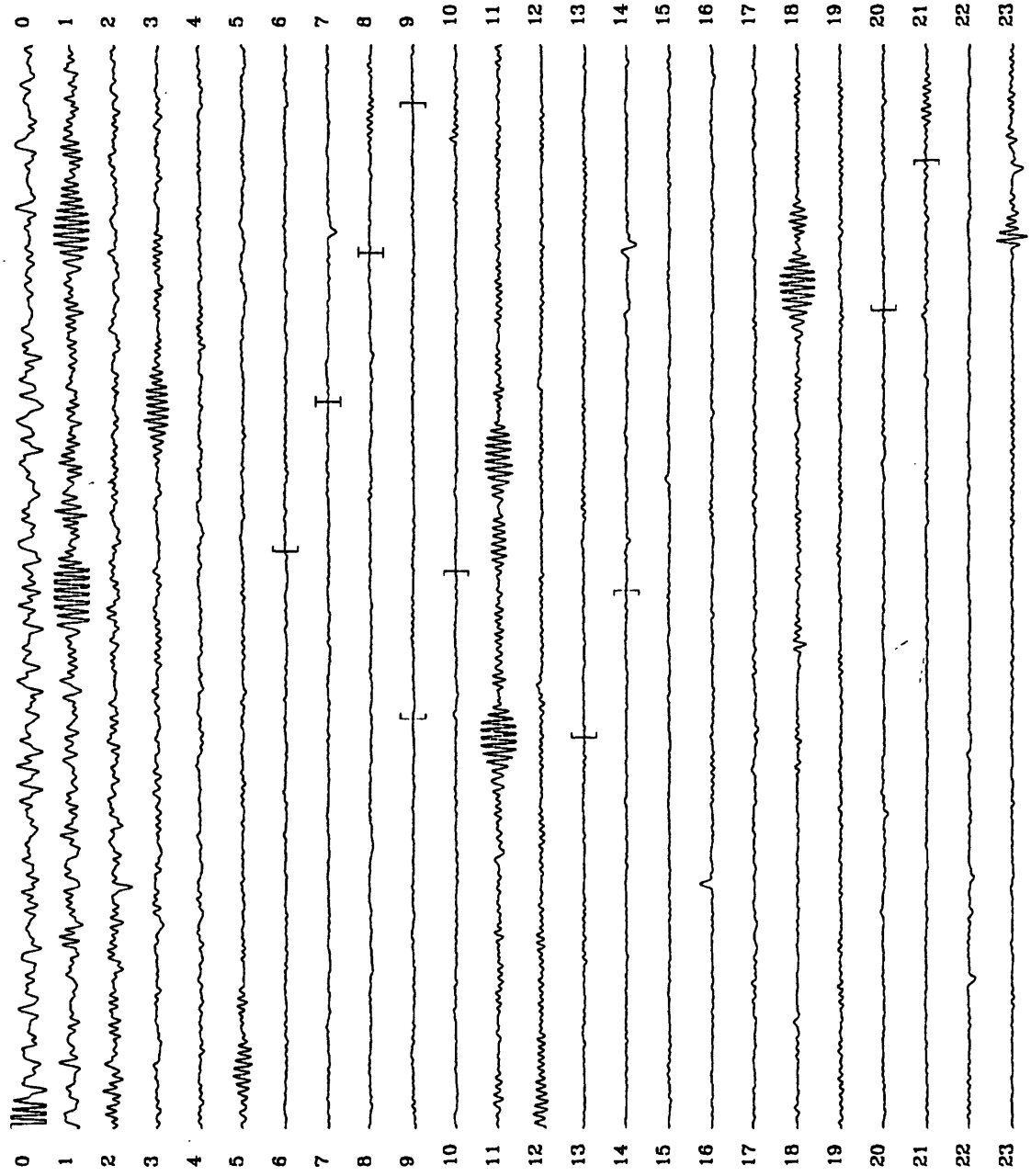

Figure 6.19 Time record for day 350 of the CMG-3S (A) horizontal when installed in a vented HGLP tank.

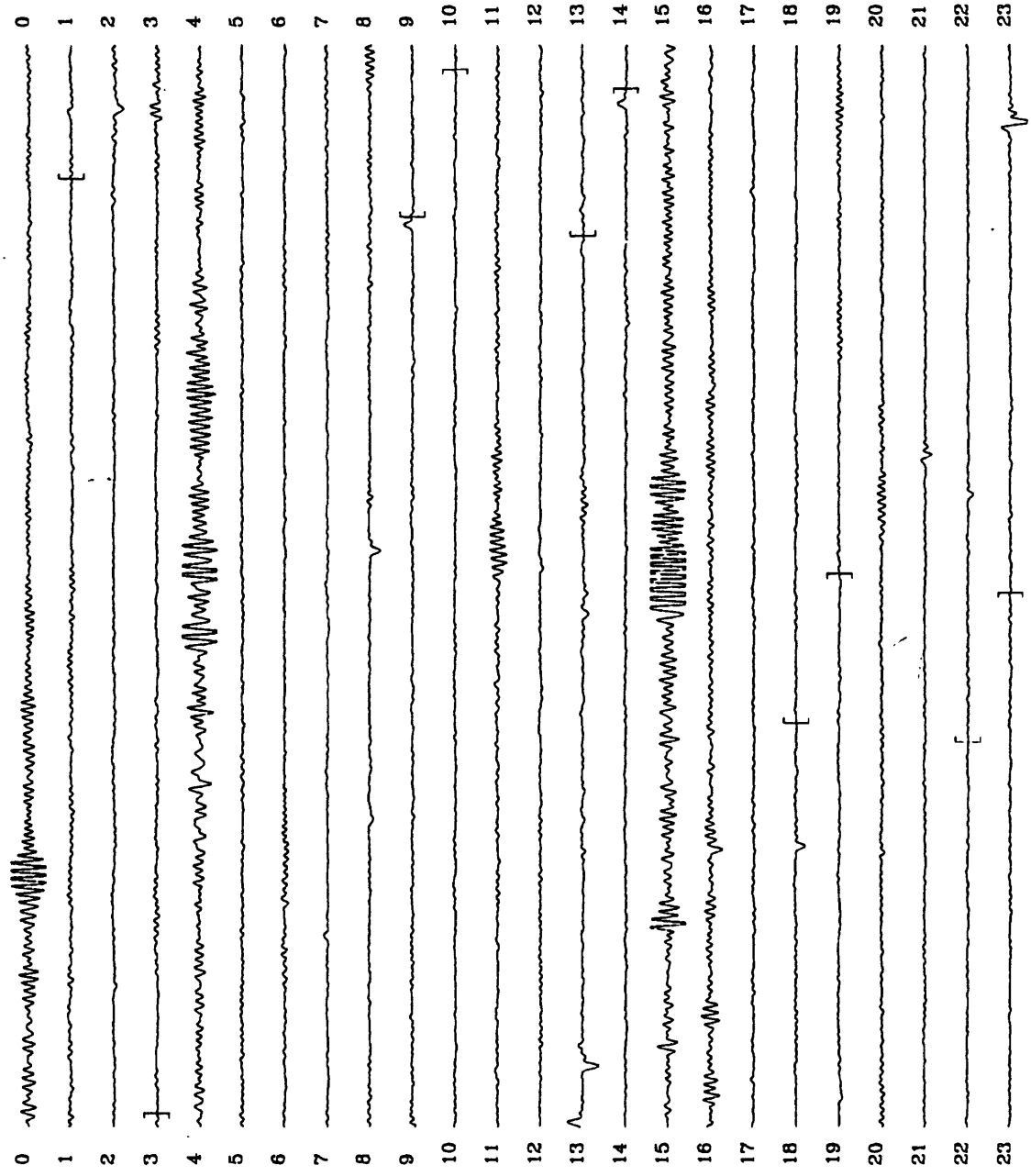

Figure 6.20 Time record for day 351 of the CMG-3S (A) horizontal when installed in a vented HGLP tank.

Figures 6.21 and 6.22 contain comparative noise estimates of the CMG-3S (B) horizontal with the STS-1 horizontal respectively during the time that the CMG-3S (B) sensor was operated in the vented tank. The CMG-3S (B) horizontal selected the segments which were included in the analysis. The segments actually selected are enclosed in square brackets in Figures 6.23 and 6.24.

A visual time domain comparison of the CMG-3S (B) horizontal operation in a vented tank contained in Figures 6.23 and 6.24 with the CMG-3S (B) horizontal operation in a sealed tank contained in Figures 6.9 through 6.12 indicates that there is no detectable difference in the time records. Both the frequency and amplitude of the burping seems to be about the same under the two conditions.

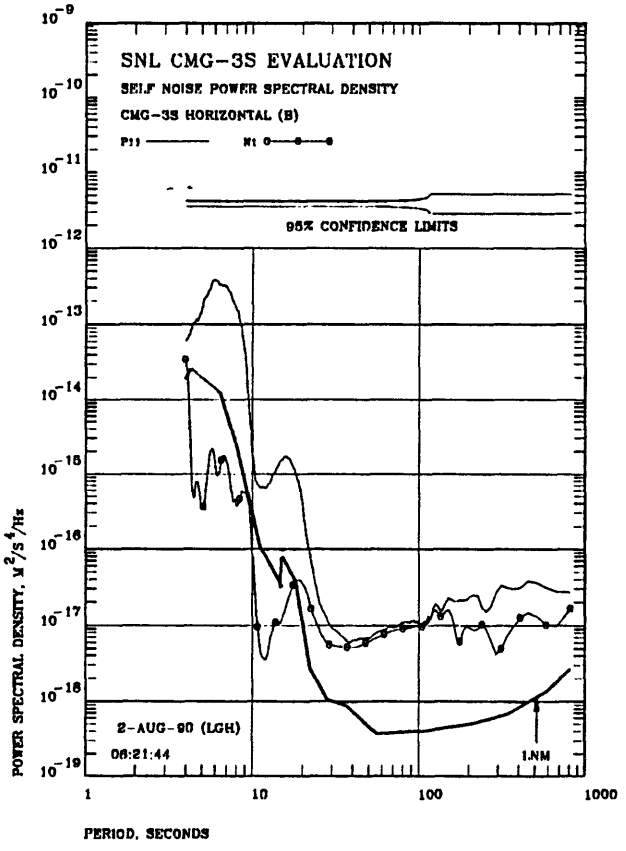

Figure 6.21 Estimated total PSD and self noise PSD of the CMG-3S (B) horizontal when installed in a vented HGLP tank. The CMG-3S (B) horizontal selected the segments.

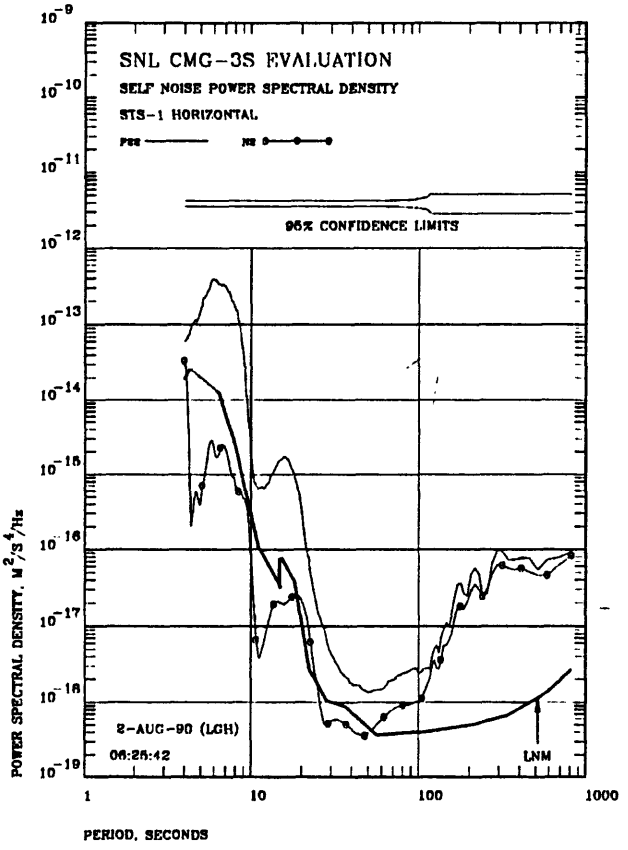

Figure 6.22 Estimated total PSD and self noise PSD of the STS-1 horizontal. The CMG-3S (B) horizontal selected the segments.

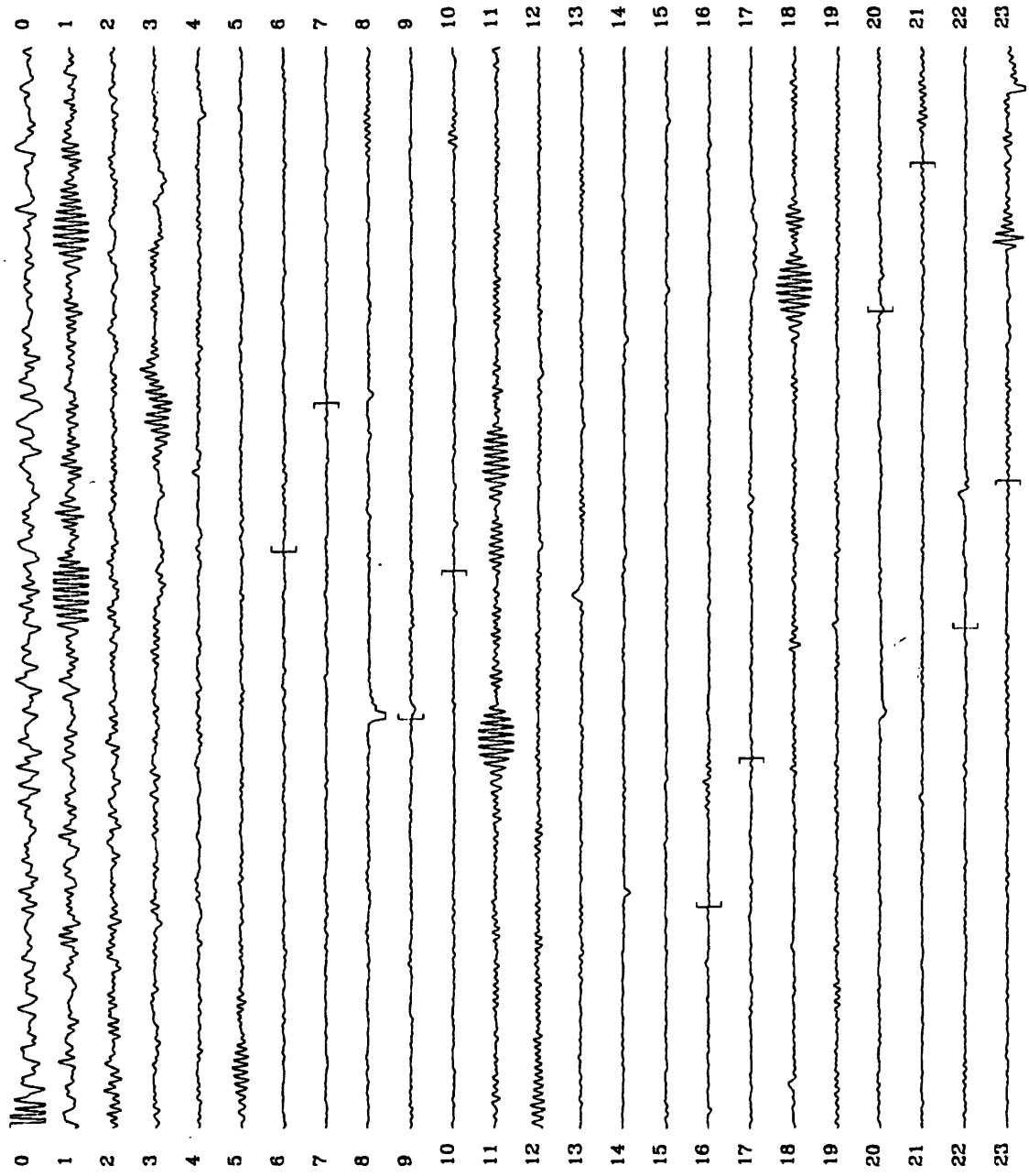

Figure 6.23 Time record for day 350 of the CMG-3S (B) horizontal when installed in a vented HGLP tank.

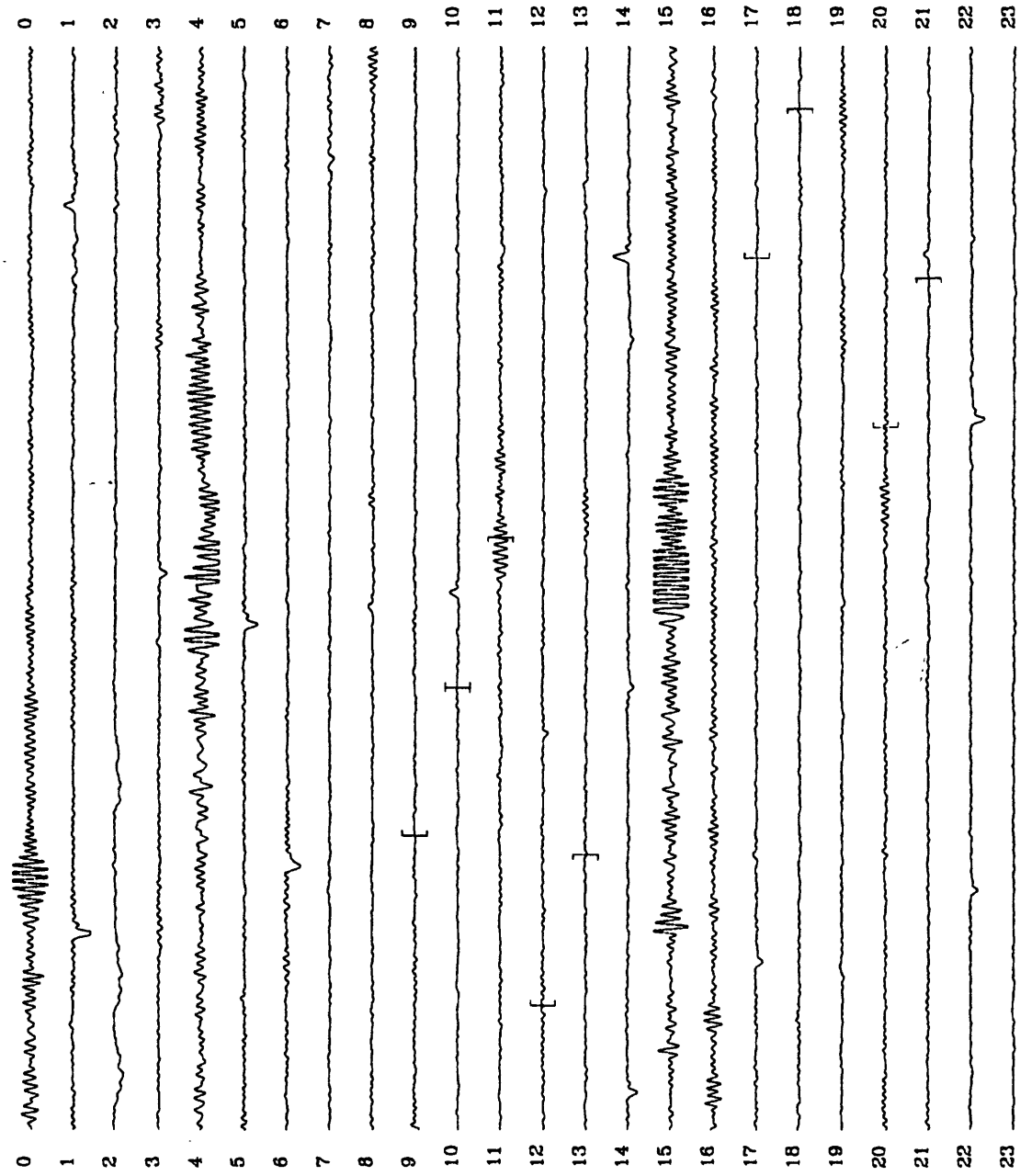

Figure 6.24 Time record for day 351 of the CMG-3S (B) horizontal when installed in a vented HGLP tank.

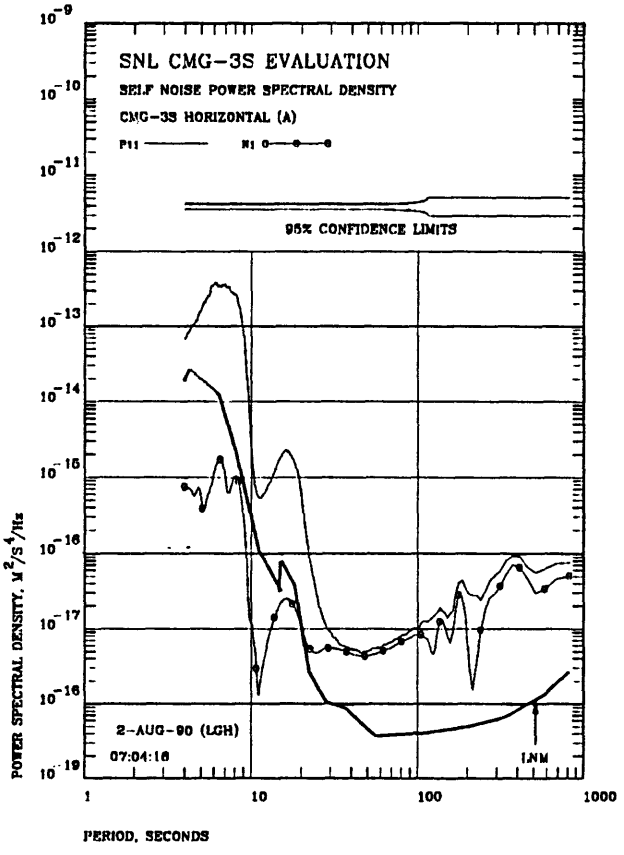

Figure 6.25 Estimated total PSD and self noise PSD of the CMG-3S (A) horizontal when installed in a vented HGLP tank. The CMG-3S (A) horizontal selected the segments.

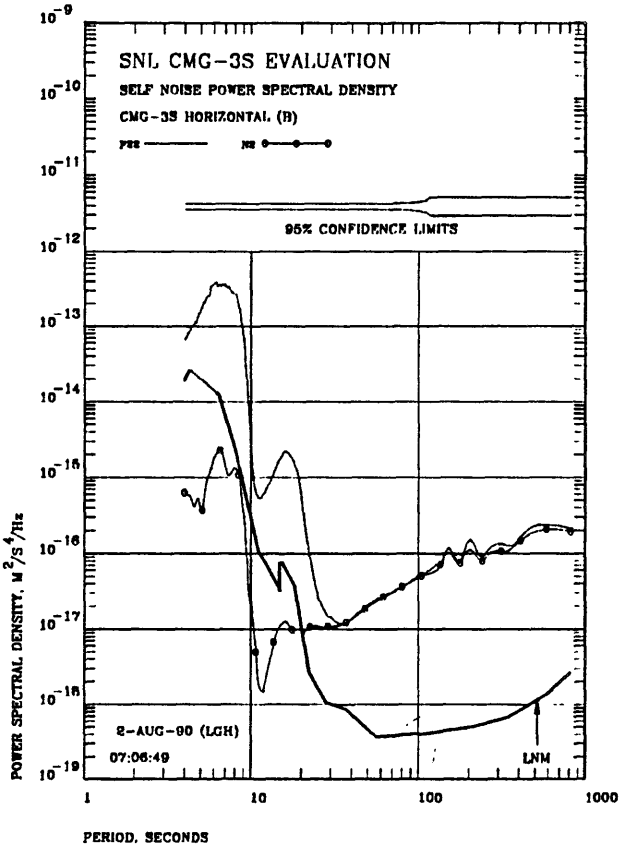

Figure 6.26 Estimated total PSD and self noise PSD of the CMG-3S (B) horizontal when installed in a vented HGLP tank. The CMG-3S (A) horizontal selected the segments.

A comparison of the estimated instrument noise levels (N_1) for vented tank operation in Figure 6.21 with the estimated instrument noise levels (N_1) for sealed tank operation in Figure 6.7 indicates that there was no detectable change in the performance of CMG-3S (B) in a vented versus a sealed tank either. The calculated noise levels are approximately the same across the band under both sealed and vented test conditions.

Figures 6.25 and 6.26 contain instrument noise estimates obtained from a direct model analysis of the two CMG-3S horizontal sensors when compared with one another while operating in a vented HGLP tank. The (A) sensor horizontal selected the segments included in the analysis; therefore, the segments included in the data are depicted in Figures 6.19 and 6.20. Notice that, above about 30 seconds, the noise estimates for the CMG-3S (A) horizontal obtained from a direct model analysis of the data from the two CMG-3S horizontals operating in a vented tank in Figure 6.25 are approximately equal to the noise estimates for the CMG-3S (A) horizontal obtained from a direct model analysis of the data from the CMG-3S (A) and STS-1 horizontals under the same conditions as shown in Figure 6.17.

Similarly, Figures 6.27 and 6.28 also contain instrument noise estimates obtained from a direct model analysis of the two CMG-3S horizontal sensors when they were compared with one another while operating in a vented HGLP tank. However, in this case, sensor (B) selected the segments; the segments included in the data are shown in Figures 6.23 and 6.24. Above about 30 seconds, the noise estimates for the CMG-3S (B) horizontal yielded by comparing the two CMG-3S horizontals in the vented tank shown in Figure 6.27 are again approximately equal to the noise estimates for the CMG-3S (B) horizontal obtained by comparing it with the STS-1 horizontal as shown in Figure 6.21.

The four sets of data presented in Figures 6.17, 6.18, 6.21, 6.22, 6.25, 6.26, 6.27, and 6.28 illustrate the power and versatility of the direct model for analyzing data from a side-by-side evaluation of two sensors. This method yields accurate and consistent estimates of sensor system noise regardless of whether the two sensors are approximately equally noisy or not.

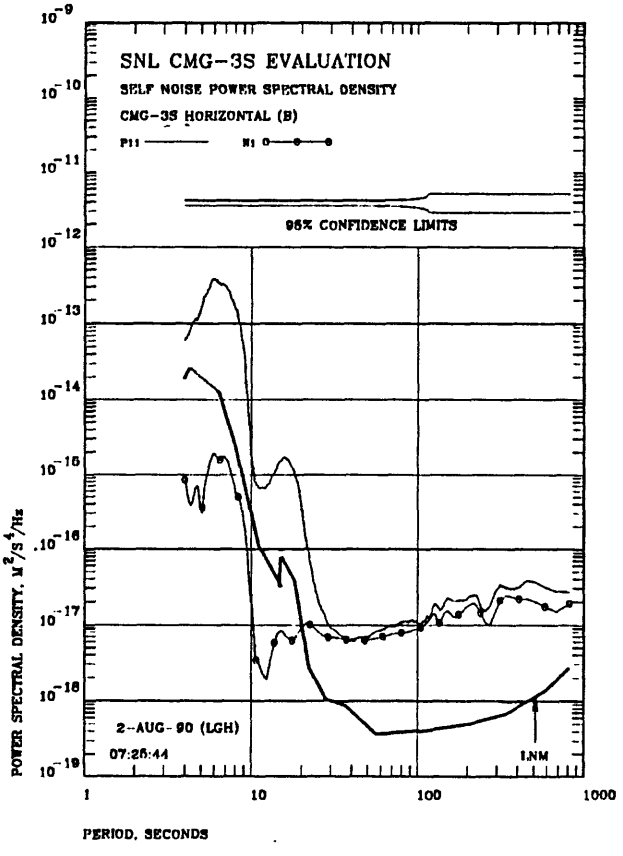

Figure 6.27 Estimated total PSD and self noise PSD of the CMG-3S (B) horizontal when installed in a vented HGLP tank. The CMG-3S (B) horizontal selected the segments.

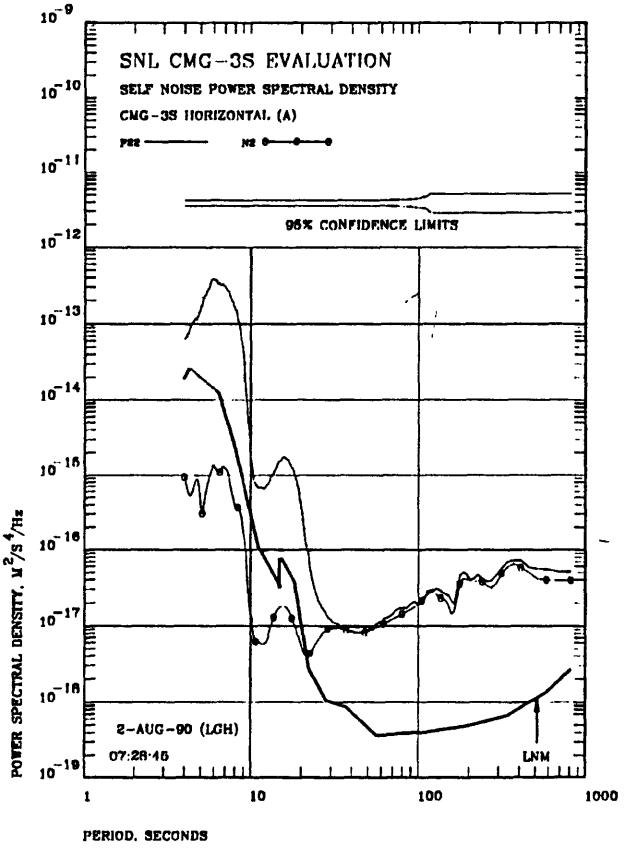

Figure 6.28 Estimated total PSD and self noise PSD of the CMG-3S (A) horizontal when installed in a vented HGLP tank. The CMG-3S (B) horizontal selected the segments.

7 POTTED IN PLASTER OF PARIS

This section presents the results of long period measurements of the two CMG-3S sensors while they were potted in the same plaster of paris block as was described in Section 5.2 on high frequency measurements. The main object of potting the sensors in plaster of paris was to improve the coupling of the sensors to the floor at high frequencies. However, it is also important to characterize their performance at long periods when enclosed in the potting material.

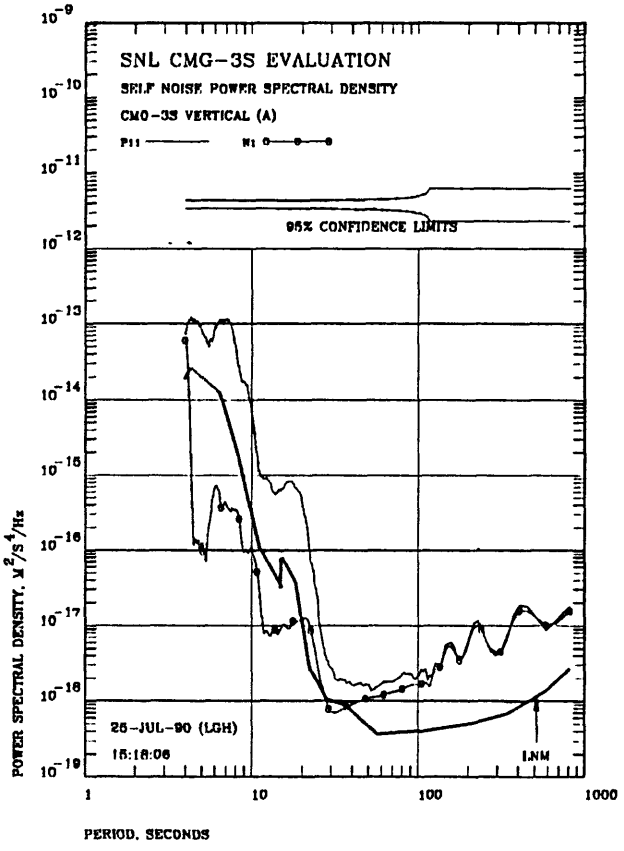

Figure 7.1 Estimated total PSD and self noise PSD of the CMG-3S (A) vertical when potted in plaster of paris. The CMG-3S (A) vertical selected the segments.

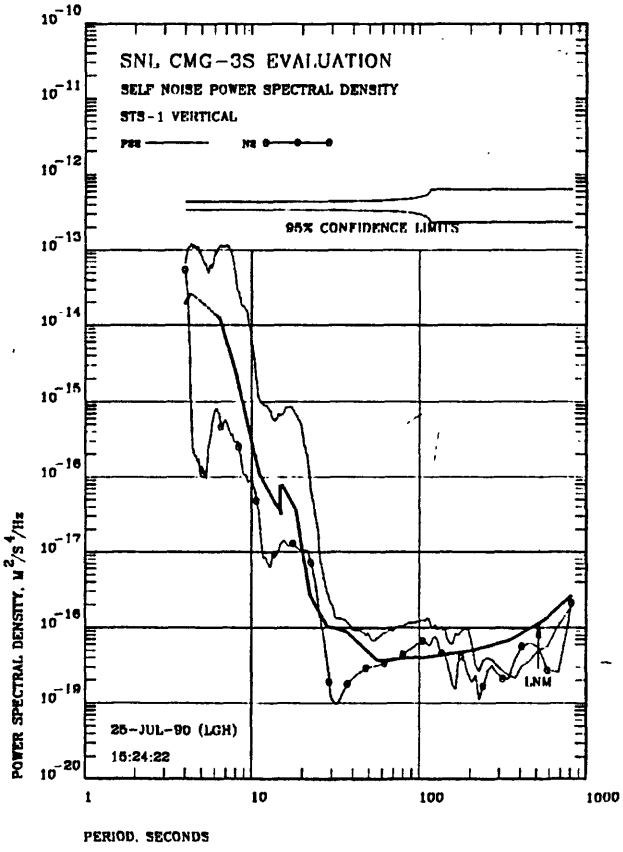

Figure 7.2 Estimated total PSD and self noise PSD of the STS-1 vertical. The CMG-3S (A) vertical selected the segments.

Space restrictions in the cross tunnel dictated that the potting experiment be located in the main ASL vault. This meant that the potted CMG-3S sensors were located approximately 10 meters from the reference STS-1 sensors located in the cross tunnel; this distance is not believed to be excessive in the period band over which the evaluation was conducted. The existing surface of the concrete floor in the ASL vault has a shiny smooth finish. Therefore, the area in which the CMG-3S sensors were to be installed was roughed up with a hammer and chisel to

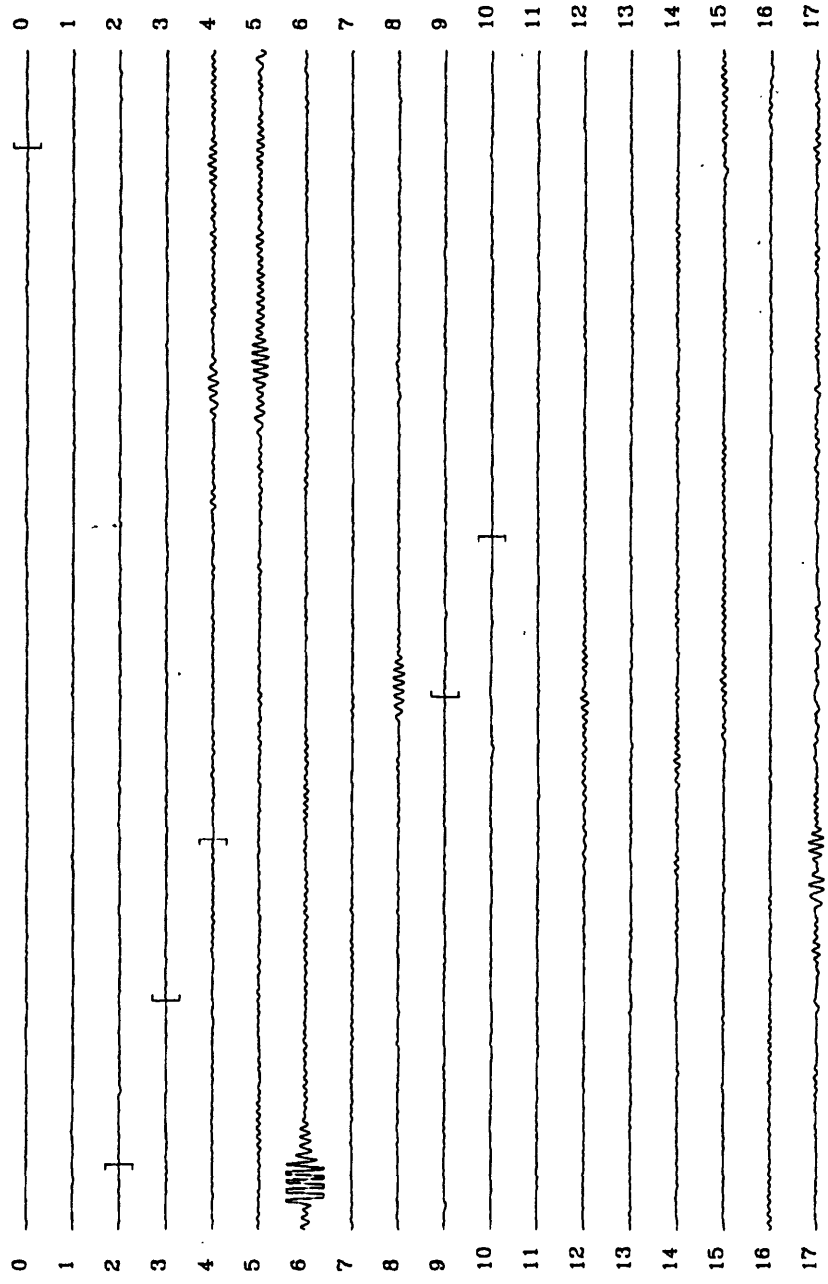

Figure 7.3 Time record for day 293 for the CMG-3S (A) vertical while it was potted showing the time segments selected by the automatic segment selection algorithm for inclusion in the direct model analysis of system noise.

create a rough surface for the potting medium to bond to. Plaster of paris was chosen as the potting material because it is readily available, easy to work with, and it would be fairly easy to remove after the experiment was completed. The two sensors were potted in a 50 cm by 50 cm by 25 cm high block of plaster of paris poured directly on the newly roughed floor of the vault. The top inch or two of the sensor projected above the plaster of paris block and the two sensors were positioned about 1 inch apart. The were visually positioned parallel to one another prior to pouring the plaster of paris in the potting form.

The whole installation was then covered with a polystyrene box to reduce the effects of air motion and resulting tilt on the horizontal sensors.

Figures 7.1 and 7.2 contain noise estimates as calculated with the direct model of a side-by-side test of the CMG-3S (A) vertical and the STS-1 vertical respectively. As noted in the figure captions, the CMG-3S (A) vertical data was used as the basis for selecting the quiet time segments to be included in the data presented in both figures. The segments actually selected by

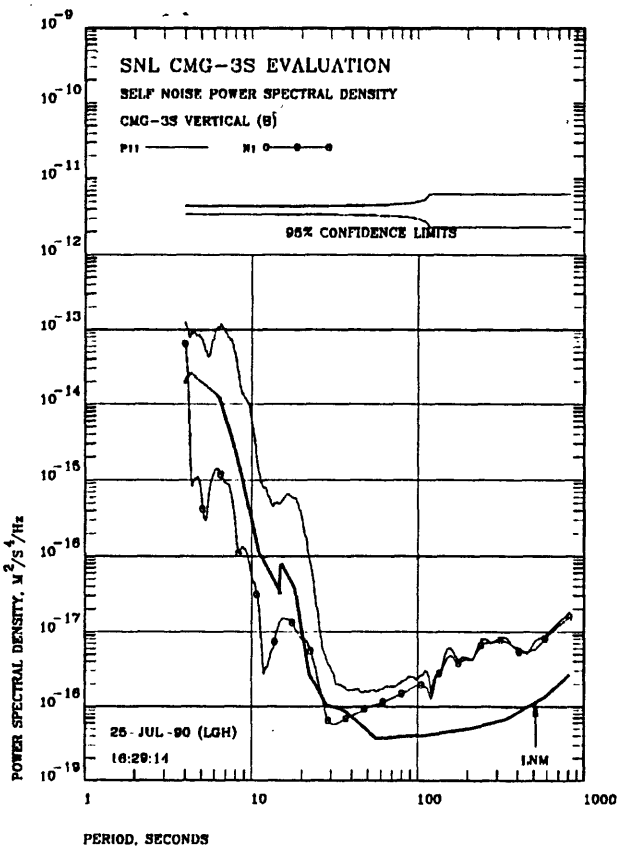

Figure 7.4 Estimated total PSD and self noise PSD of the CMG-3S (B) vertical when potted in plaster of paris. The CMG-3S (B) vertical selected the segments.

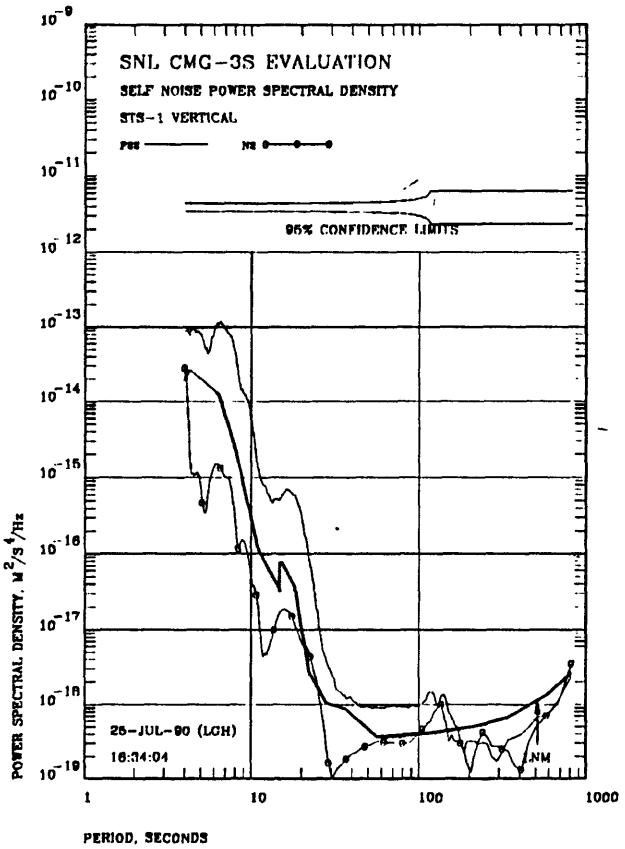

Figure 7.5 Estimated total PSD and self noise PSD of the STS-1 vertical. The CMG-3S (B) vertical selected the segments.

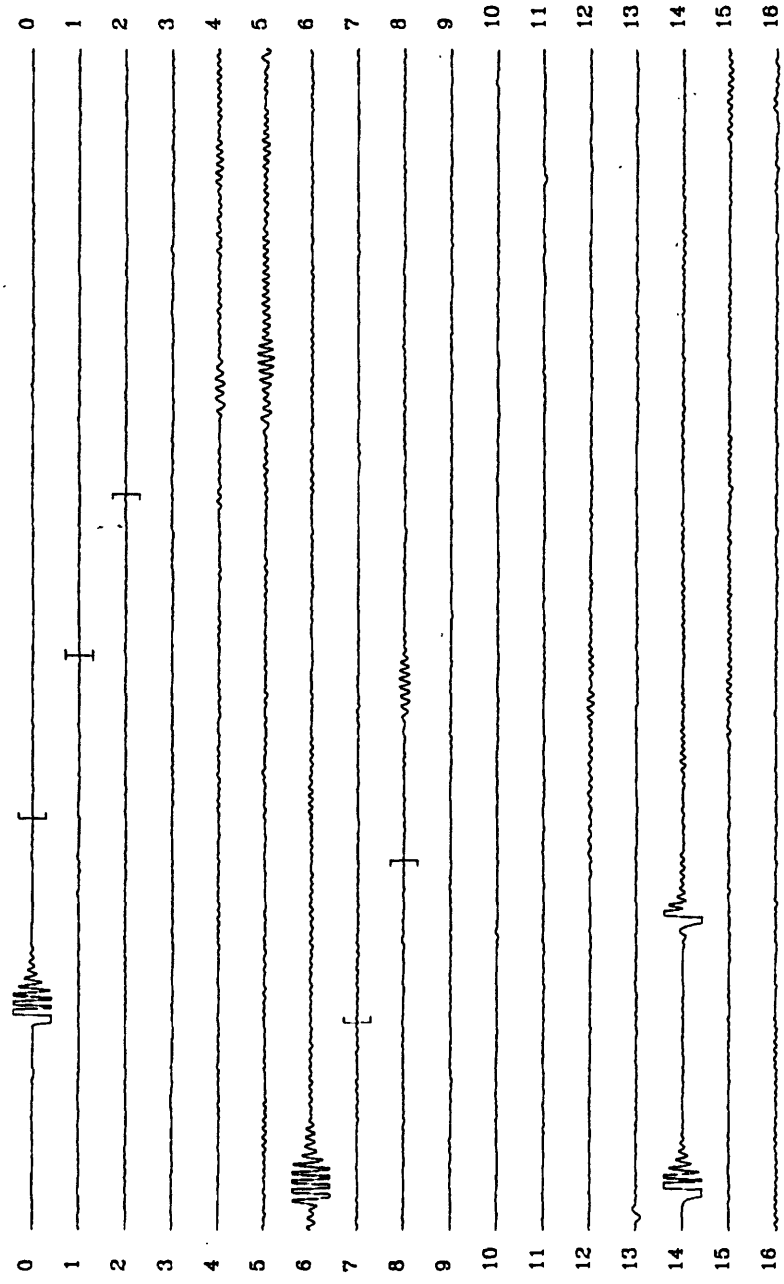

Figure 7.6 Time record for day 293 for the CMG-3S (B) vertical while it was potted showing the time segments selected by the automatic segment selection algorithm for inclusion in the direct model analysis of system noise.

the automatic segment selection algorithm are depicted in Figure 7.3, which contains a time domain plot of all of the data actually collected for the CMG-3S (A) vertical. Each segment is approximately one hour and eight minutes long; the selected segments are enclosed by square brackets in Figure 7.3.

Note that the two total PSD estimates (P_{11} and P_{22}) in Figures 7.1 and 7.2 virtually overlay one another out to around 25 seconds. Above 25 seconds, the total PSD estimate for the CMG-3S vertical becomes progressively larger than that for the STS-1 vertical at longer periods. Note also that the estimated noise levels (N_1 and N_2) for both of the instruments are quite similar from 4 to approximately 25 seconds.

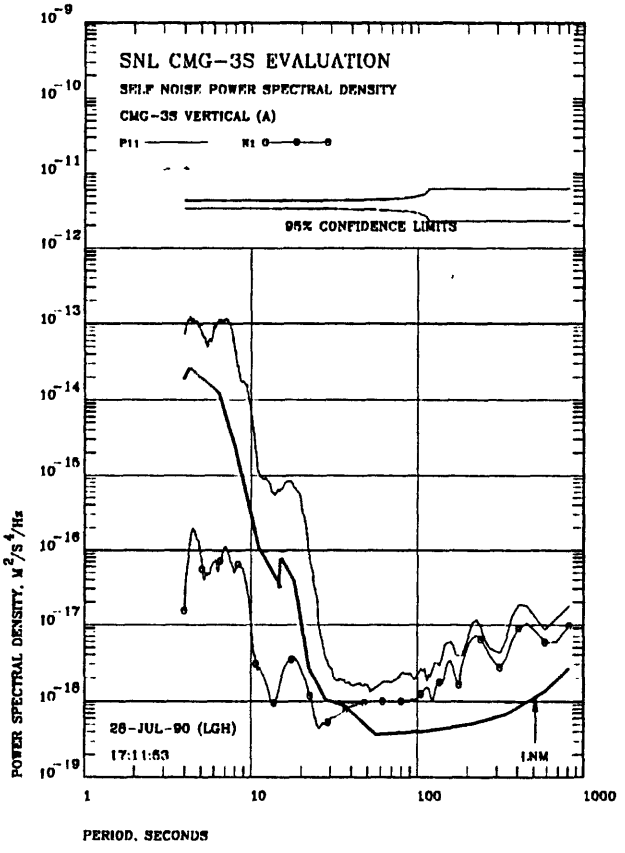

Figure 7.7 Estimated total PSD and self noise PSD of the CMG-3S (A) vertical when potted in plaster of paris. The CMG-3S (A) vertical selected the segments.

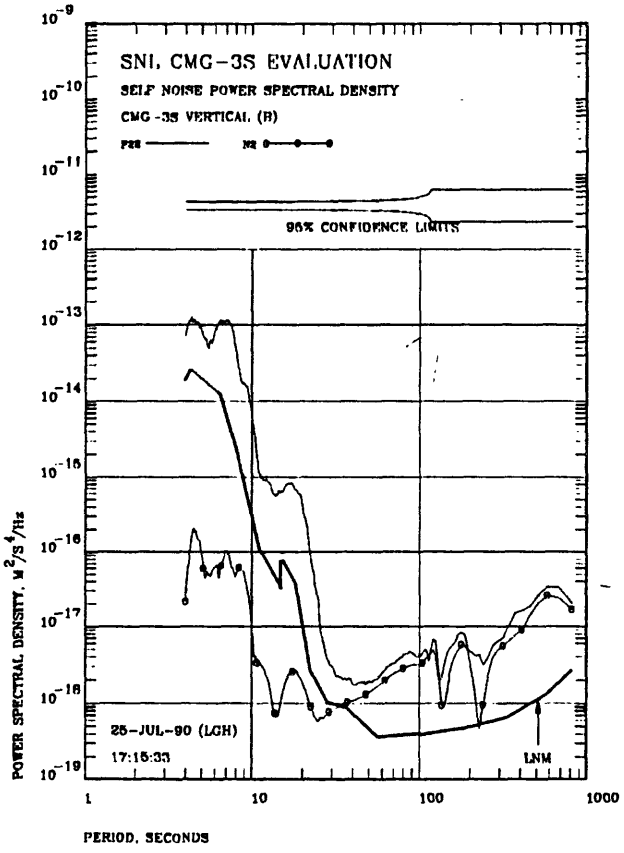

Figure 7.8 Estimated total PSD and self noise PSD of the CMG-3S (B) vertical when potted in plaster of paris. The CMG-3S (A) vertical selected the segments.

The estimated noise PSD in this part of the band is probably not representative of the true noise level in either instrument. Instead, it is probably due to alignment error between the two vertical components. An earlier analysis (see Holcomb, 1990) demonstrated that errors in alignment in side-by-side tests results in apparent system noise, which is shaped more or less like the seismic background, and which lies at a fixed distance below the seismic background across the band. The PSD noise estimates in both Figures 7.1 and 7.2 from 4 to 25 seconds approximate these characteristics quite well. Both noise estimates (N_1 and N_2) lie a factor of 1000 to 100 below the total power estimate (P_{11} and P_{22}) (the total power estimate should be very close to the seismic background in this part of the spectrum because sensor noise is typically far below background signals in this band) and their shape approximates the total power estimate. Ratios of 1000 to 100 translate into possible misalignments of from 2° to 10° (see Figures 6.20 and 6.21 of Holcomb, 1990). The true instrument noise in the band extending from 4 to 25 seconds for both sensors probably lies somewhat below the levels shown in the two figures; it is probably well below the indicated levels at shorter periods.

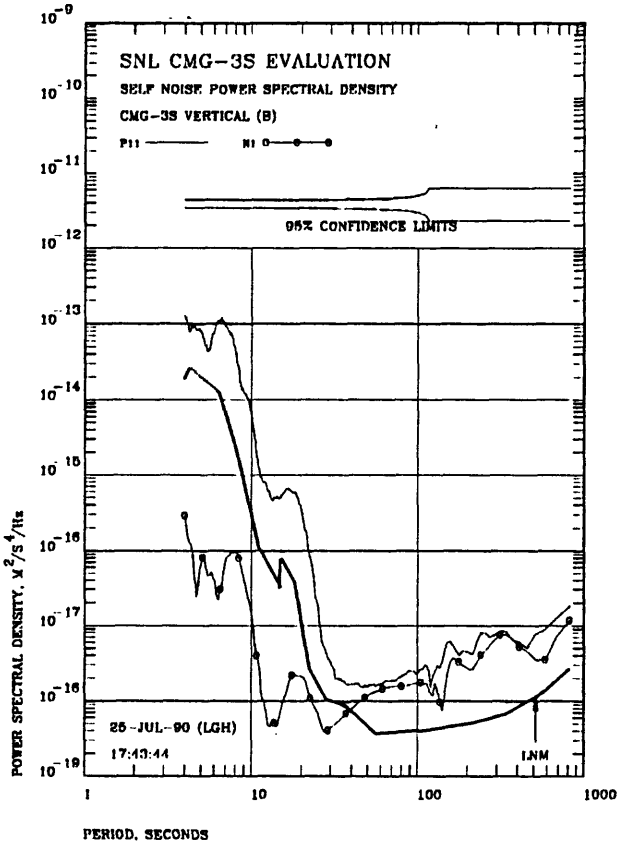

Figure 7.9 Estimated total PSD and self noise PSD of the CMG-3S (B) vertical when potted in plaster of paris. The CMG-3S (B) vertical selected the segments.

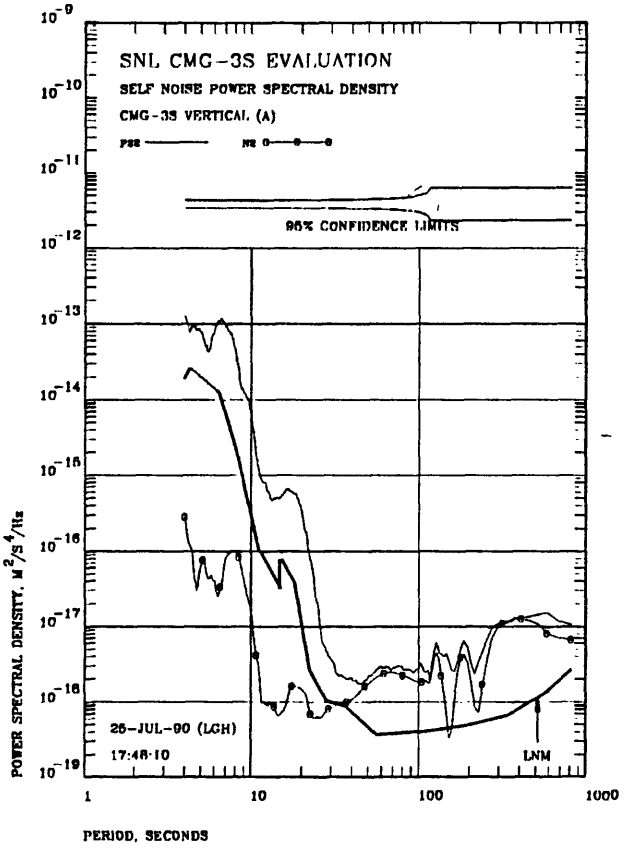

Figure 7.10 Estimated total PSD and self noise PSD of the CMG-3S (A) vertical when potted in plaster of paris. The CMG-3S (B) vertical selected the segments.

Above 25 seconds the estimated noise level for the CMG-3S vertical is progressively larger than that for the STS-1 vertical. In addition, both noise estimates lie less than a factor of 100 below their respective total power estimates. Since a given misalignment error creates a fixed separation between the seismic background and the alignment generated noise, and since the estimated noise levels above 25 seconds are unique, these estimates are probably representative of true instrument noise in this part of the spectrum.

Figures 7.4 and 7.5 contain direct model noise estimates for the side-by-side evaluation of the CMG-3S (B) vertical and the STS-1 vertical. In these two figures, the quiet segments from the CMG-3S (B) vertical data were used to select the data to be included in the two figures. The time domain segments selected by the segment selection algorithm are shown in Figure 7.6. The STS-1 vertical used in this evaluation is the same vertical used in the CMG-3S (A) evaluation above.

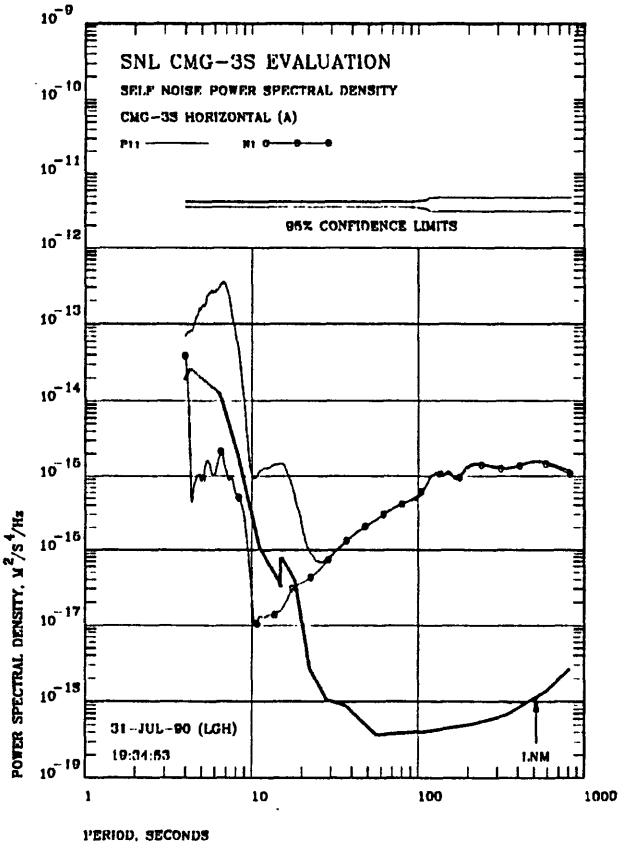

Figure 7.11 Estimated total PSD and self noise PSD of the CMG-3S (A) horizontal when potted in plaster of paris. The CMG-3S (A) horizontal selected the segments.

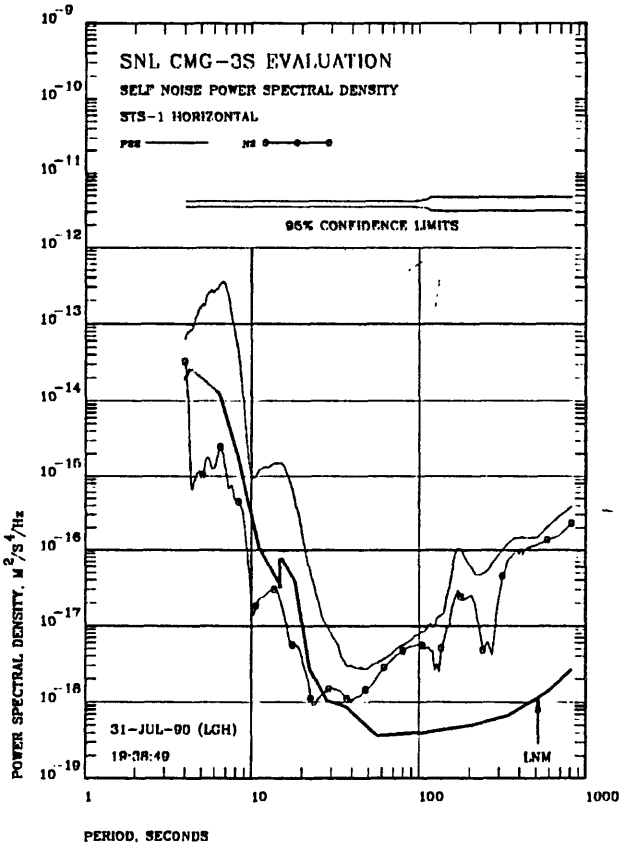

Figure 7.12 Estimated total PSD and self noise PSD of the STS-1 horizontal. The CMG-3S (A) horizontal selected the segments.

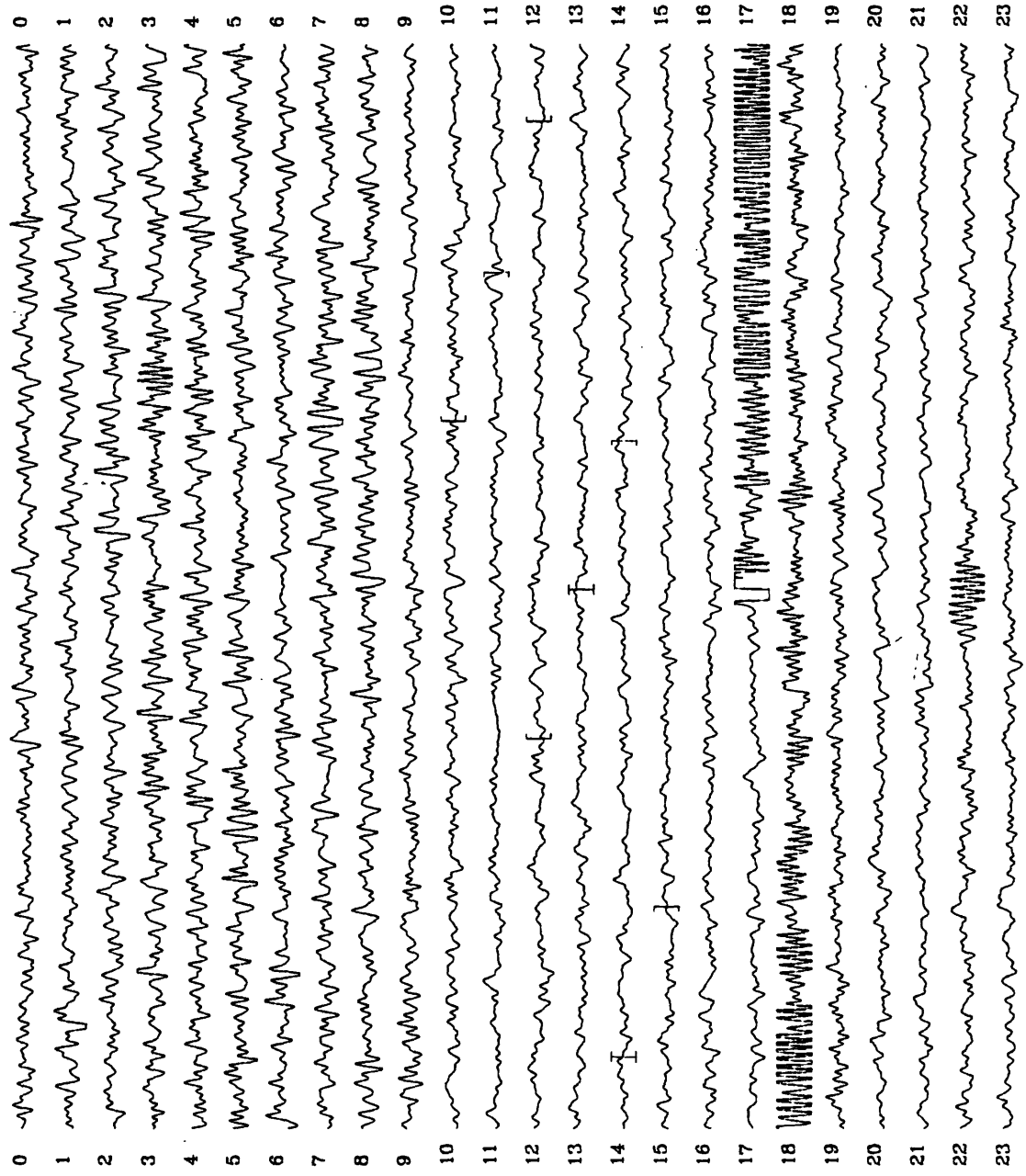

Figure 7.13 Time record for day 299 of the CMG-3S (A) horizontal showing the time segments selected by the automatic segment selection algorithm for inclusion in the direct model analysis of system noise.

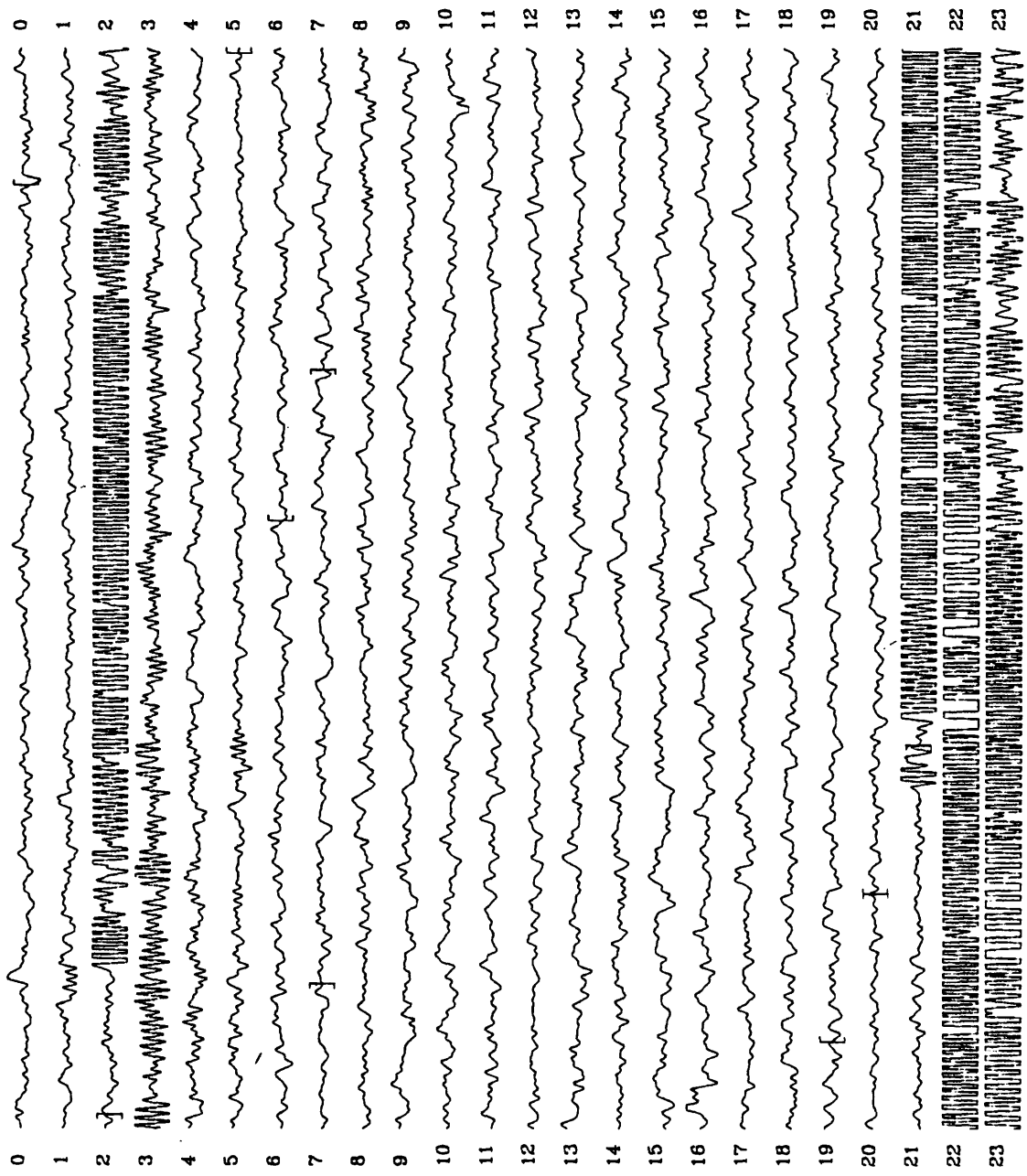

Figure 7.14 Time record for day 300 of the CMG-3S (A) horizontal showing the time segments selected by the automatic segment selection algorithm for inclusion in the direct model analysis of system noise.

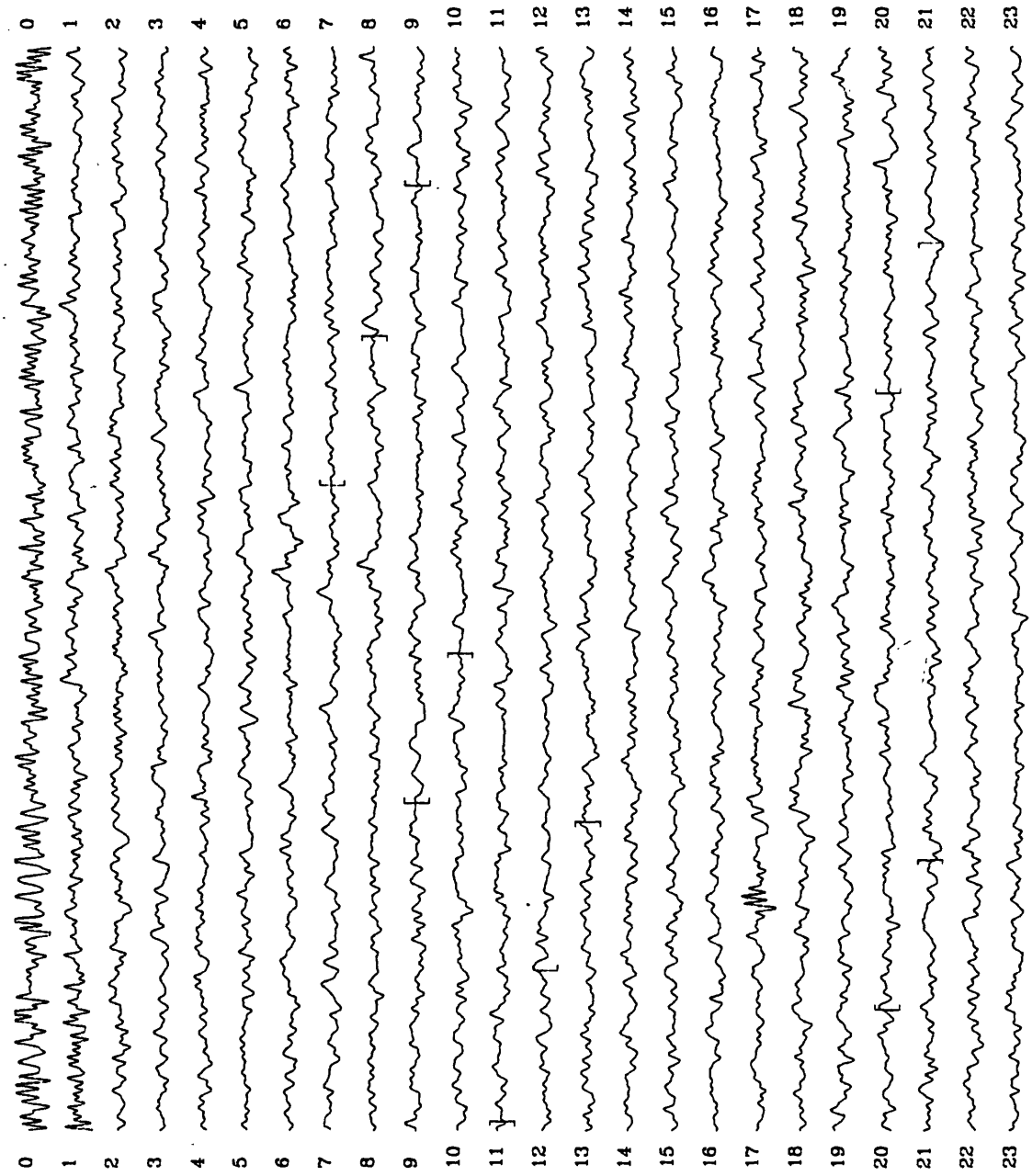

Figure 7.15 Time record for day 301 of the CMG-3S (A) horizontal showing the time segments selected by the automatic segment selection algorithm for inclusion in the direct model analysis of system noise.

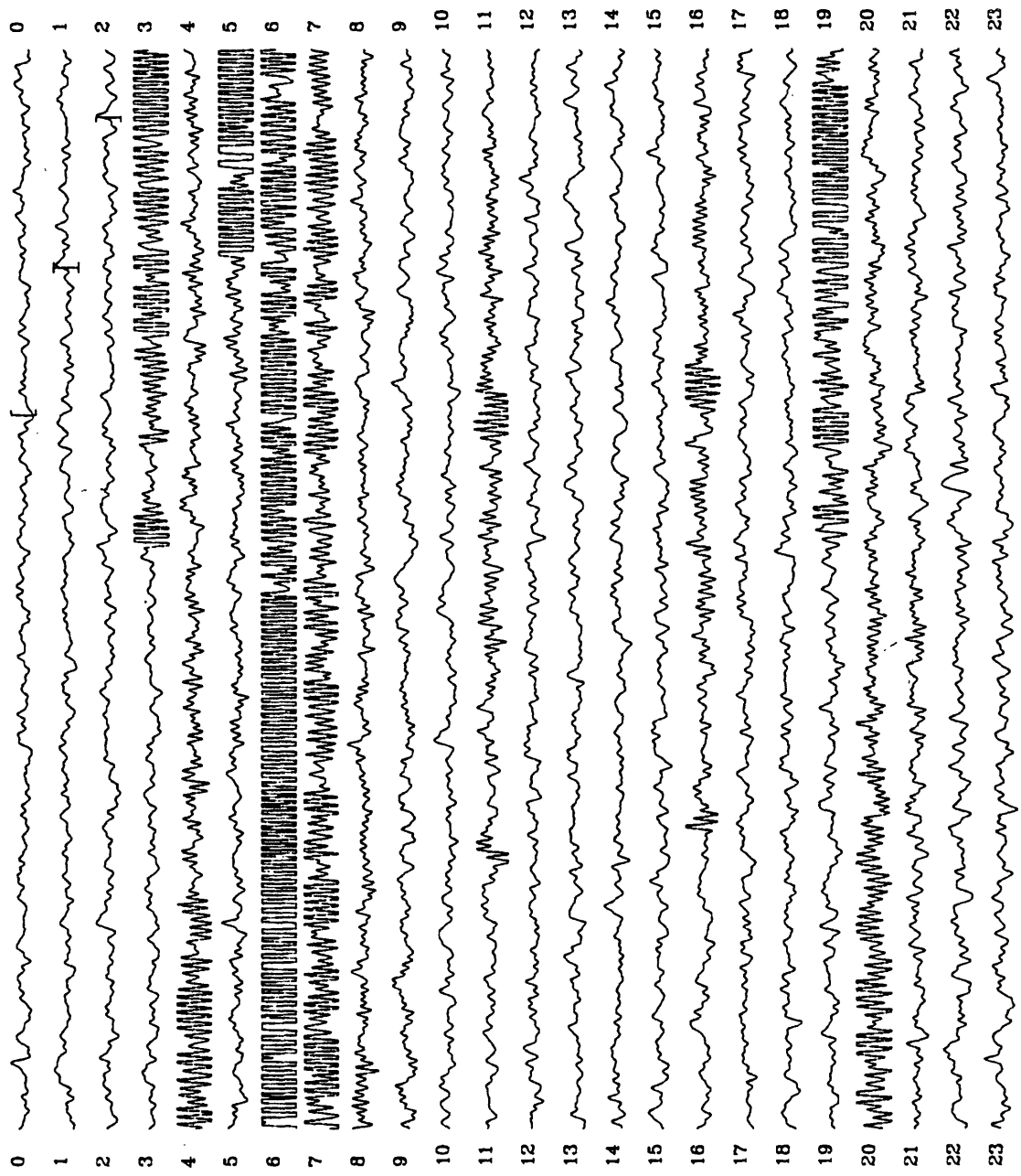

Figure 7.16 Time record for day 302 of the CMG-3S (A) horizontal showing the time segments selected by the automatic segment selection algorithm for inclusion in the direct model analysis of system noise.

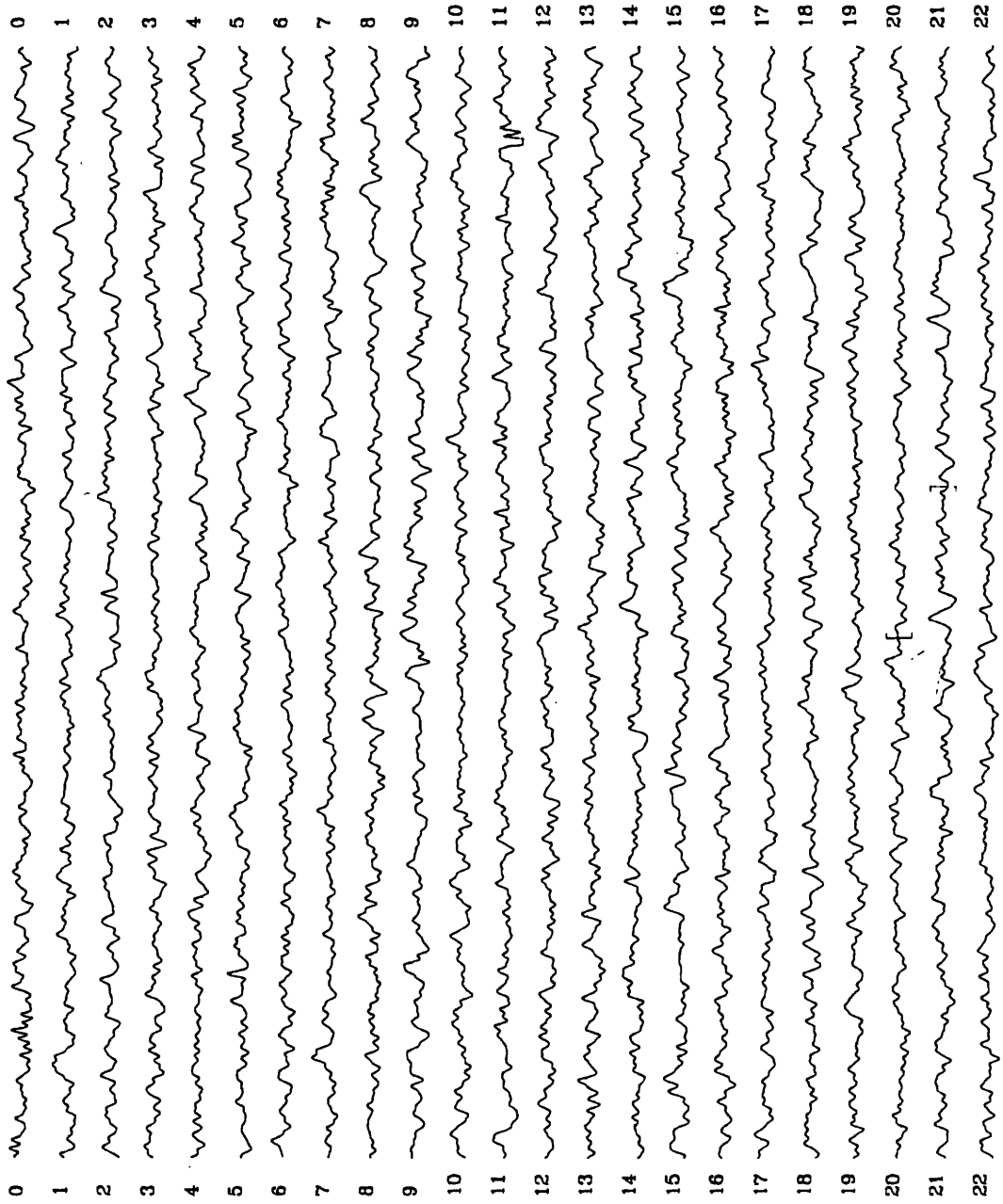

Figure 7.17 Time record for day 303 of the CMG-3S (A) horizontal showing the time segments selected by the automatic segment selection algorithm for inclusion in the direct model analysis of system noise.

As Figures 7.4 and 7.5 demonstrate, the general character of the noise estimates for the CMG-3S (B) vertical are approximately the same as those obtained for the (A) vertical above. Here again, the noise estimates for the CMG-3S (B) vertical and the STS-1 vertical are nearly the same from 4 to approximately 25 seconds thereby indicating that the calculated noise estimates in this band are due to instrument misalignment. The general level of the noise estimates in the band extending from 4 to 25 seconds for CMG-3S (B) and the STS-1 in Figures 7.3 and 7.4 are approximately the same as those in the same band for CMG-3S (A) and the STS-1 in Figures 7.1 and 7.2; therefore, the degree of misalignment must be approximately the same for the two evaluations. Above 25 seconds, the noise estimates for the two instruments are unique and comparable to those obtained above. From 25 to 100 seconds, the noise estimates for sensors A and B are virtually identical; above 100 seconds sensor B may be slightly quieter.

Figures 7.7, 7.8, 7.9, and 7.10 contain noise estimates obtained from a direct model analysis of the data from CMG-3S (A) and the CMG-3S (B) verticals. Figures 7.7 and 7.8 contain the results of using the CMG-3S (A) vertical as the basis for selecting the quiet segments whereas Figures 7.9 and 7.10 contain the results of using the CMG-3S (B) vertical to select the quiet segments. The actual segments selected are the same as those shown in Figures 7.3 and 7.6 above. The estimated noise levels for the CMG-3S (A) vertical when compared with the STS-1 vertical as shown in Figure 7.1 are approximately the same as those for the CMG-3S (A) vertical when compared with the CMG-3S (B) vertical as shown in Figure 7.7. Similarly, the estimated noise levels for the CMG-3S (B) vertical when compared with the STS-1 vertical as shown in Figure 7.4 are approximately the same as those for the CMG-3S (B) vertical when compared with the CMG-3S (A) vertical as shown in Figure 7.9. However, there are slight differences; the estimated noise levels are slightly lower when two CMG-3S sensors are compared to one another than when one CMG-3S sensor is compared with a STS-1.

Between 4 and 25 seconds, the noise estimates for the two CMG-3S vertical components compared with one another, as shown in Figures 7.7, 7.8, 7.9, and 7.10 are lower by roughly a factor of 10 in power than those shown in Figures 7.1 and 7.3 in which the two CMG-3S verticals are compared with the STS-1 vertical. This fact probably means that the two CMG-3S verticals were more closely aligned with one another than either of them was with the STS-1 vertical. In Figures 7.7, 7.8, 7.9, and 7.10, the 4 to 25 second estimated noise level is approximately a factor of 1000 down from the total power level. This SNR is indicative of an angular misalignment of approximately 1° to 3° (see Holcomb, 1990, Figures 6.20 and 6.21).

Above 25 seconds, the noise estimates in Figures 7.7 and 7.9 are slightly lower than the corresponding estimates for the CMG-3S verticals in Figures 7.1 and 7.4. The noise estimates for the CMG-3S (A) vertical may be nearly a factor of two lower in Figure 7.7 than in Figure 7.1 whereas there is not quite as much improvement for the CMG-3S (B) vertical.

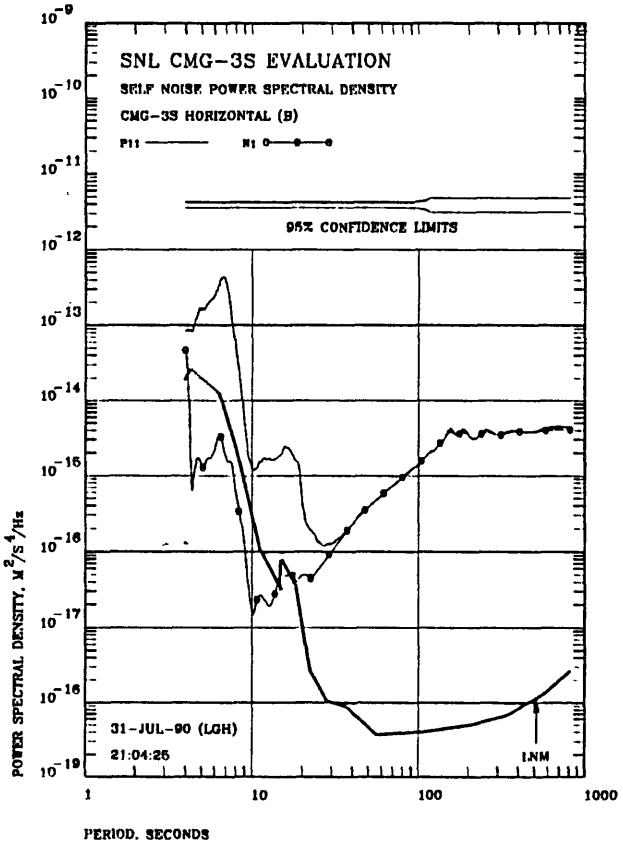

Figure 7.18 Estimated total PSD and self noise PSD of the CMG-3S (B) horizontal when potted in plaster of paris. The CMG-3S (B) horizontal selected the segments.

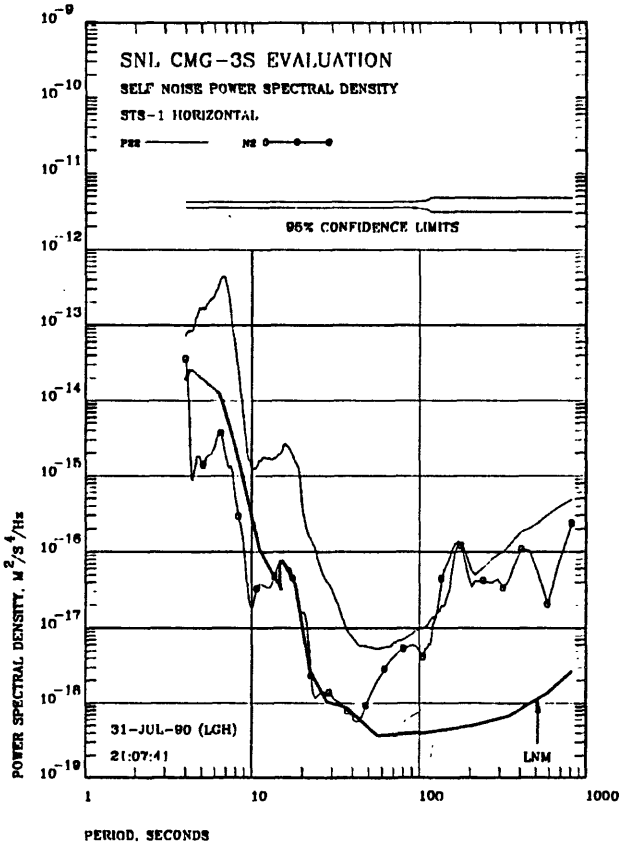

Figure 7.19 Estimated total PSD and self noise PSD of the STS-1 horizontal. The CMG-3S (B) horizontal selected the segments.

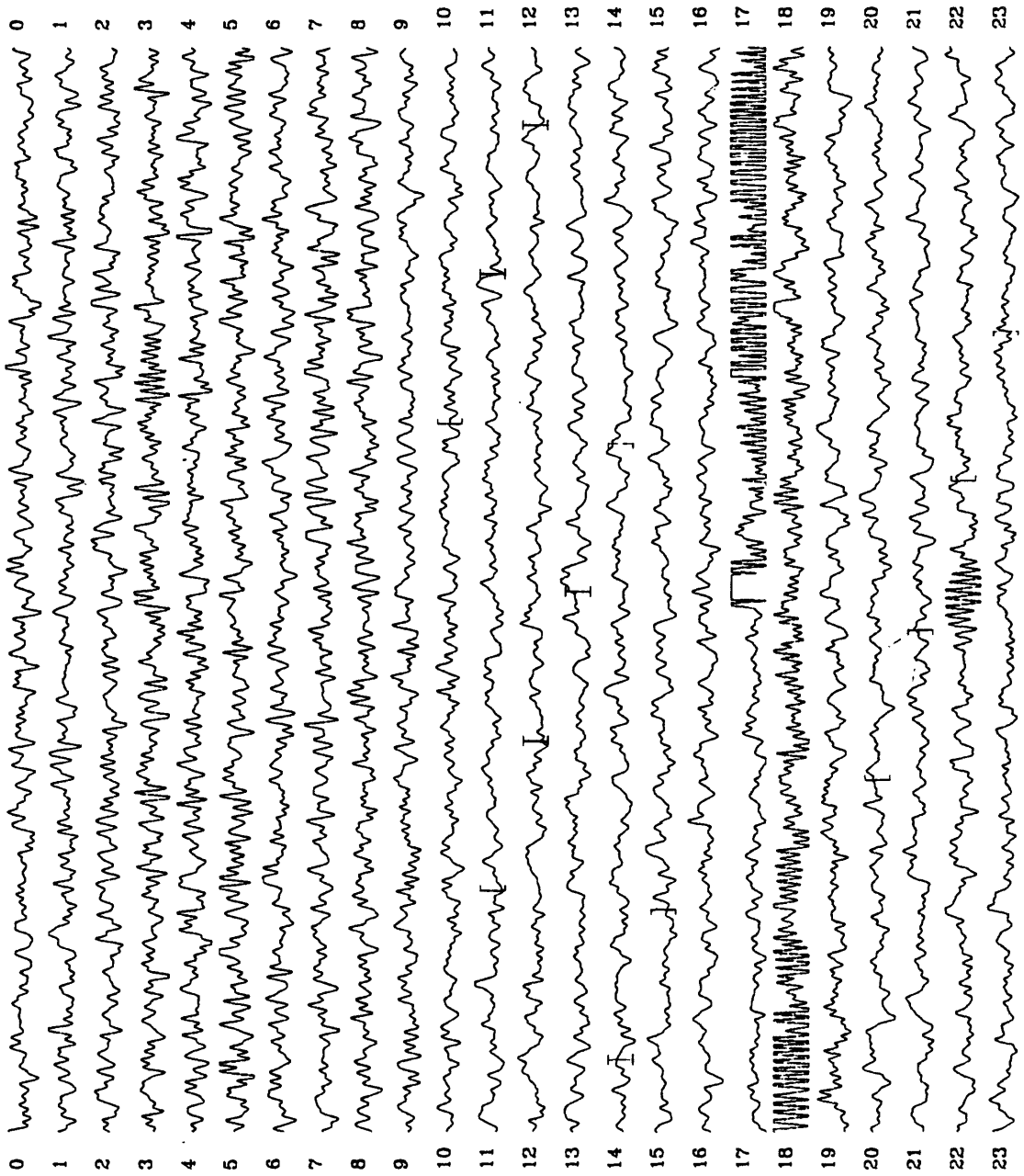

Figure 7.20 Time record for day 299 for the CMG-3S (B) horizontal showing the time segments selected by the automatic segment selection algorithm for inclusion in the direct model analysis of system noise.

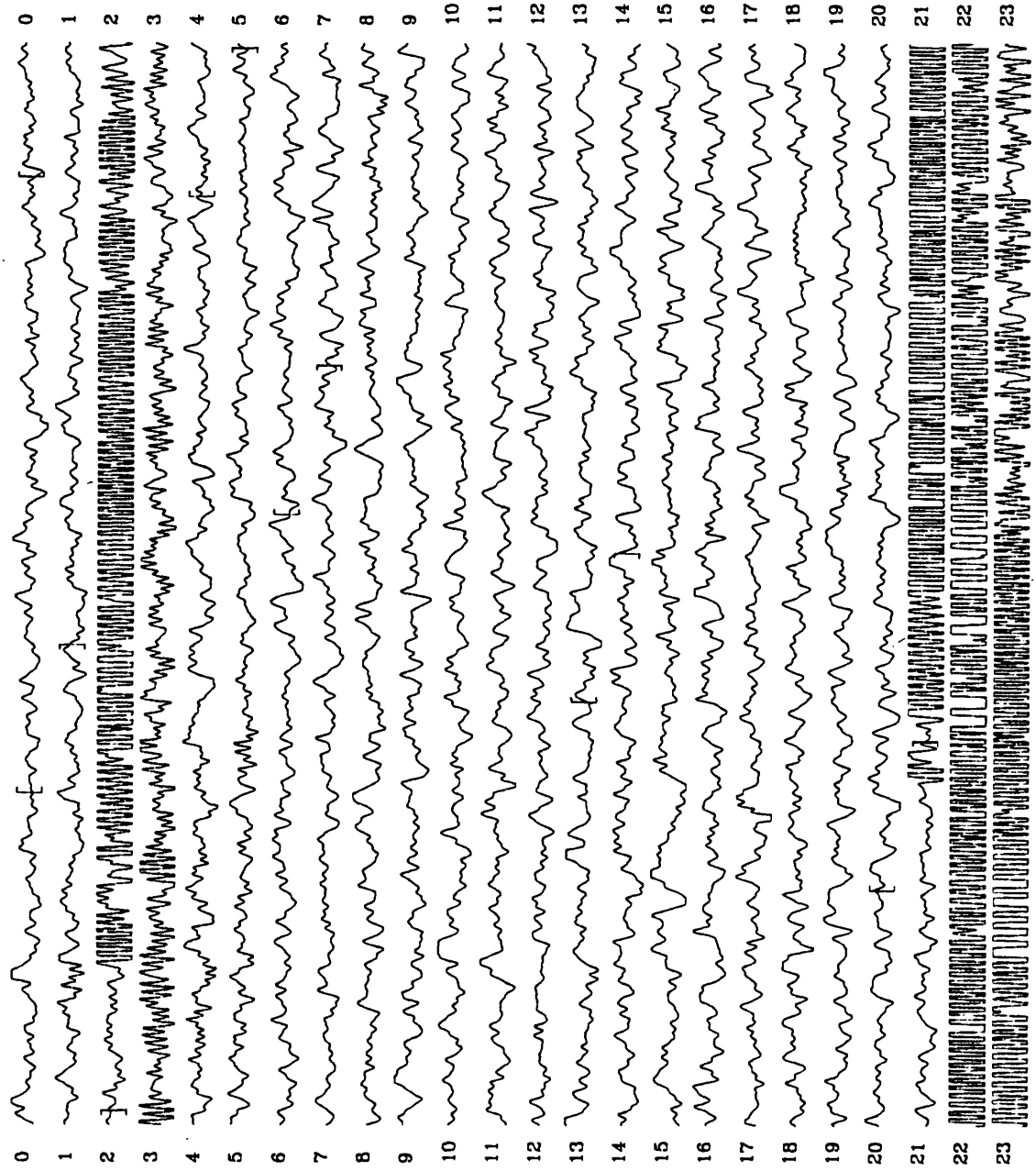

Figure 7.21 Time record for day 300 for the CMG-3S (B) horizontal showing the time segments selected by the automatic segment selection algorithm for inclusion in the direct model analysis of system noise.

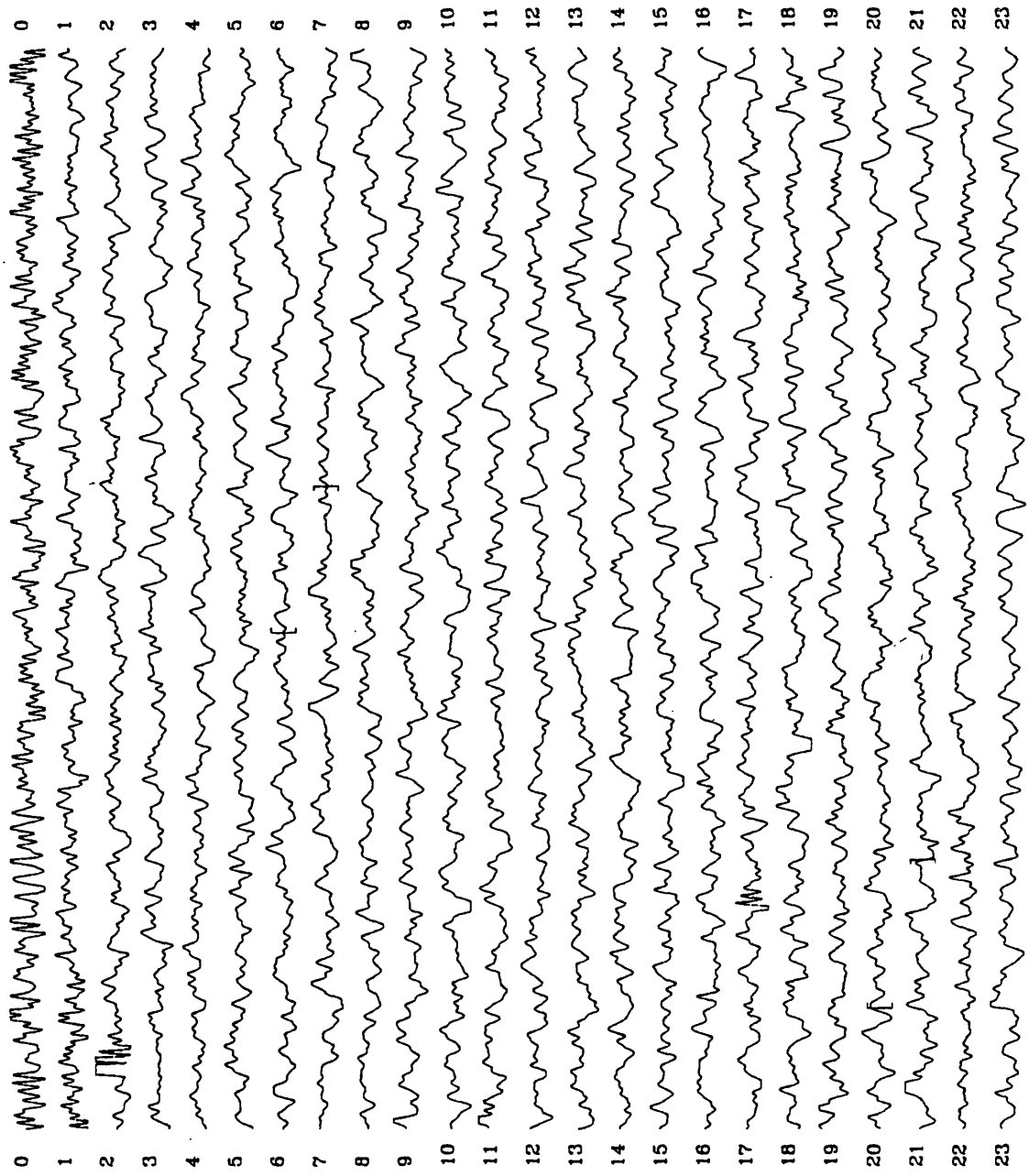

Figure 7.22 Time record for day 301 for the CMG-3S (B) horizontal showing the time segments selected by the automatic segment selection algorithm for inclusion in the direct model analysis of system noise.

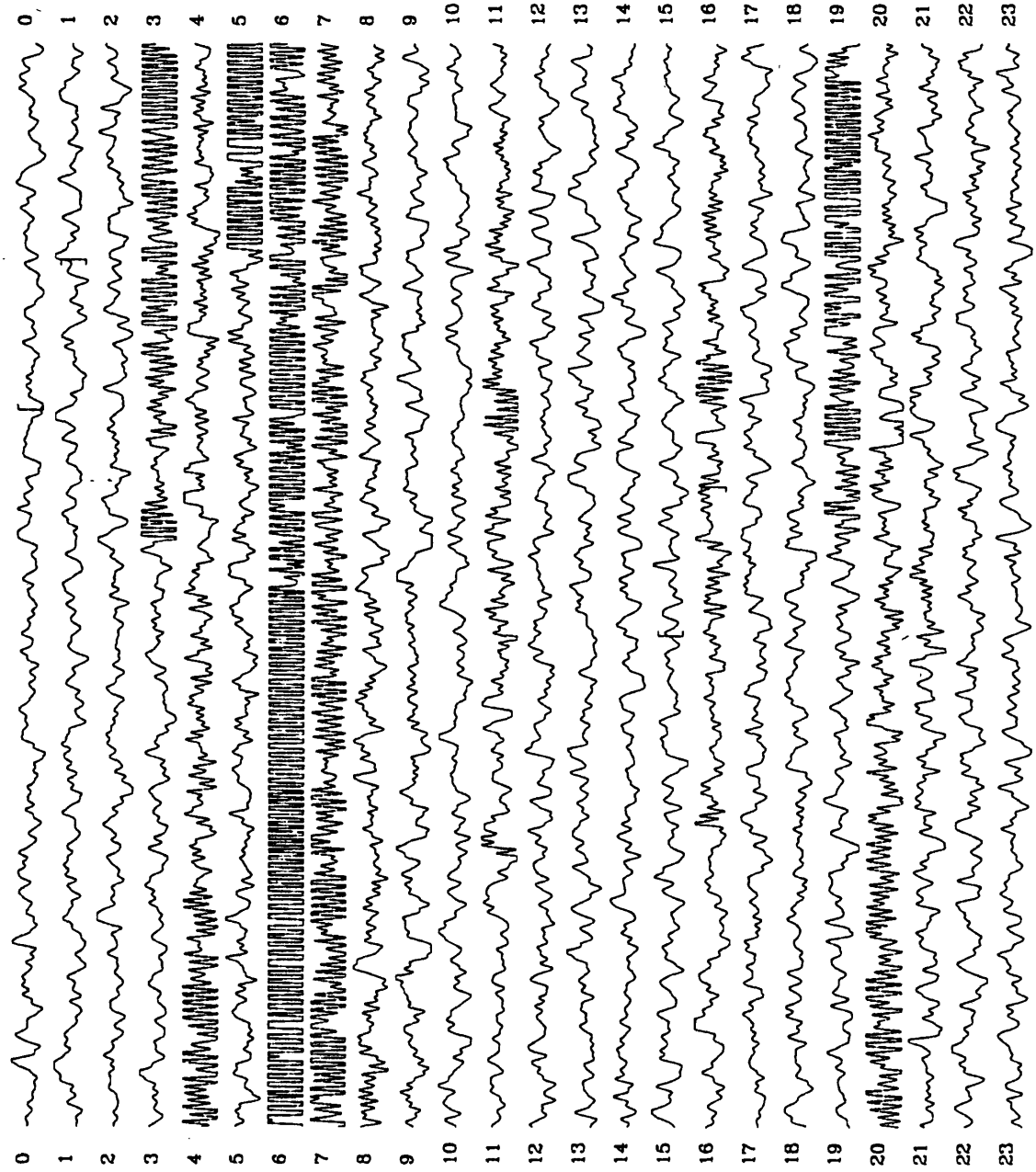

Figure 7.23 Time record for day 302 for the CMG-3S (B) horizontal showing the time segments selected by the automatic segment selection algorithm for inclusion in the direct model analysis of system noise.

Figures 7.11 and 7.12 contain the total PSD and noise PSD estimates for the horizontal components of the CMG-3S (A) and the STS-1 sensors respectively. In these figures, the data from the CMG-3S (A) was used to select the quiet segments; the selected segments are denoted in Figures 7.13, 7.14, 7.15, 7.16, and 7.17. Between 4 and 10 seconds the noise PSD estimates for both the CMG-3S and STS-1 horizontals are nearly identical in both shape and amplitude. This indicates that these noise estimates are probably dominated by misalignment error and that they are therefore not indicative of the true instrument noise levels in this portion of the spectrum. True instrument noise probably lies considerably below the levels shown in the figures. The indicated misalignment error is nearly 10° as indicated by Figures 6.20 and 6.21 in Holcomb, 1990.

Unfortunately, at long periods the performance of the CMG-3S horizontal component was not nearly as good as for the vertical component. Note that in Figure 7.11 the CMG-3S (A) horizontal is very noisy above about 10 seconds. The noise level is so high that it is readily evident in the time domain as can be observed by comparing Figures 7.3 and 7.6 with Figures 7.13 through 7.17. The same is true of the CMG-3S (B) horizontal whose total and noise PSD estimates are shown in Figure 7.18 and whose time domain data is shown in Figures 7.20 through 7.23. Even the PSD estimates for the STS-1 horizontal as shown in Figures 7.12 and 7.19 are higher than one would expect above 20 seconds. However, the higher than normal PSD estimates for the STS-1 horizontal is probably explainable by the fact that the CMG-3S horizontal data was used to select the quiet segments. Since the CMG-3S data is so noisy, the automatic quiet segment selection algorithm probably failed to discriminate against small events or windy periods of time. Judging from the character of the PSD estimates above 20 seconds for the STS-1 horizontals, it appears that the data is contaminated by wind generated tilt.

The source of the long period noise in the two CMG-3S horizontal sensors is not known for sure but the most probable suspected source is the plaster of paris block. Program time constraints did not permit the luxury of allowing the plaster of paris to cure and dry out thoroughly; hence, it is likely that the block was still curing during the data acquisition period. The curing process definitely involves the evaporation of water and probably results in the generation of micro-cracks within the material. Therefore, it is quite possible that the curing process causes tilt in the horizontals, which appears as excess noise in the figures. This possibility should be investigated in the future in a long term investigation lasting perhaps two months or more.

Figures 7.24 and 7.25 contain instrument noise estimates obtained from a direct model analysis of the two CMG-3S horizontal sensors when compared with one another while potted in plaster of paris. Sensor (A) selected the segments included in the analysis and they are indicated by square brackets in Figures 7.13 through 7.17. Note that the estimated noise levels (N_1 and N_2) in Figures 7.24 and 7.25 respectively are much lower in the 4 to 10 second part of the spectrum than was observed before. This indicates that the sensors were aligned better when potted in plaster of paris than they were in the pressure sensitivity investigations presented previously in Section 6. The SNR in the 4 to 10 second period range in Figure 7.24 lies between 1,000 and 10,000; SNR's in this range correspond to misalignment angles of less than 2° (see Holcomb, 1990).

A comparison of Figure 7.24 with Figure 7.11 indicates a significantly lower calculated estimated noise level for the CMG-3S (A) horizontal when it is compared with the CMG-3S (B) sensor as shown in Figure 7.24 than when it is compared with the STS-1 horizontal as shown in Figure 7.11. This may seem odd at first, but it becomes quite plausible when the probable effects of tilt are considered. If the plaster of paris block was still curing, it was probably generating tilt

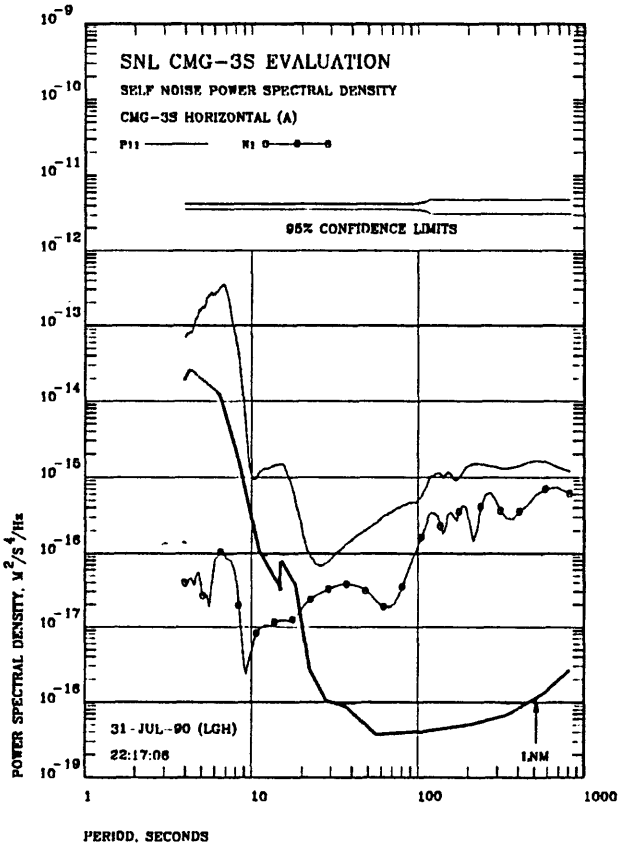

Figure 7.24 Estimated total PSD and self noise PSD of the CMG-3S (A) horizontal when potted in plaster of paris. The CMG-3S (A) horizontal selected the segments.

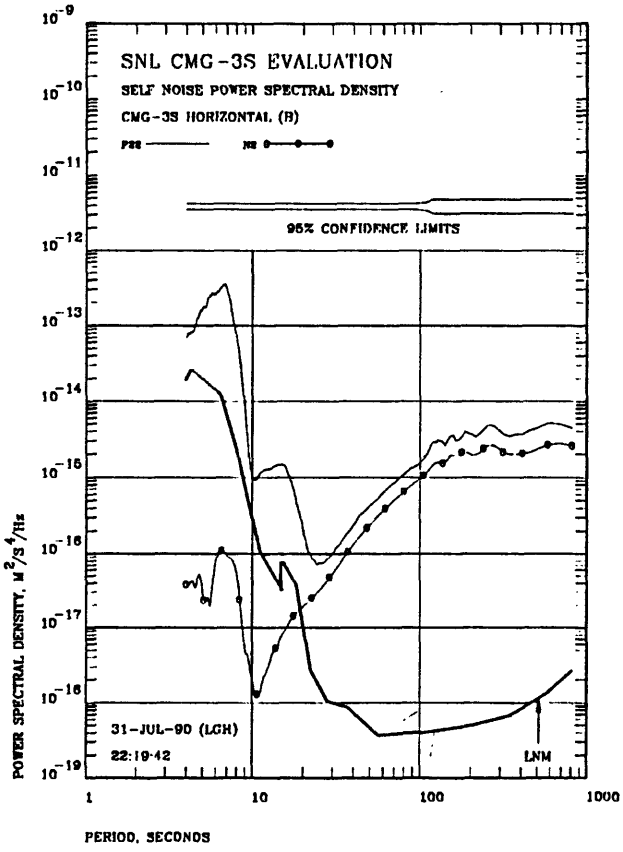

Figure 7.25 Estimated total PSD and self noise PSD of the CMG-3S (B) horizontal when potted in plaster of paris. The CMG-3S (A) horizontal selected the segments.

in the sensors as was mentioned earlier. Some of these tilt motions were probably coherent between the sensors because the plaster of paris block coupled the two sensors together fairly rigidly. Coherent tilt between the two CMG-3S horizontals can not be separated from coherent ground motion. Therefore, the calculated system noise level, when analyzing the outputs of the two CMG-3S horizontals with the direct model as shown in Figure 7.24, does not include coherent tilt in the noise estimates. On the other hand, the calculated system noise level, when analyzing the outputs of the CMG-3S (A) and STS-1 horizontals with the direct model as shown in Figure 7.11, includes this tilt noise as part of the estimated system noise because it is not coherent with the STS-1 horizontal.

Figures 7.26 and 7.27 contain instrument noise estimates obtained from a direct model analysis of the two CMG-3S horizontal sensors when potted with the CMG-3S (B) sensor selecting the segments. The segments actually selected are denoted by square brackets in Figures 7.20 through 7.23. From 4 to about 10 seconds, the calculated SNR is quite close to that observed in Figures 7.24 and 7.25 where the roles of the two CMG-3S horizontals were reversed. The indicated misalignment is of the order of 2°or less.

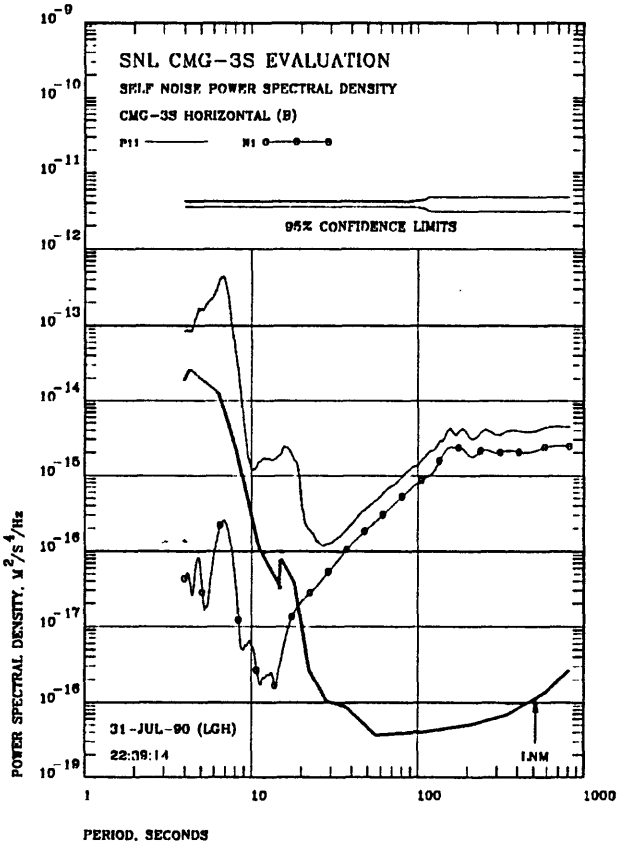

Figure 7.26 Estimated total PSD and self noise PSD of the CMG-3S (B) horizontal when potted in plaster of paris. The CMG-3S (B) horizontal selected the segments.

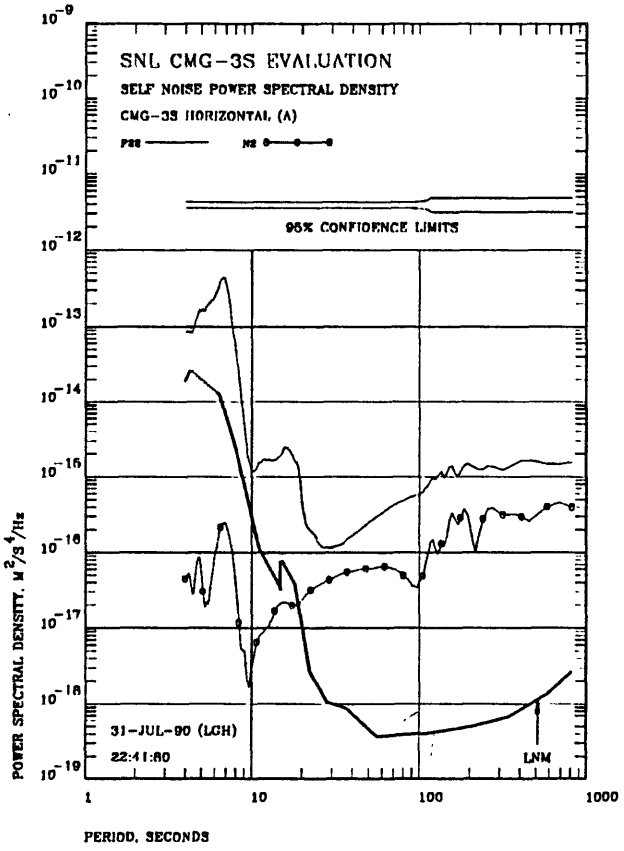

Figure 7.27 Estimated total PSD and self noise PSD of the CMG-3S (A) horizontal when potted in plaster of paris. The CMG-3S (B) horizontal selected the segments.

A comparison of Figures 7.26 and 7.18 indicates that the calculated estimated noise level above about 10 seconds is less when the two CMG-3S sensors are compared with each other in Figure 7.26 than when CMG-3S (B) is compared with the STS-1 horizontal in figure 7.18. Once again, the explanation for this difference lies in the curing of the plaster of paris and coherent tilt in the two CMG-3S horizontal sensors.

8 LOW PRESSURE PERFORMANCE

There was a possibility that air motion within the sensor cases was causing noise at long periods. This problem has been observed in long period sensors in the past thereby necessitating the evacuation of the sensor or the introduction of carefully selected gasses. Therefore, we attempted to evaluate the possibility that air motion was present within the CMG-3S cases by operating them at reduced pressure to see if the long period noise levels decreased. First, CMG-3S (A) was evacuated with a roughing pump and then sealed and operated side-by-side with CMG-3S (B) at atmospheric pressure in a vented HGLP tank for several days while the performance of the verticals was monitored. Then both sensors were evacuated and operated side-by-side in a vented HGLP tank while the performance of the horizontals was monitored.

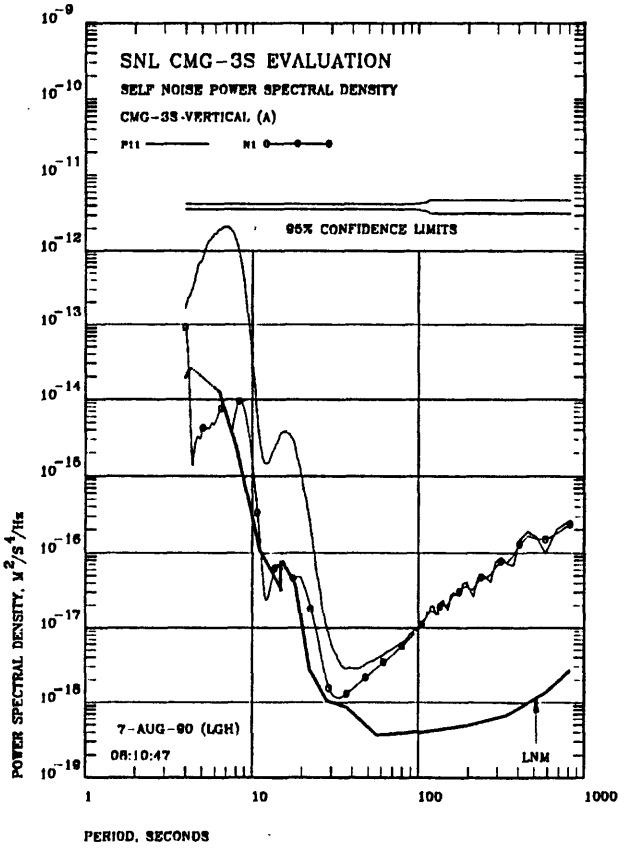

Figure 8.1 Estimated total PSD and self noise PSD of the CMG-3S (A) vertical when pumped down. The CMG-3S (A) vertical selected the segments.

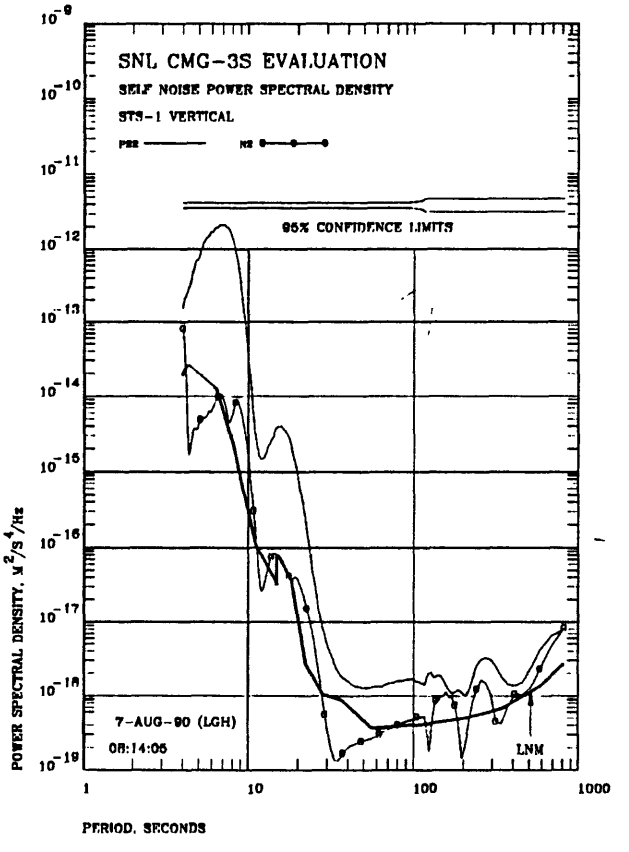

Figure 8.2 Estimated total PSD and self noise PSD of the STS-1 vertical. The CMG-3S (A) vertical selected the segments.

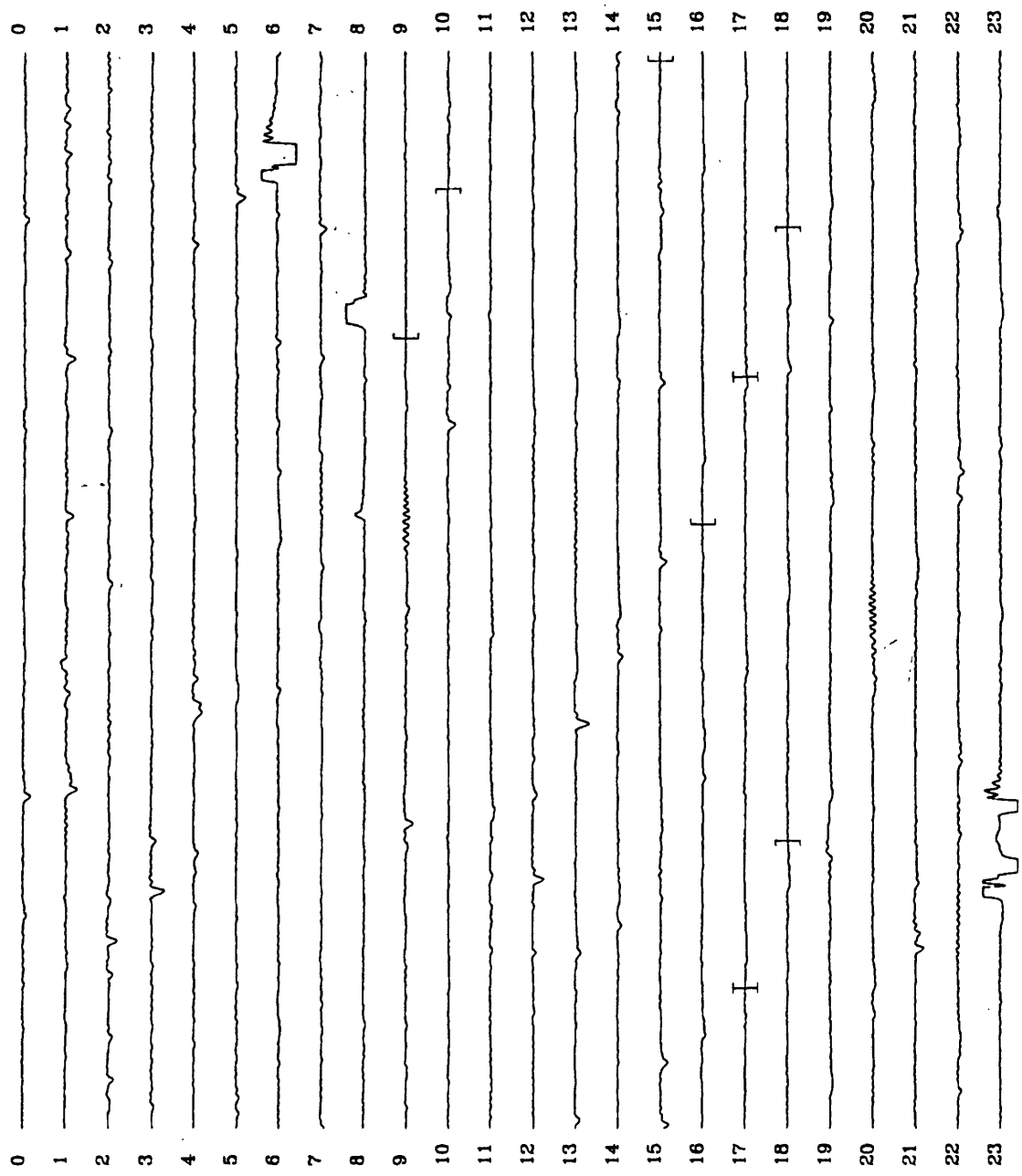

Figure 8.3 Time record for day 356 of the CMG-3S (A) vertical when under a vacuum.

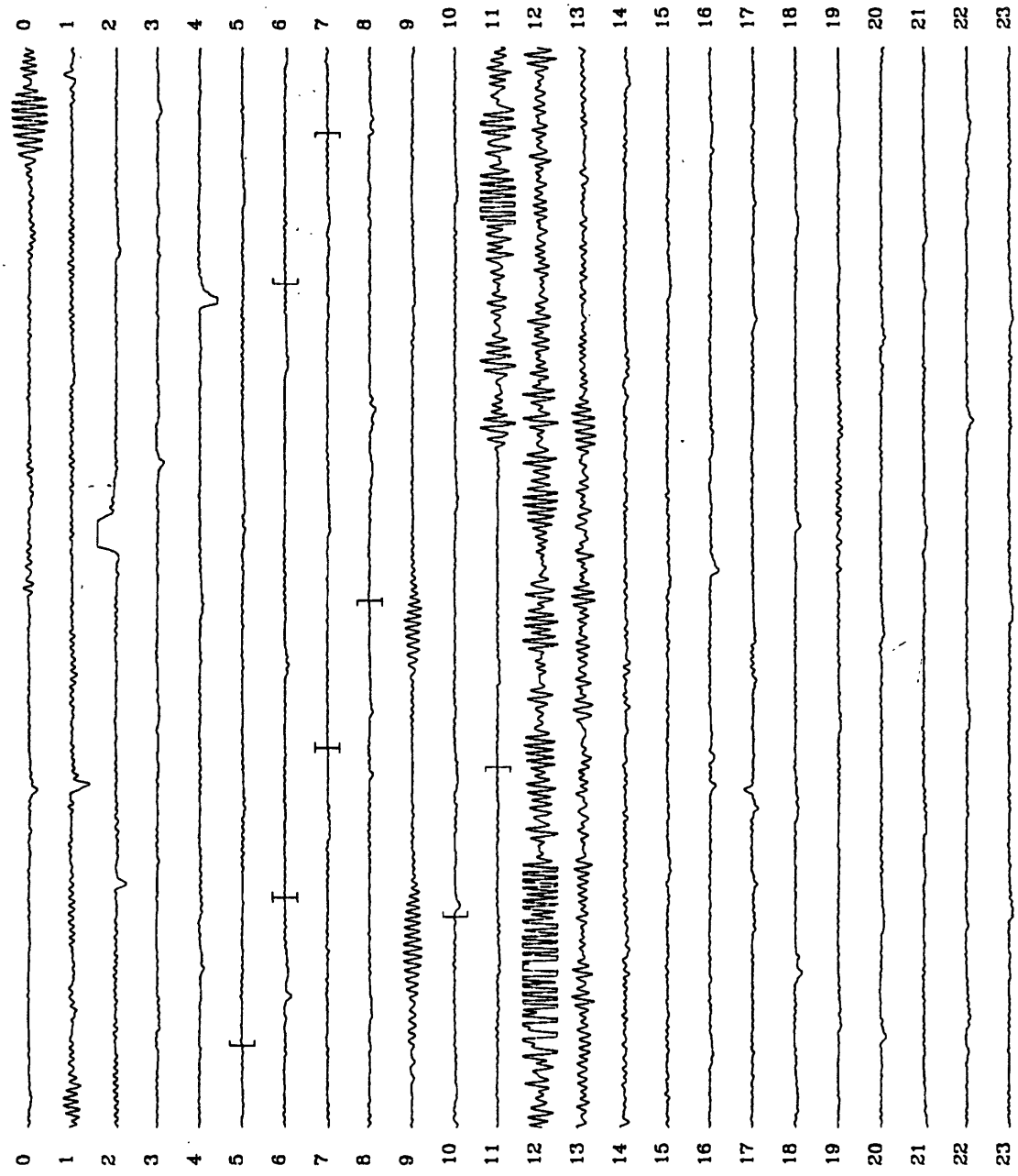

Figure 8.4 Time record for day 357 of the CMG-3S (A) vertical when under a vacuum.

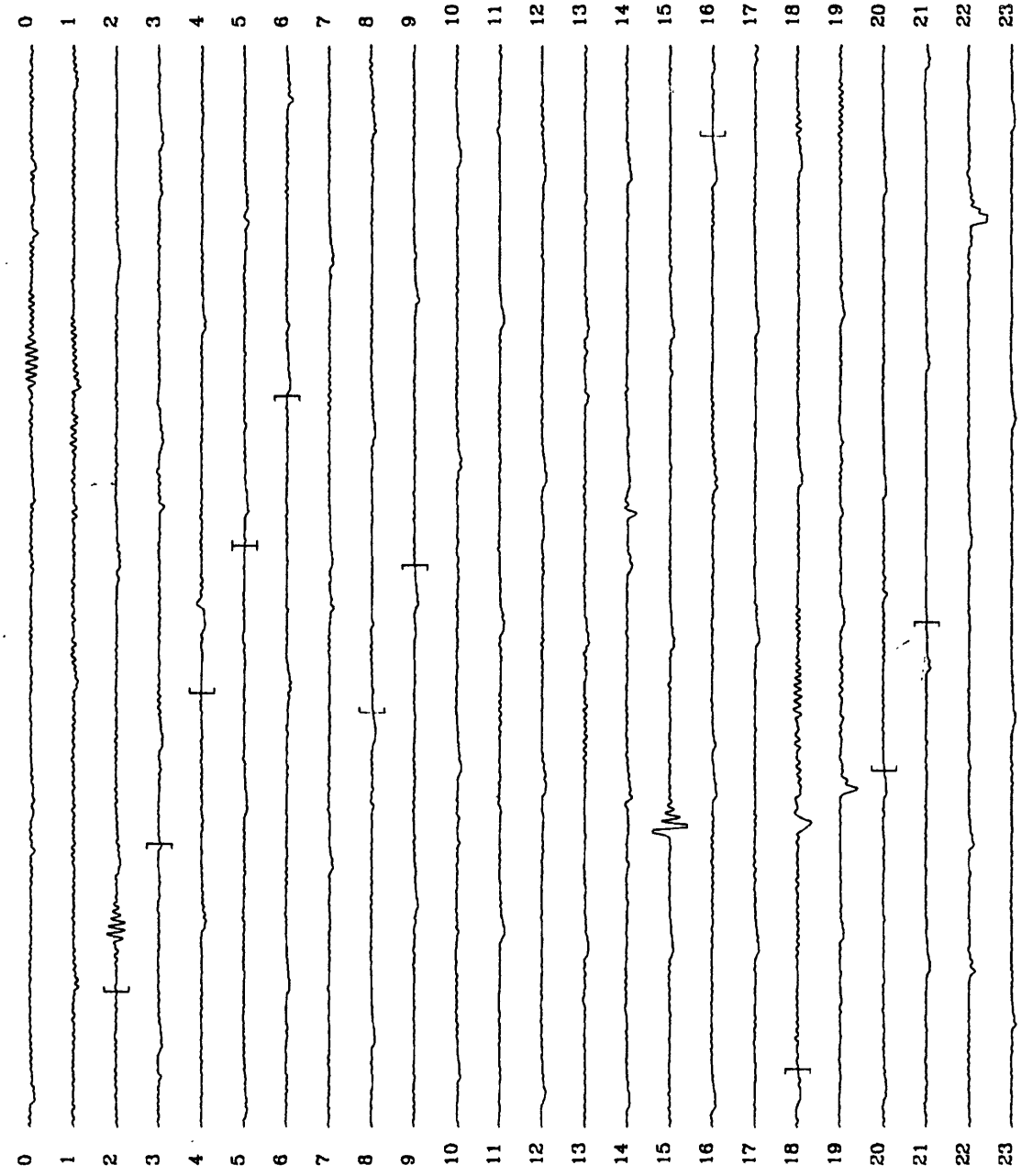

Figure 8.5 Time record for day 358 of the CMG-3S (A) vertical when under a vacuum.

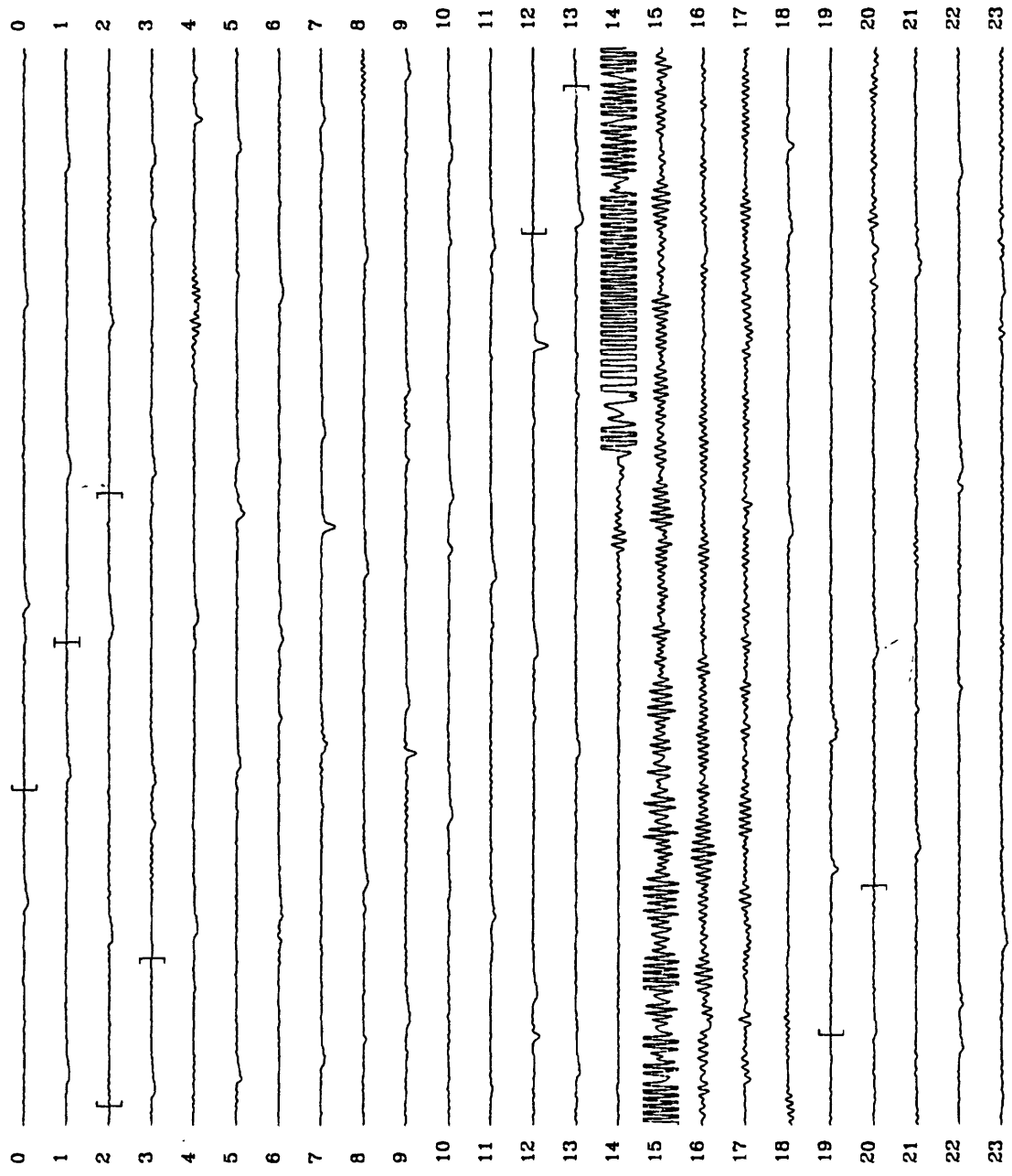

Figure 8.6 Time record for day 359 of the CMG-3S (A) vertical when under a vacuum.

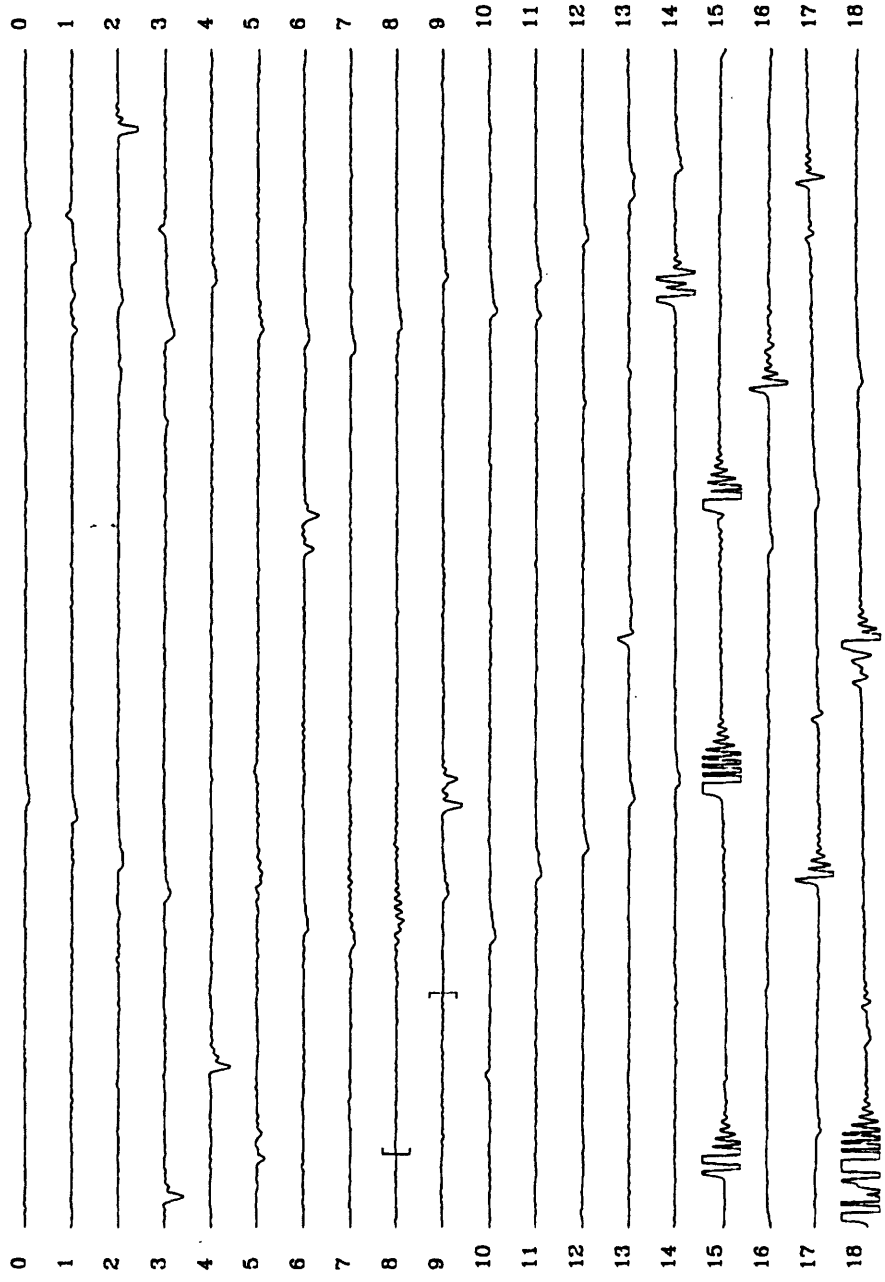

Figure 8.7 Time record for day 360 of the CMG-3S (A) vertical when under a vacuum.

8.1 VERTICAL PERFORMANCE AT ONE ATMOSPHERE VERSUS PUMPED DOWN

First, CMG-3S (A) was evacuated with a roughing pump and then sealed and operated side-by-side with CMG-3S (B) at atmospheric pressure in a vented HGLP tank for several days while the performance of the verticals was monitored. Data was recorded from the two CMG-3S verticals and the STS-1 vertical located in the vault cross tunnel.

Figures 8.1 and 8.2 contain noise PSD estimates for the CMG-3S (A) vertical and the STS-1 vertical during the time period in which CMG-3S (A) was pumped down. Here again, the noise estimates for both instruments appear to be dominated by misalignment noise from 4 to about 30 seconds. True instrument noise probably lies considerably below the indicated levels in both figures especially at shorter periods. Above 30 seconds, the noise levels for each instrument are unique and are probably indicative of true internal sensor noise.

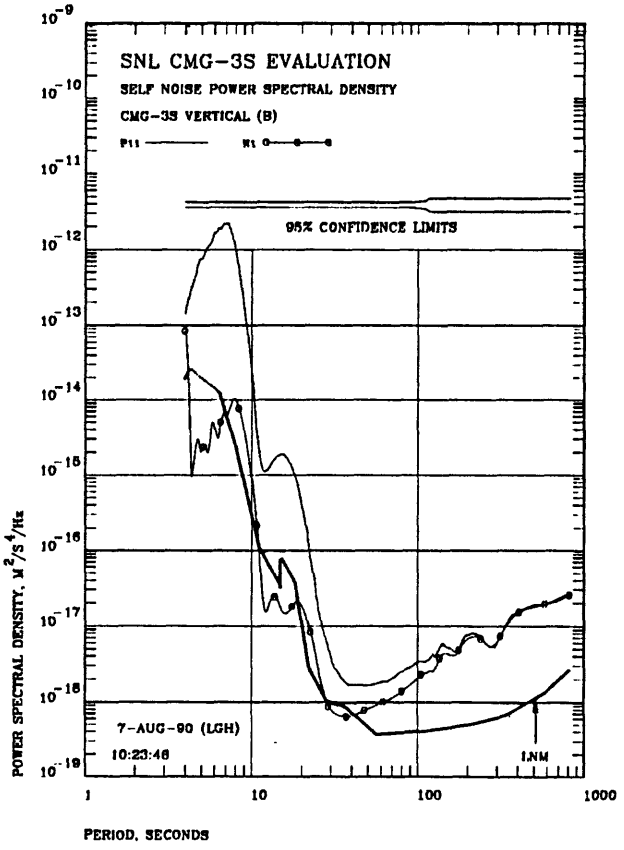

Figure 8.8 Estimated total PSD and self noise PSD of the CMG-3S (B) vertical when at one atmosphere of pressure. The CMG-3S (B) vertical selected the segments.

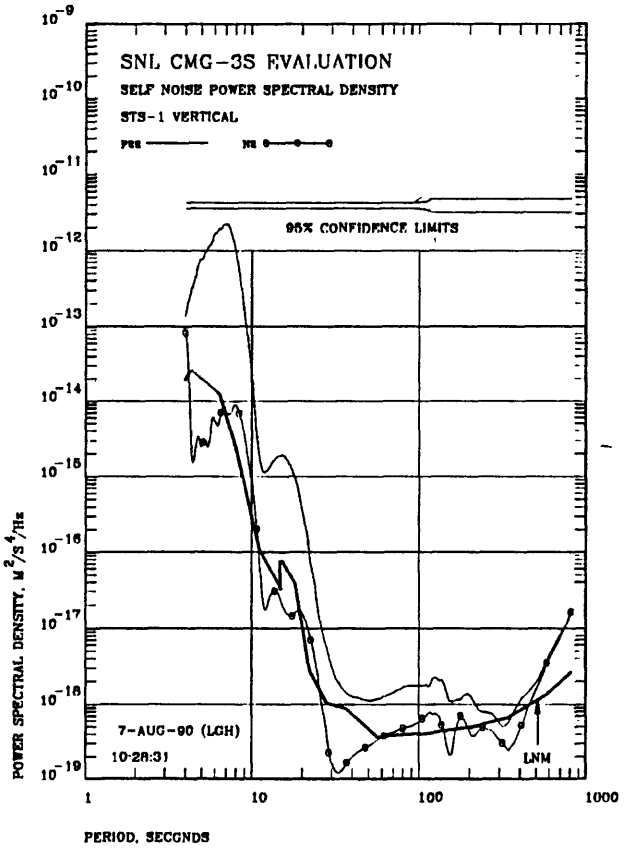

Figure 8.9 Estimated total PSD and self noise PSD of the STS-1 vertical. The CMG-3S (B) vertical selected the segments.

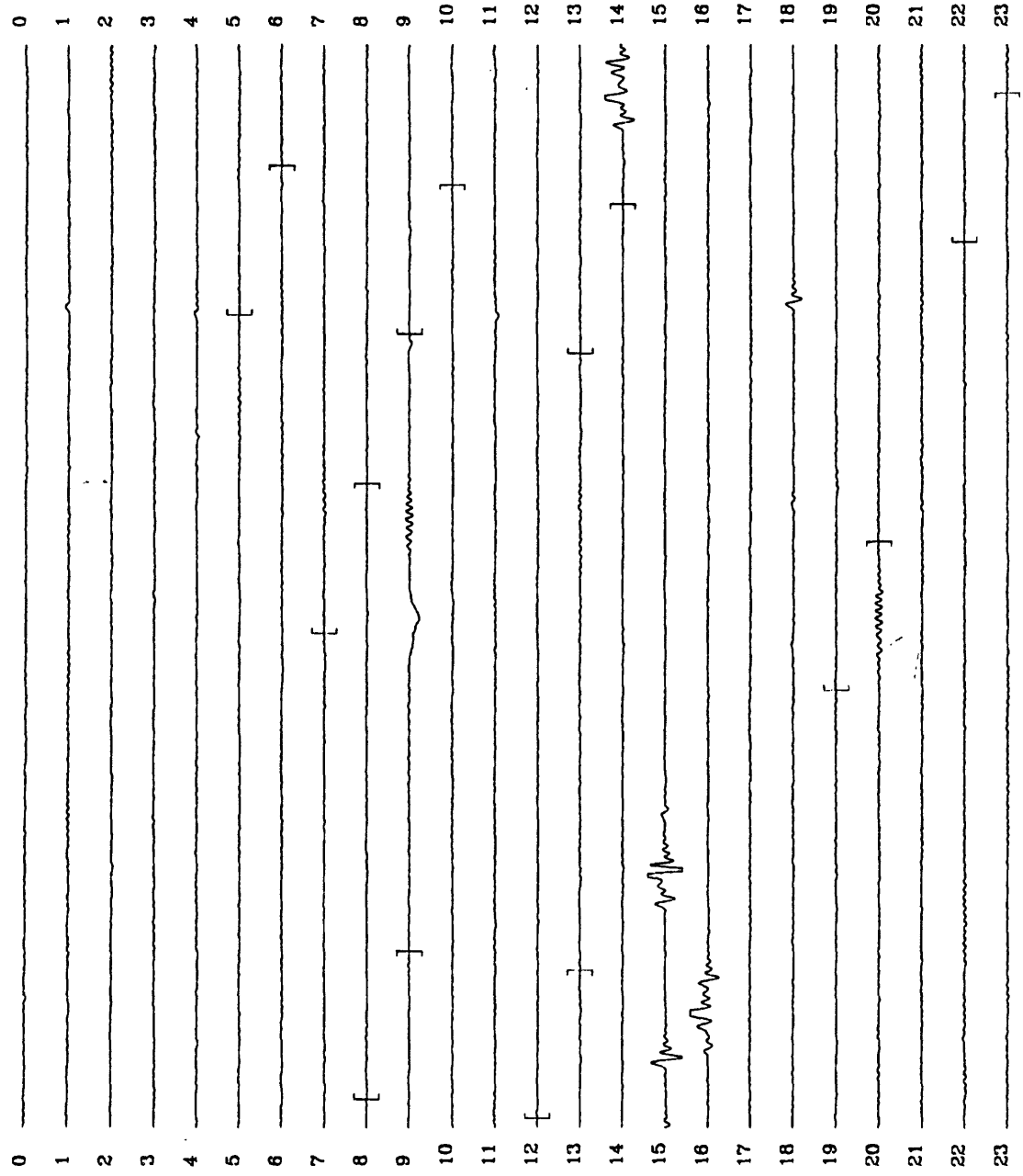

Figure 8.10 Time record for day 356 of the CMG-3S (B) vertical at atmospheric pressure.

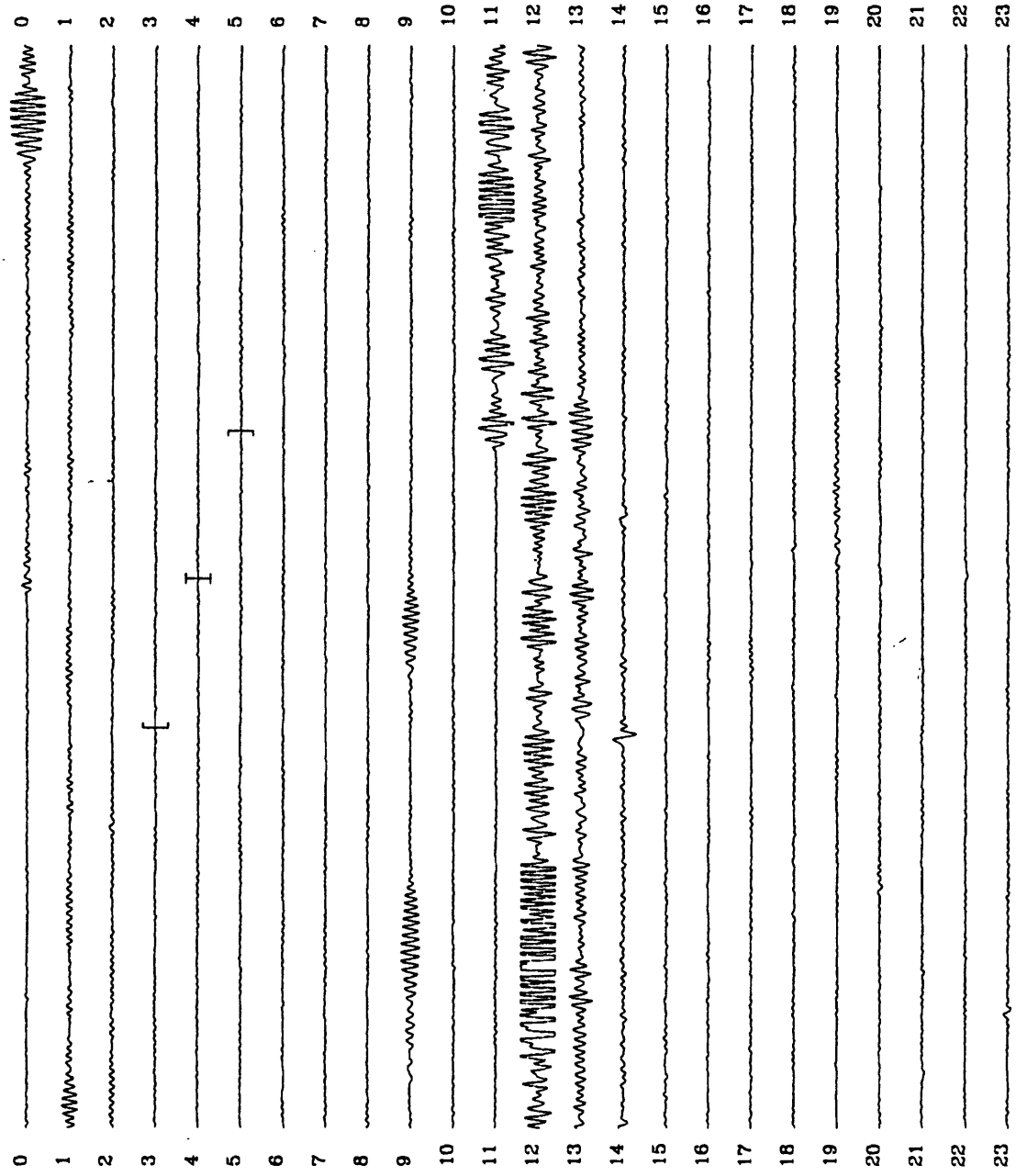

Figure 8.11 Time record for day 357 of the CMG-3S (B) vertical at atmospheric pressure.

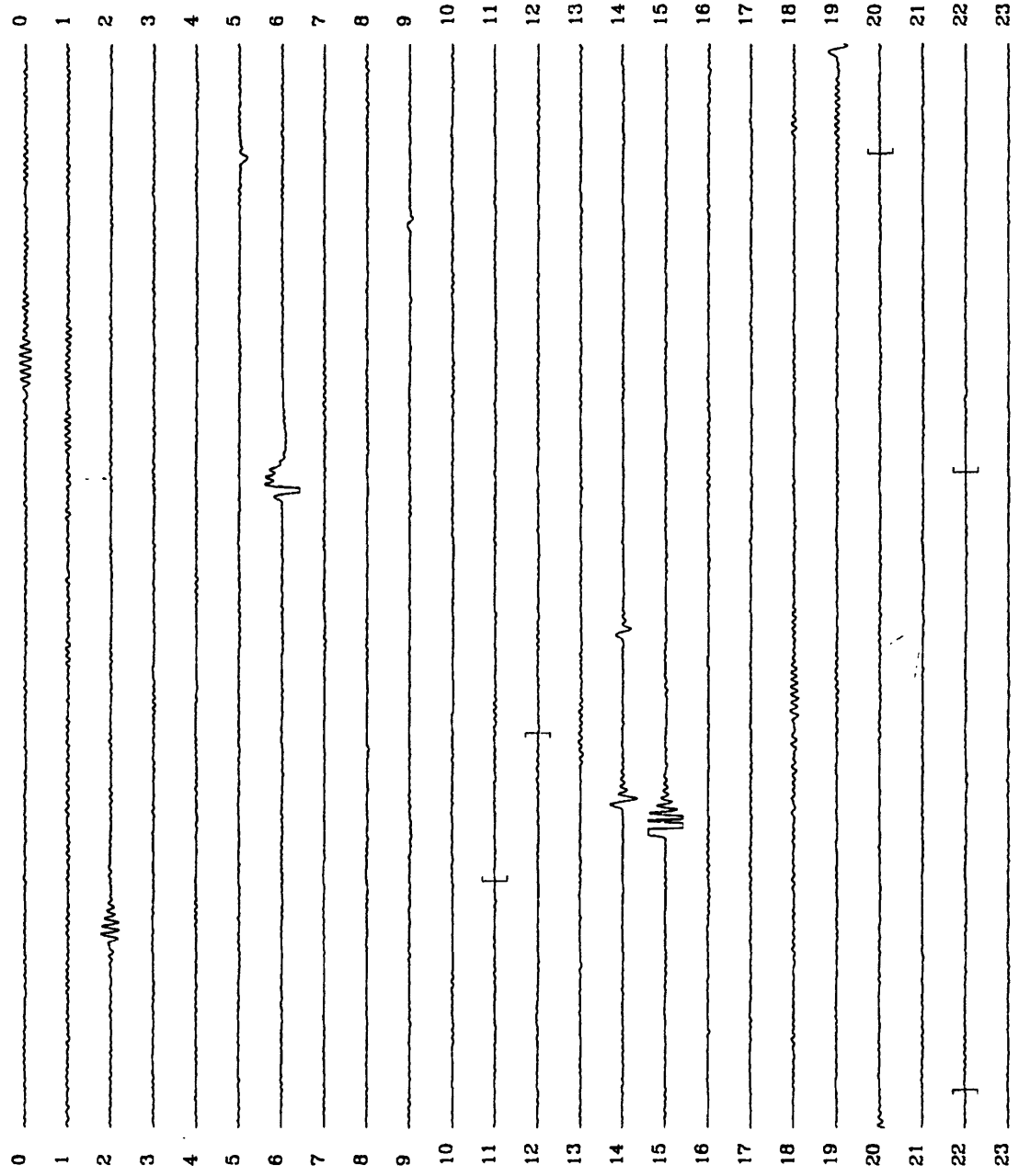

Figure 8.12 Time record for day 358 of the CMG-3S (B) vertical at atmospheric pressure.

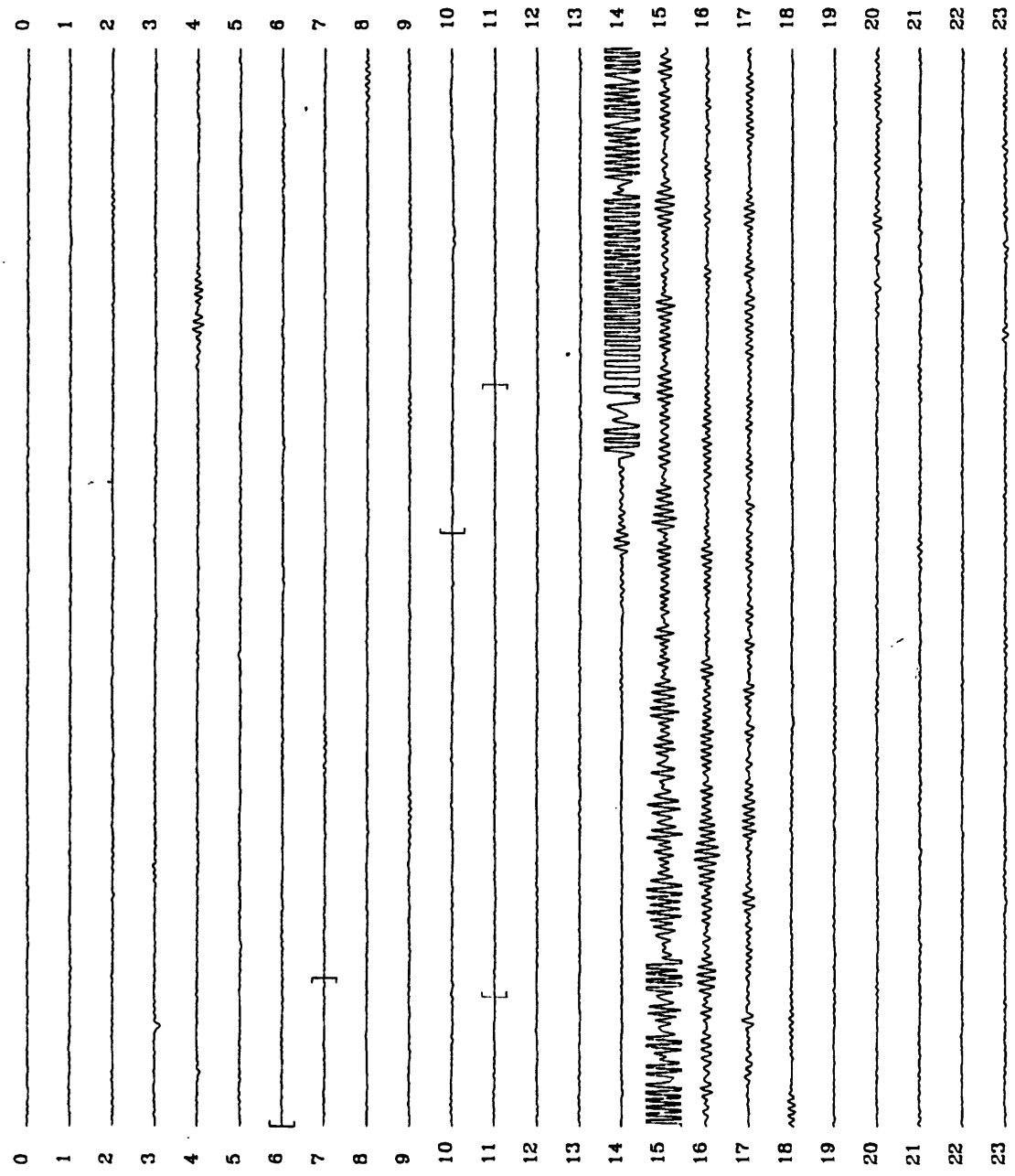

Figure 8.13 Time record for day 359 of the CMG-3S (B) vertical at atmospheric pressure.

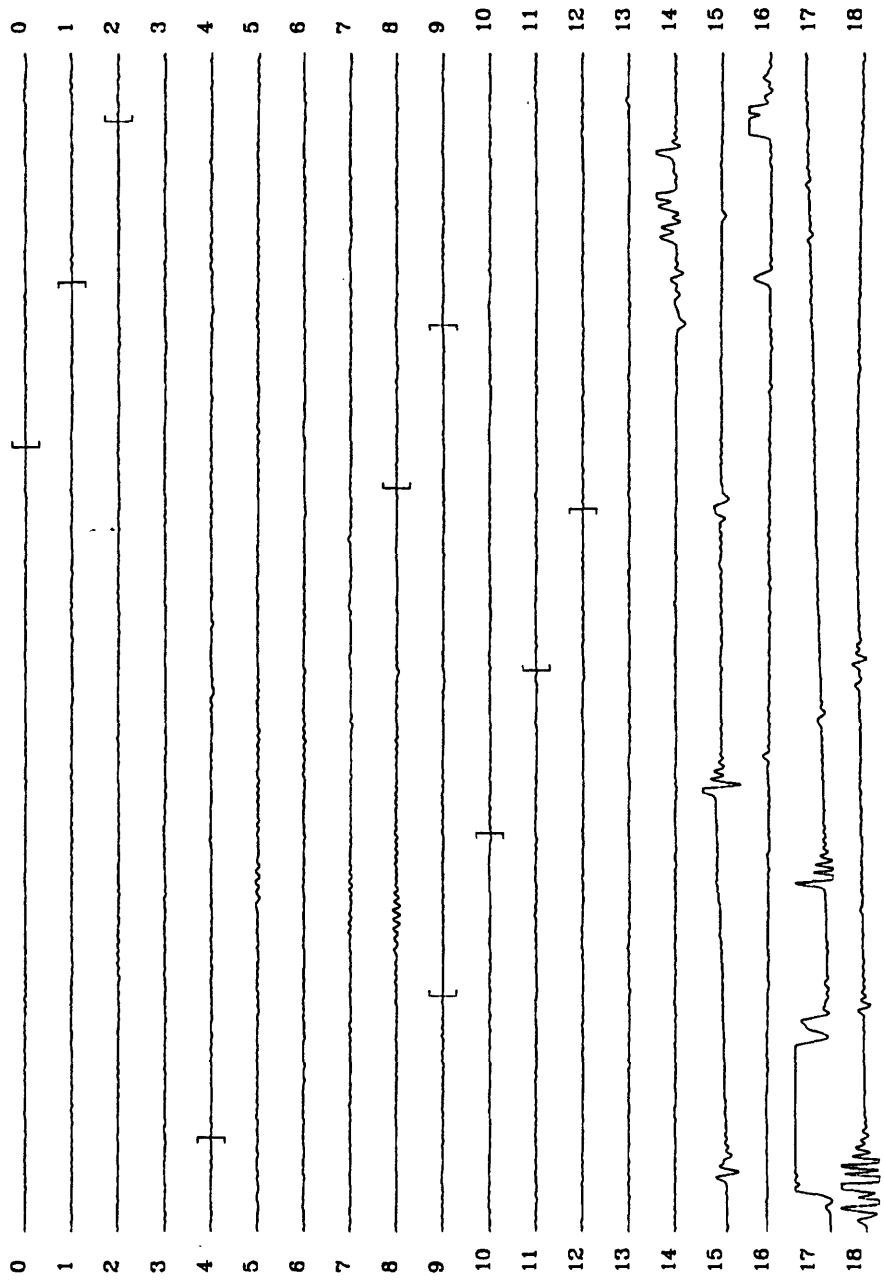

Figure 8.14 Time record for day 360 of the CMG-3S (B) vertical at atmospheric pressure.

Figures 8.3 through 8.7 contain the time domain histories for the CMG-3S (A) vertical showing the time segments actually included in the analysis to generate the noise estimates in Figures 8.1 and 8.2.

Figures 8.8 and 8.9 contain noise PSD estimates for the CMG-3S (B) vertical and the STS-1 vertical during the time period in which CMG-3S (B) was at one atmosphere. In these figures, misalignment noise dominates the noise estimates from 4 to about 30 seconds, but above 30 seconds, the noise estimates are probably representative of true system noise.

The important observation to make is that the estimated noise spectra for CMG-3S (B) above 30 seconds (at one atmosphere) in Figure 8.8 is significantly lower than the estimated noise spectra for CMG-3S (A) above 30 seconds (pumped down) in Figure 8.1. Instead of getting quieter as a result of evacuating the air from sensor (A), the vertical component became noisier. Inspection of Figures 8.3 through 8.7 as compared with Figures 8.10 through 8.14 reveals that the reason for the increase in long period noise is probably the fact that the CMG-3S (A) vertical was burping badly whereas the CMG-3S (B) vertical was relatively burp free.

Burps are evident throughout all five days of data from the CMG-3S (A) vertical shown in Figures 8.3 through 8.7. There were so many burps on sensor (A) that the segment selection algorithm was not able to find enough quiet "burp free" segments to fulfill the 10% of time criteria. Therefore, small burps are present in several of the segments which were included in the analysis. For instance, there is at least one burp in the segment which includes most of hour 10 for day 356 (see Figure 8.3 at about 10:40). There are also probably two burps which occur at approximately 08:20 on day 357 (see Figure 8.4); this time period lies within a selected segment.

In contrast, there are very few discernable burps in the five days of data from the CMG-3S (B) vertical shown in Figures 8.10 through 8.14. There are a few relatively large burps; for instance, several large burps are present beginning at about 14:50 and extending to about 16:10 on day 356 in Figure 8.10. However, the burp frequency in the CMG-3S (B) vertical data was low enough that the segment selection algorithm appears to have been able to completely eliminate burps from the segments included in the (B) vertical noise estimates. If any burps are included, they are so small that they can not be visually detected in the time histories.

The most probable cause of the marked increase in the severity of burping in the CMG-3S (A) vertical over that observed in the CMG-3S (B) vertical lies in the fact that sensor (A) was evacuated. Evacuation places new mechanical stress on the sensor assembly: the differential air pressure forces the sides, the top, and the bottom of the package to bow inward. Past experience gained over many years of working with long period instrumentation has shown that anytime a long period system is physically disturbed it will start to burp. Normally, the frequency of occurrence and amplitude of the burps will decrease with time until they are no longer discernable. Pumping a sensor down and the resulting stress induced change in mechanical dimensions is a severe disturbance to a long period sensor.

Experience gained over the years leads the authors to believe that, if left alone, the evacuated sensor's burps would decay off in both frequency of occurrence and amplitude with time. Eventually, it would probably become at least as quiet as it was before evacuation; if evacuation improved its performance, it would become quieter. Judging from the qualitative severity of the burping shown above, it might take several months for the system to settle down. Only a long term quantitative test could determine if the behavior we forecast would actually be observed.

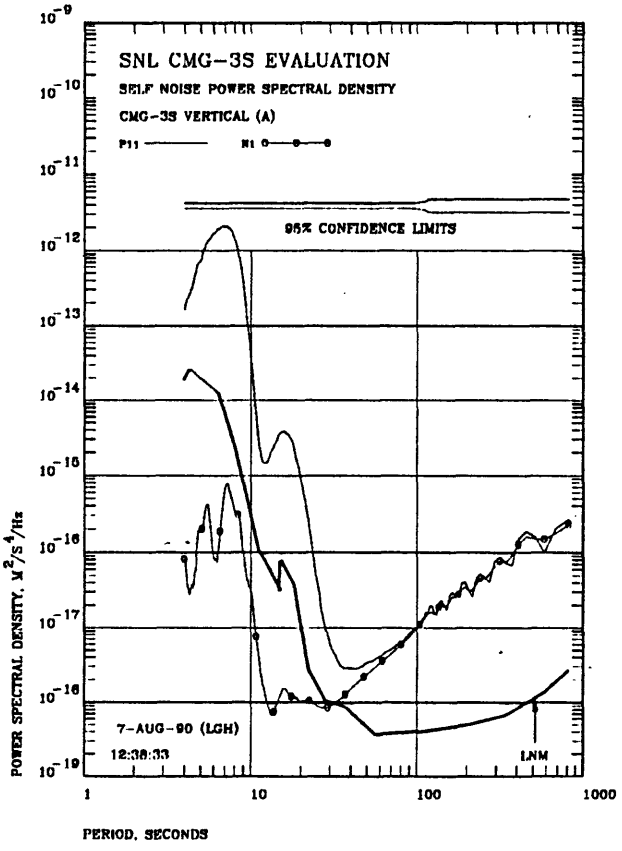

Figure 8.15 Estimated total PSD and self noise PSD of the CMG-3S (A) vertical when pumped down. The CMG-3S (A) vertical selected the segments.

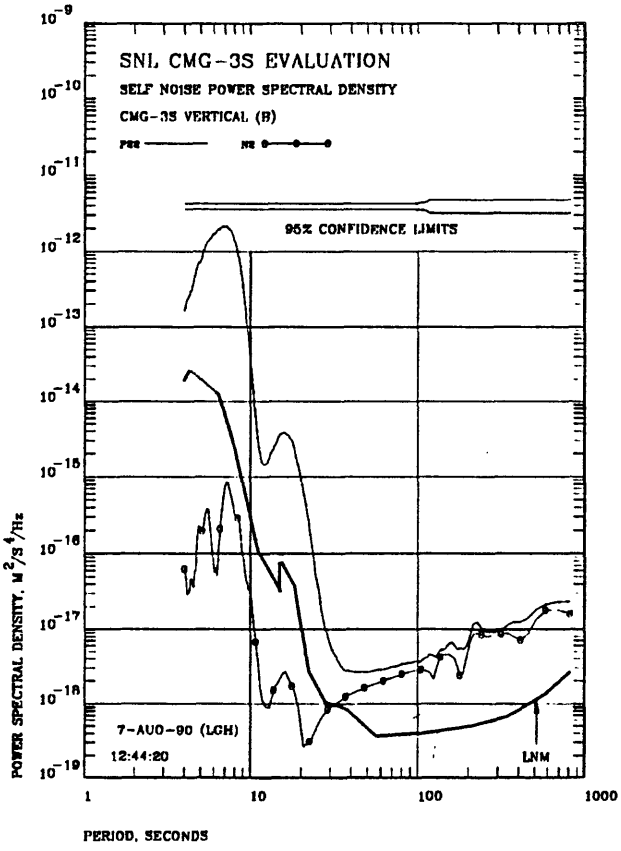

Figure 8.16 Estimated total PSD and self noise PSD of the CMG-3S (B) vertical when at one atmosphere. The CMG-3S (A) vertical selected the segments.

Figures 8.15 and 8.16 contain PSD estimates obtained from a direct model comparison of the CMG-3S (A) evacuated vertical with the CMG-3S (B) atmospheric pressure vertical. The CMG-3S (A) evacuated vertical selected the segments. It is evident that, even with the evacuated vertical (A) selecting the segments, the evacuated vertical is considerably noisier than the atmospheric pressure vertical. With the situation reversed as in Figures 8.17 and 8.18 in which the CMG-3S (B) atmospheric pressure vertical selected the segments, the noise levels in the CMG-3S (A) vertical are incredibly high.

It is quite clear that evacuating the CMG-3S case does not improve the performance of the vertical component in the short term. The behavior in the long term would probably be better than the short term because the burps would probably die out with time. Whether or not the evacuated instrument's long term performance would improve over the atmospheric performance can not be ascertained with the information at hand; only a long term experiment can resolve this question.

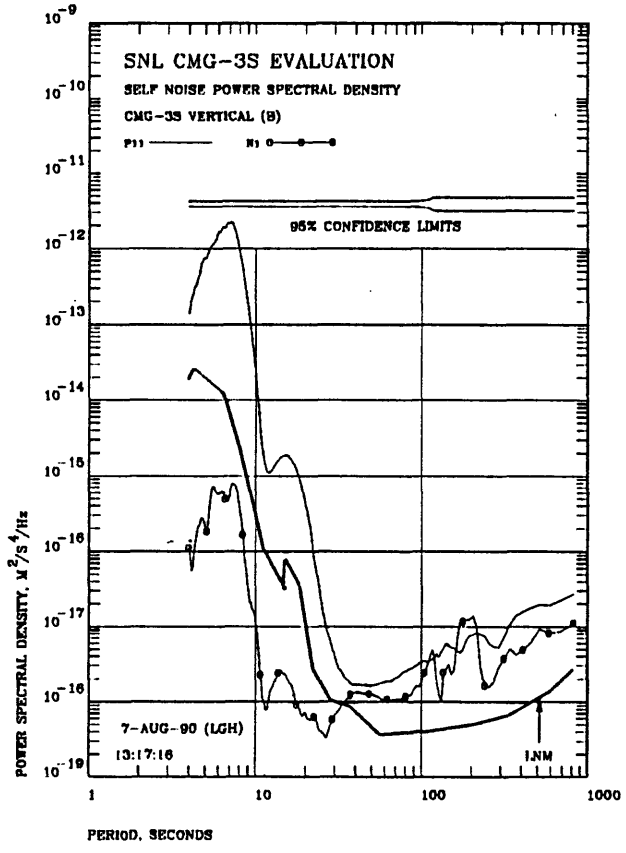

Figure 8.17 Estimated total PSD and self noise PSD of the CMG-3S (B) vertical when at one atmosphere. The CMG-3S (B) vertical selected the segments.

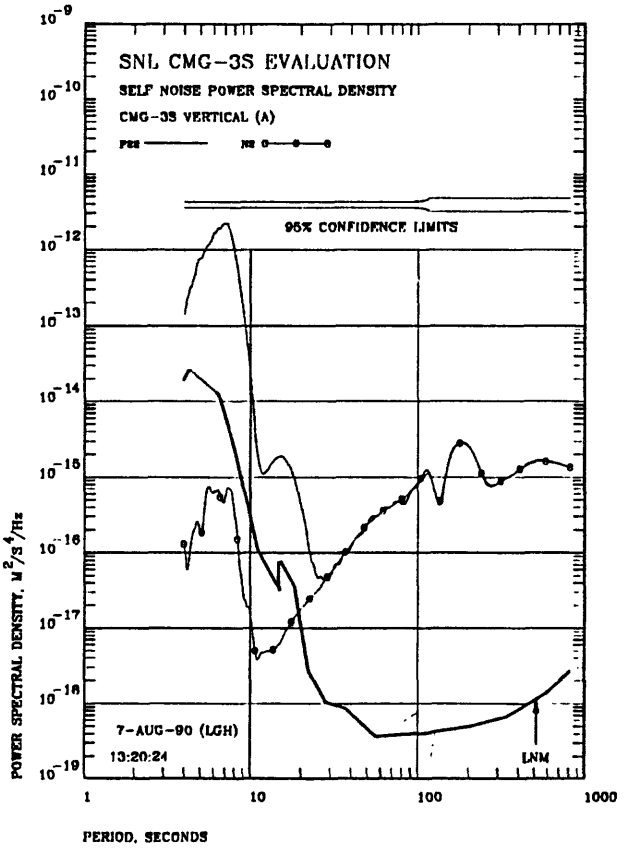

Figure 8.18 Estimated total PSD and self noise PSD of the CMG-3S (A) vertical when pumped down. The CMG-3S (B) vertical selected the segments.

8.2 HORIZONTAL PERFORMANCE WHEN PUMPED DOWN

Next, both sensors were evacuated with a roughing pump and operated side-by-side in a vented HGLP tank while the performance of the horizontals was monitored. Data was recorded from the two evacuated CMG-3S horizontals and a STS-1 horizontal located in the vault cross tunnel.

Figures 8.19 and 8.20 contain comparative PSD estimates for the CMG-3S (A) horizontal when it was evacuated and the STS-1 horizontal. As noted in the figures, the CMG-3S (A) horizontal selected the segments used to obtain all of the estimates in the figures. The segments actually selected are depicted in the time domain plots of the data collected are shown in Figures 8.21, 8.22, and 8.23.

From 4 to about 15 seconds the estimated PSD noise levels for both the CMG-3S (A) horizontal and the STS-1 horizontal are approximately the same. As discussed in detail in Section 6.1, this noise is probably due to sensor misalignment and is probably not indicative of the true internal noise level of either instrument. Above 15 seconds, the two noise estimates are distinct; the estimate for the CMG-3S (A) horizontal shown in Figure 8.19 above 15 seconds is believed to be the true noise level in the instrument. However, the STS-1 horizontal noise level shown in Figure 8.20 is probably true instrument noise only above approximately 30 seconds. Below 30 seconds, the estimated PSD data is probably dominated by misalignment noise.

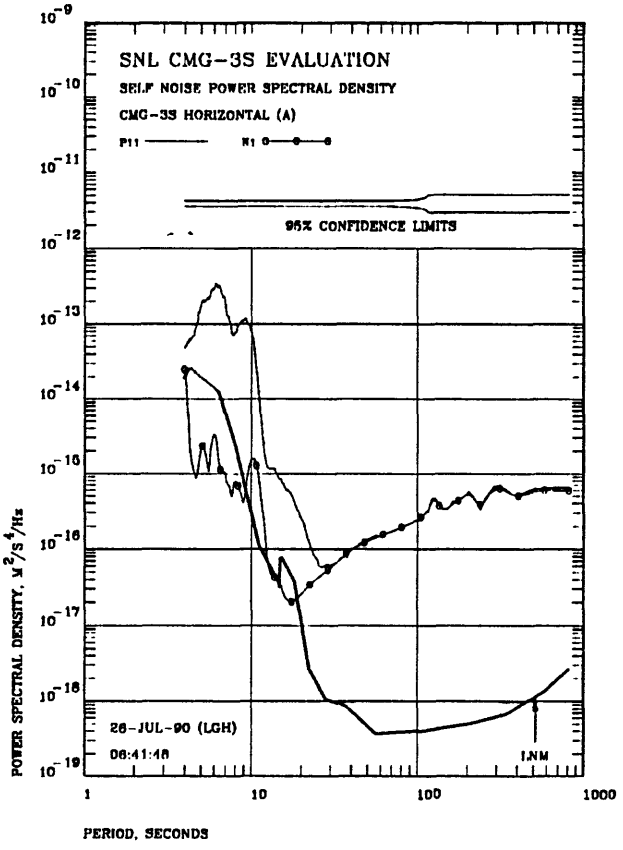

Figure 8.19 Estimated total PSD and self noise PSD of the CMG-3S (A) horizontal under a vacuum. The CMG-3S (A) horizontal selected the segments.

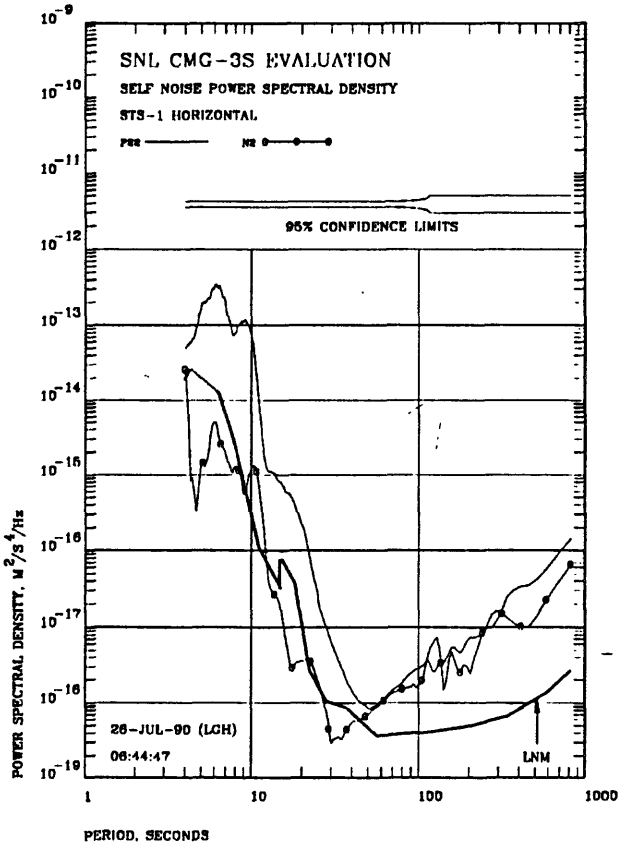

Figure 8.20 Estimated total PSD and self noise PSD of the STS-1 horizontal. The CMG-3S (A) horizontal selected the segments.

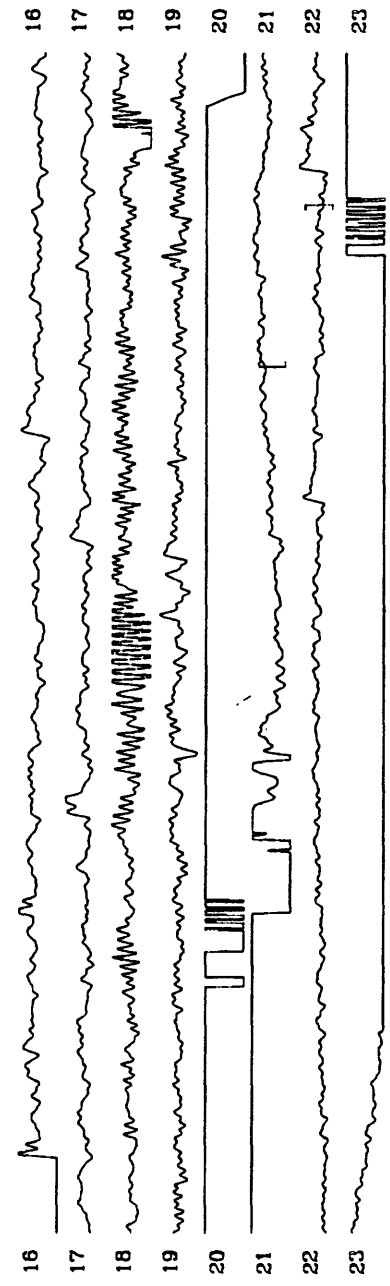

Figure 8.21 Time record for day 307 of the CMG-3S (A) horizontal when under a vacuum.

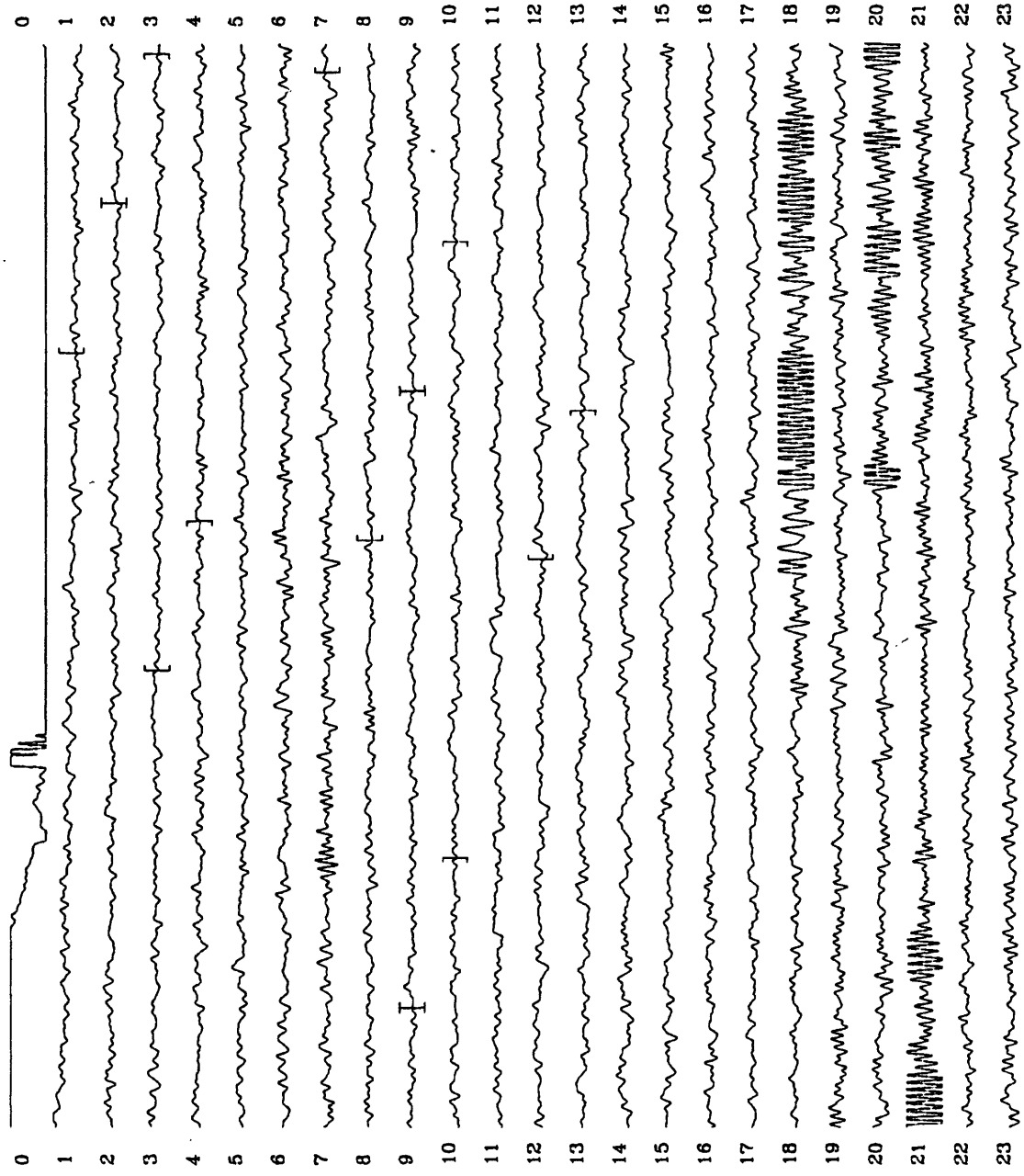

Figure 8.22 Time record for day 308 of the CMG-3S (A) horizontal when under a vacuum.

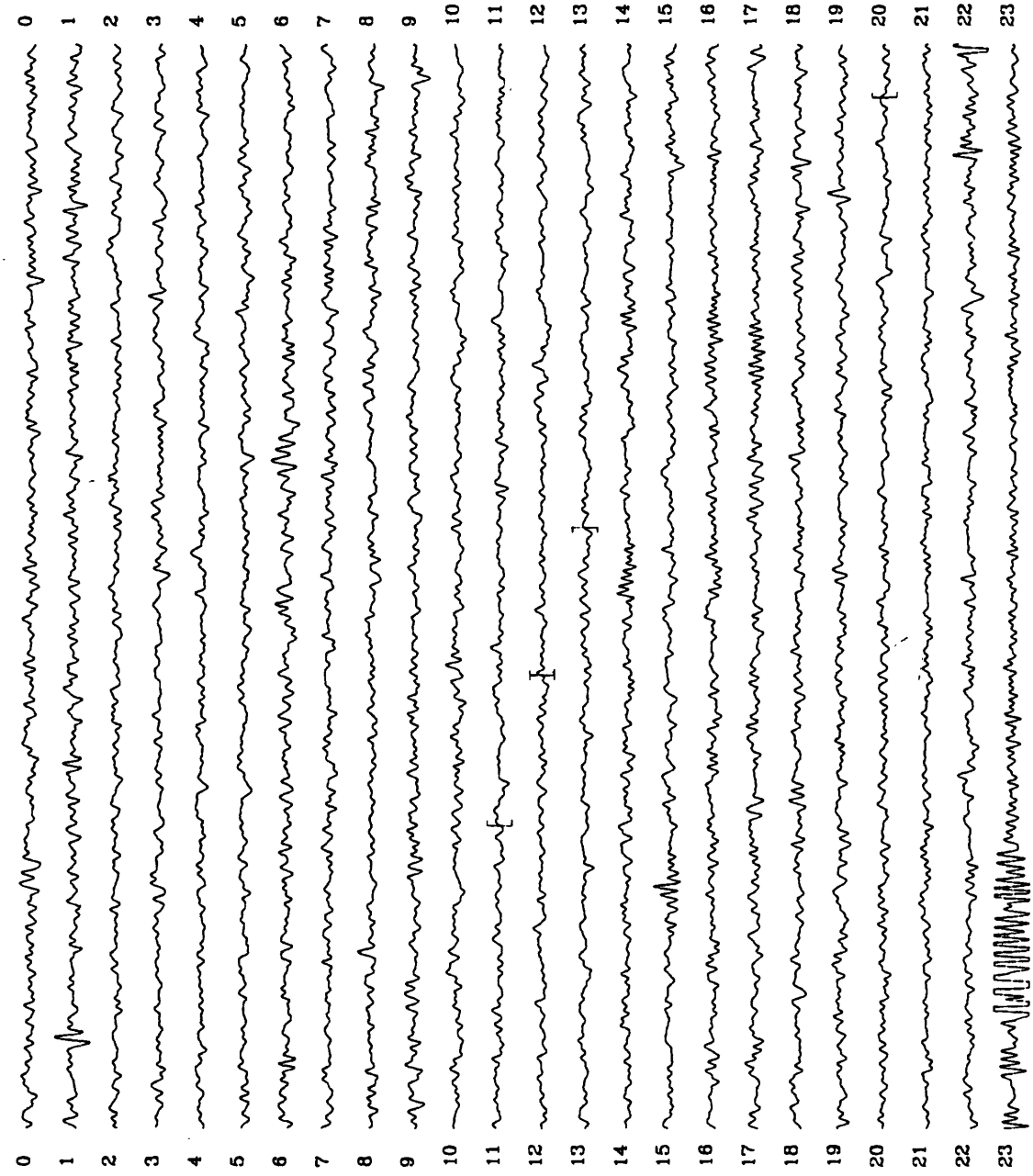

Figure 8.23 Time record for day 309 of the CMG-3S (A) horizontal when under a vacuum.

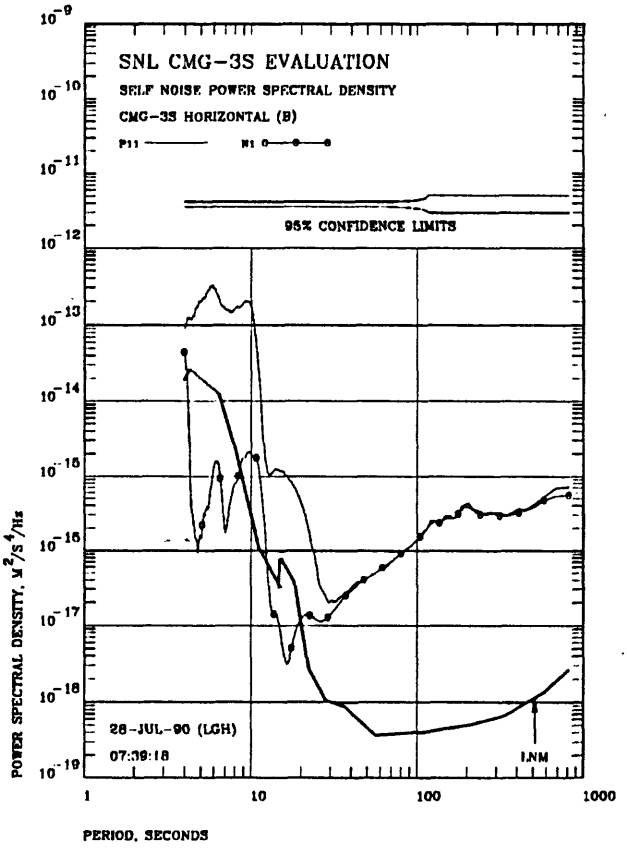

Figure 8.24 Estimated total PSD and self noise PSD of the CMG-3S (B) horizontal under a vacuum. The CMG-3S (B) horizontal selected the segments.

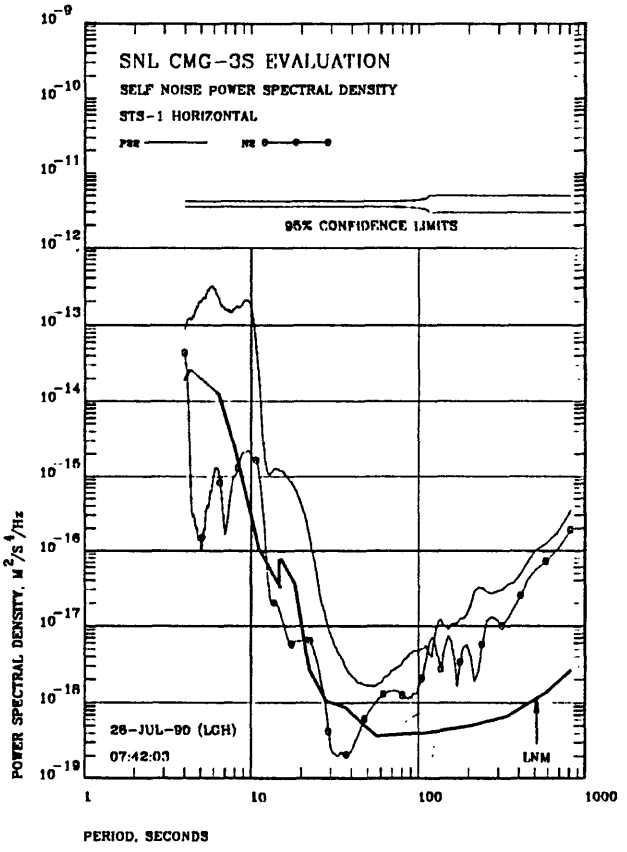

Figure 8.25 Estimated total PSD and self noise PSD of the STS-1 horizontal. The CMG-3S (B) horizontal selected the segments.

The noise PSD estimates for the CMG-3S (B) as compared with the STS-1 horizontal are shown in Figures 8.24 and 8.25 respectively. Here again, the noise estimates for the two instruments are quite similar below about 20 seconds thereby indicating misalignment whereas the estimates diverge above 25 seconds. The noise PSD estimates above 25 seconds in both figures should be indicative of instrument noise in the individual instruments.

When they were evacuated, both the CMG-3S (A) horizontal and the CMG-3S (B) horizontal were very noisy above 20 seconds or so. This noise is evident in both the noise PSD estimates for the two instruments shown in Figures 8.19 and 8.24, and in the time domain data contained in Figures 8.21 through 8.23 and Figures 8.26 through 8.29. The most logical explanation for the excess noise is that some how it was associated with the fact that the sensors were evacuated. The precise mechanism for creating the noise by simply evacuating the sensor

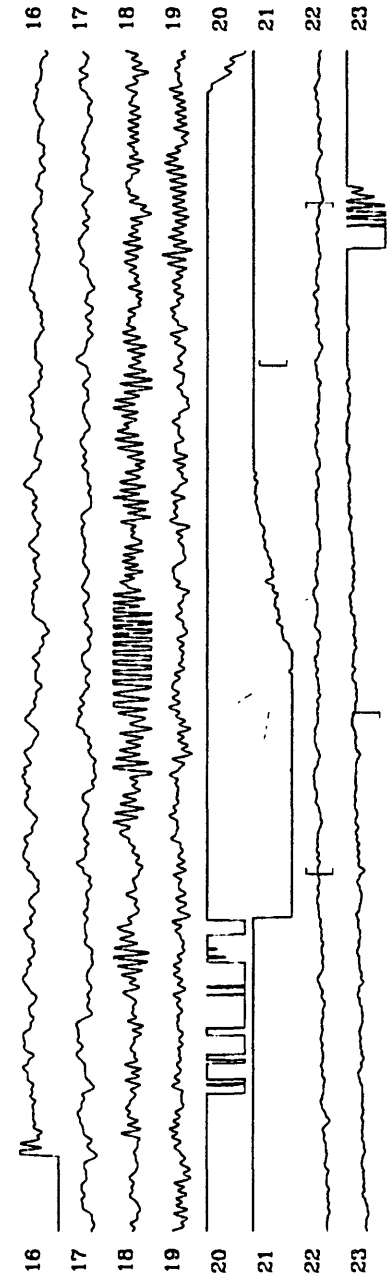

Figure 8.26 Time record for day 347 of the CMG-3S (B) horizontal when under a vacuum.

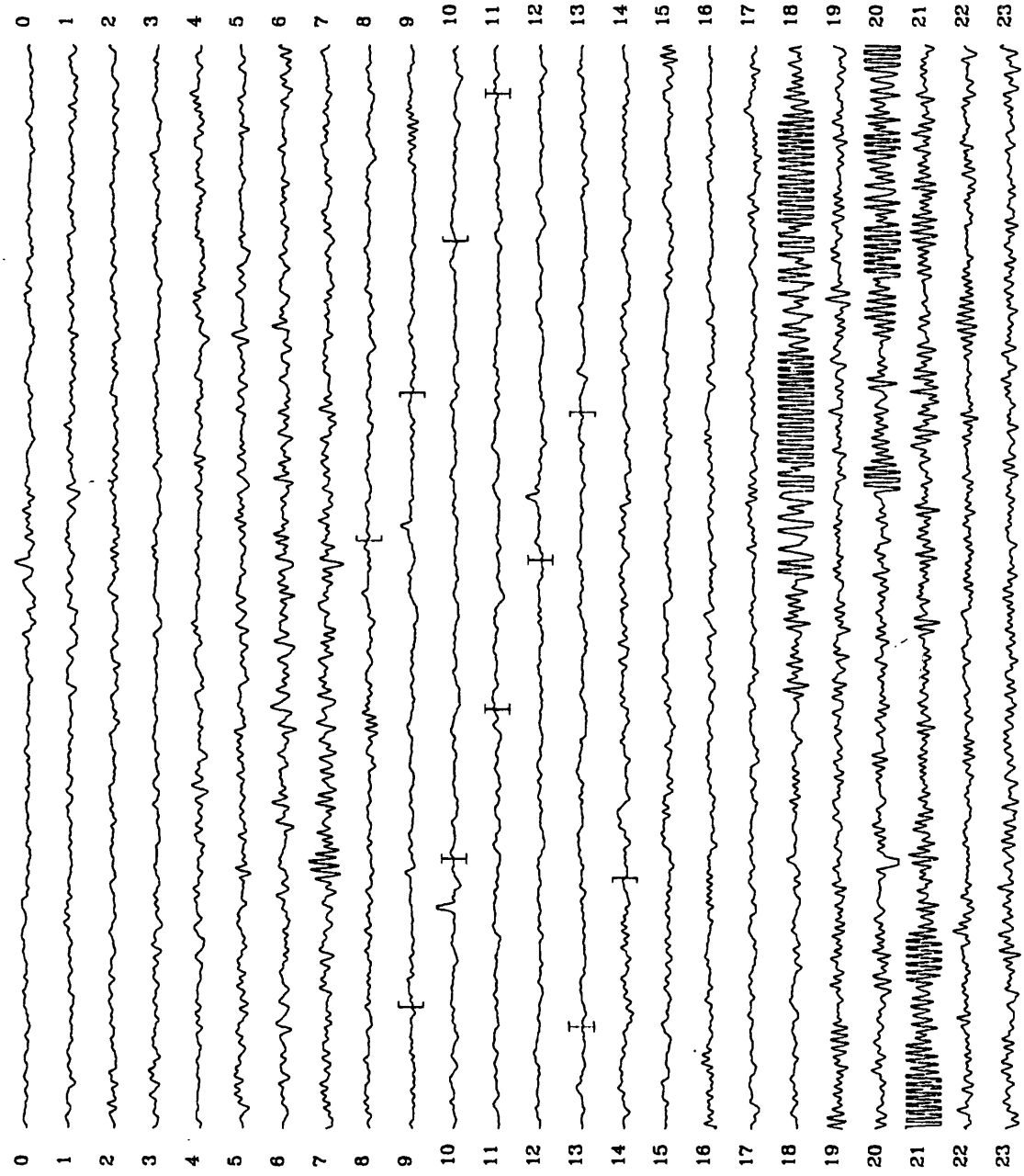

Figure 8.27 Time record for day 348 of the CMG-3S (B) horizontal when under a vacuum.

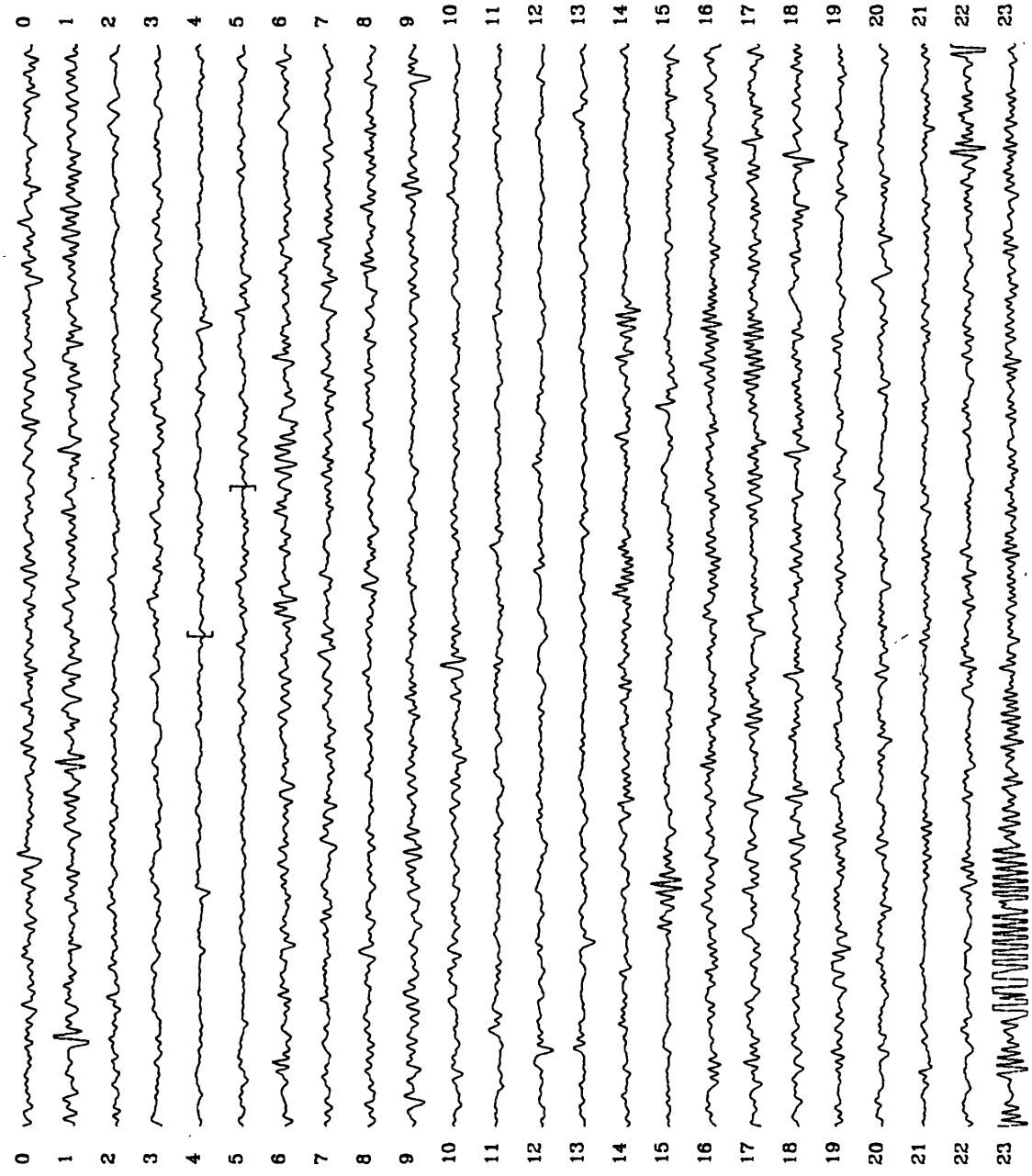

Figure 8.28 Time record for day 349 of the CMG-3S (B) horizontal when under a vacuum.

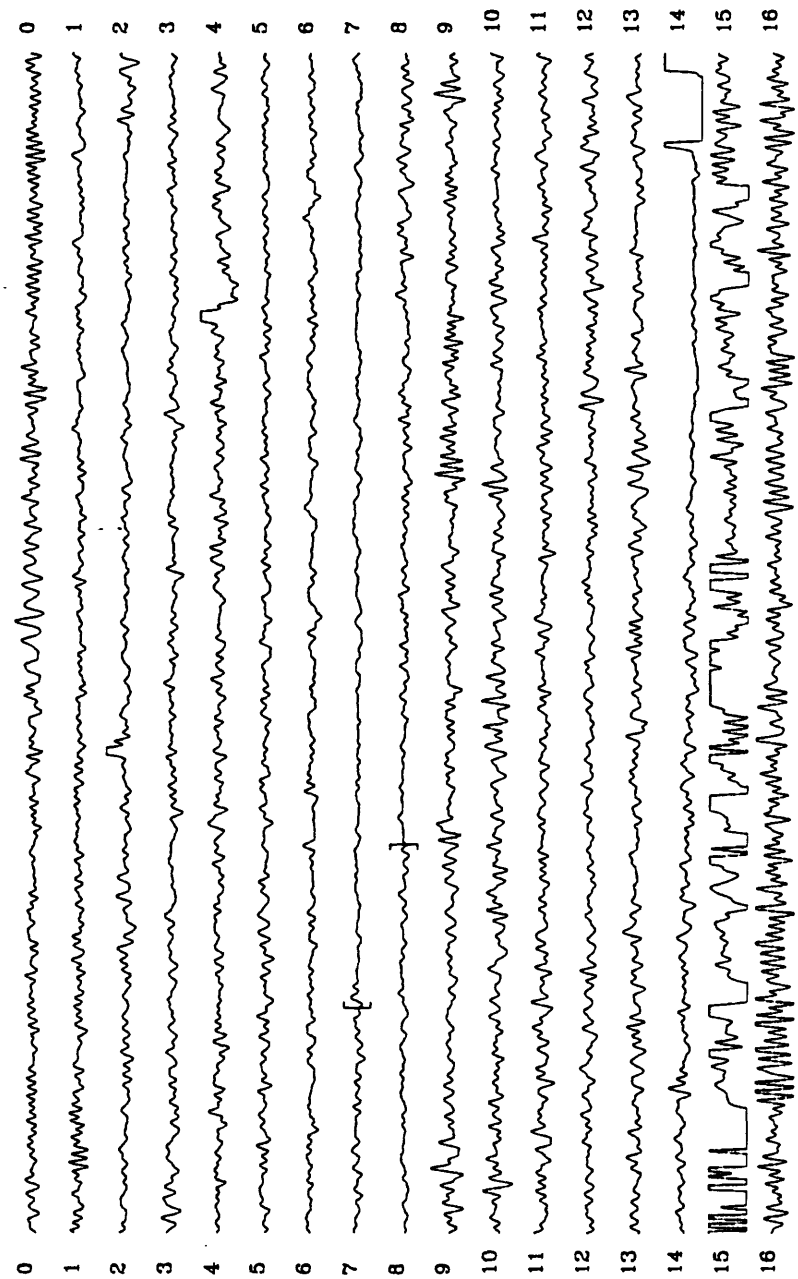

Figure 8.29 Time record for day 350 of the CMG-3S (B) horizontal when under a vacuum.

cases is not clear. Burps are visible in the time records, but there appears to be a noise source over and above the burps. One possibility is that both sensor cases were leaking at a very slow rate. Air motion inside the case created by the incoming jet of air caused by a leak would probably drive the masses quite significantly. However, a leak should also influence the vertical component; no evidence of a leak was observed previously in the vertical evacuation tests discussed in Section 8.1.

9 NORMAL SIDE-BY-SIDE OPERATION OF TWO CMG-3S's

As a final evaluation of the performance of the CMG-3S sensor system, all three components of both sensors were tested side-by-side in the "as is" configuration they were delivered in from the factory. Both sensors were sealed at atmospheric pressure. They were both installed on three point leveling plates inside a vented HGLP tank approximately 12 cm apart. The horizontal components were visually aligned with one another. A lighted 60 watt light bulb was placed on top of the HGLP tank to stratify the air inside the tank to subdue air convection.

The data from the three channels of sensor (A) was recorded on the 24 bit channels of ALQX and the data from the three channels of sensor (B) was recorded on the 16 bit channels of ALQX. Data was recorded from 1989,362,19:00:00 to 1990,001,18:00:00; however only data extending from 1989,362,19:00:00 to about 1989,365,23:00:00 was included in the analysis because a bug in ALQX-ASL software prevented the analysis of data extending over a change in year.

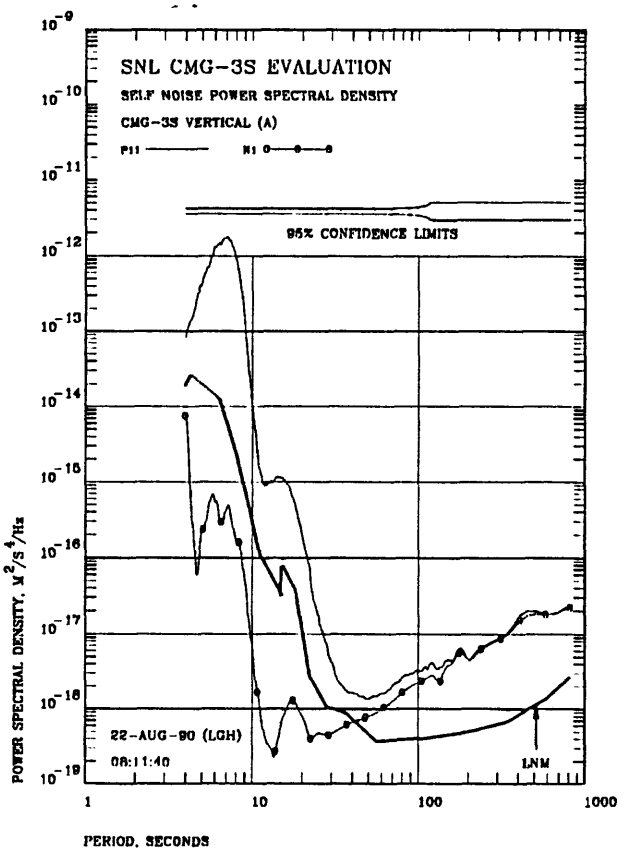

Figure 9.1 Estimated total PSD and self noise PSD of the CMG-3S (A) vertical. The CMG-3S (A) vertical selected the segments.

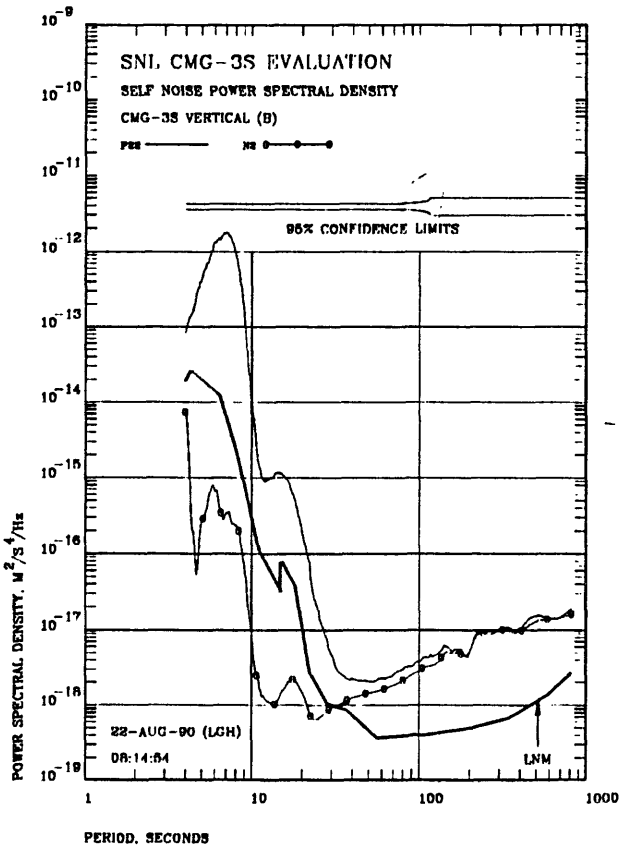

Figure 9.2 Estimated total PSD and self noise PSD of the CMG-3S (B) vertical. The CMG-3S (A) vertical selected the segments.

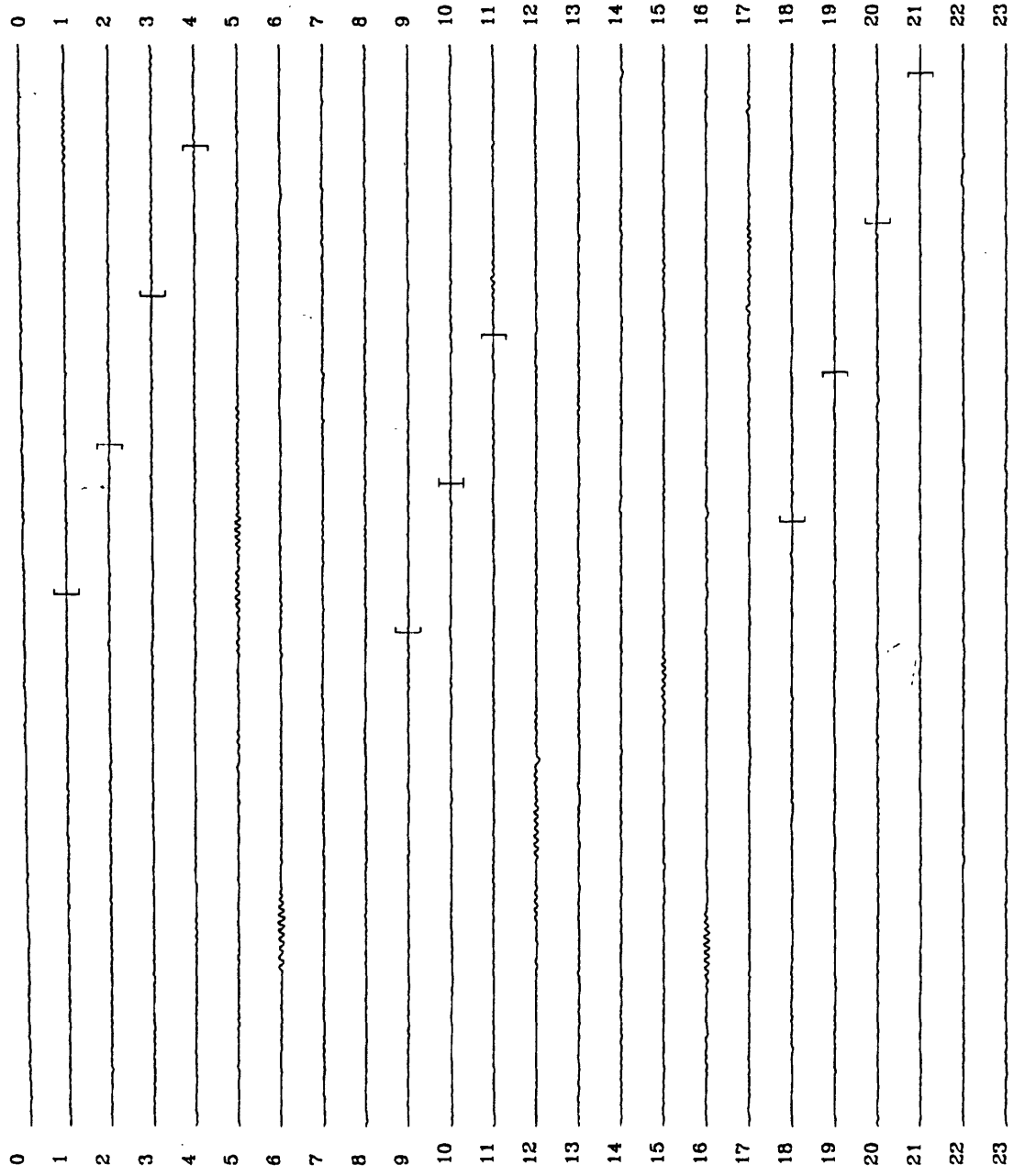

Figure 9.3 Time record for day 363 of the CMG-3S (A) vertical.

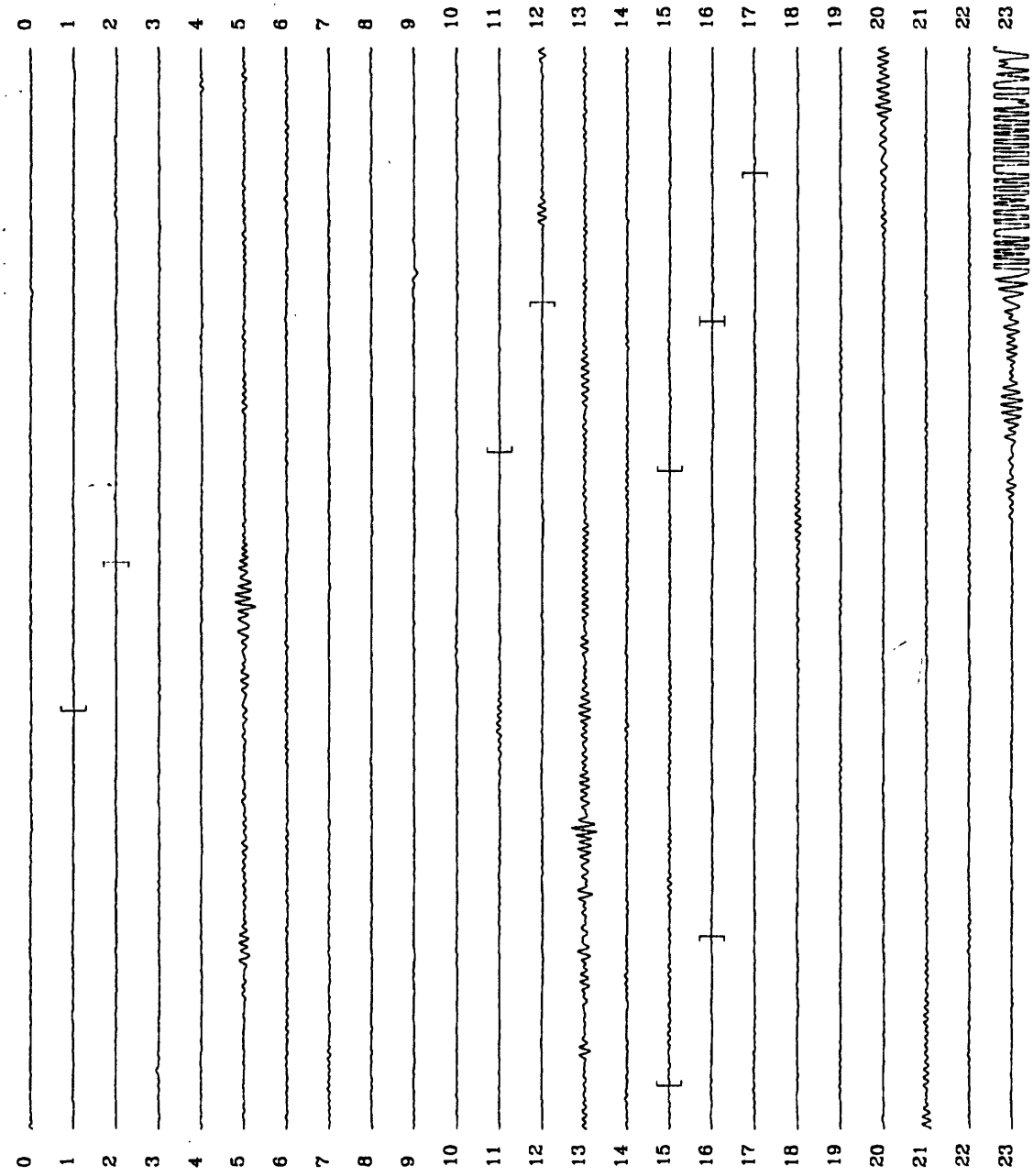

Figure 9.4 Time record for day 364 of the CMG-3S (A) vertical.

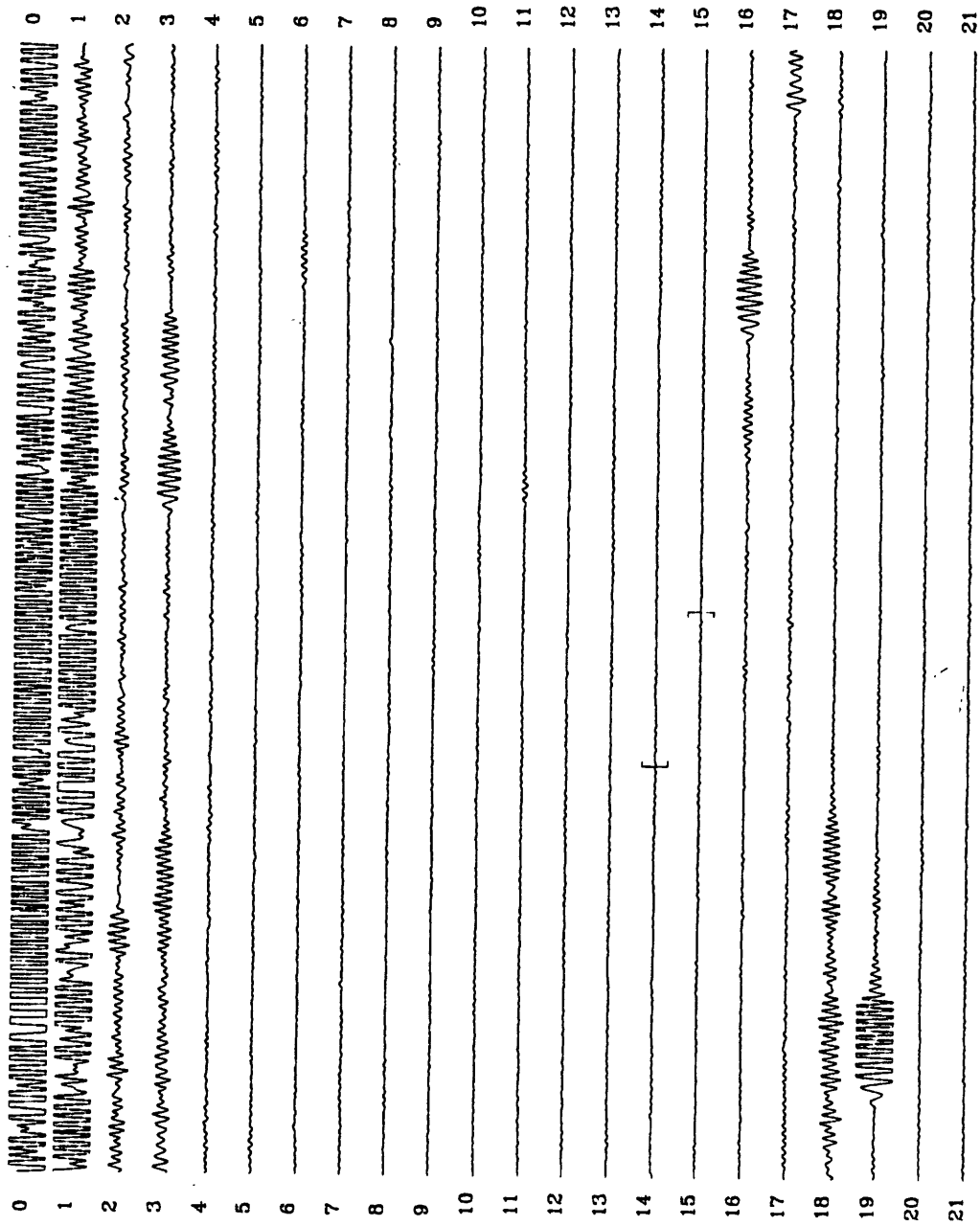

Figure 9.5 Time record for day 365 of the CMG-3S (A) vertical.

Figures 9.1 and 9.2 contain noise PSD estimates for the CMG-3S (A) and the CMG-3S (B) verticals. The time segments as selected for these estimates by the CMG-3S (A) vertical are shown in Figures 9.3 through 9.5. From 4 to 10 seconds, the noise estimates for both the (A) and (B) sensors in Figures 9.1 and 9.2 respectively are nearly identical. In this portion of the spectrum, the noise estimates are probably dominated by misalignment noise. From 10 seconds to 100 seconds, the noise estimate for sensor (A) is slightly lower than that for sensor (B). This difference may be due to the fact that sensor (A) selected the segments thereby favoring sensor (A). Above 100 seconds, the noise estimates are essentially identical.

The vertical time domain data for sensor (A) in Figures 9.3 through 9.5 is relatively but not completely burp free. For instance, there is a readily identifiable but quite small burp at about 9:45 on day 364 in Figure 9.4. However, inspection of the data in this figure indicates that this burp was not included in the analysis. The authors have been unable to identify any burps in the segments of data which were included in the analysis. However, small burps may exist in the included segments; they may just be so small that they are indistinguishable at the magnifications (300K) in the figures.

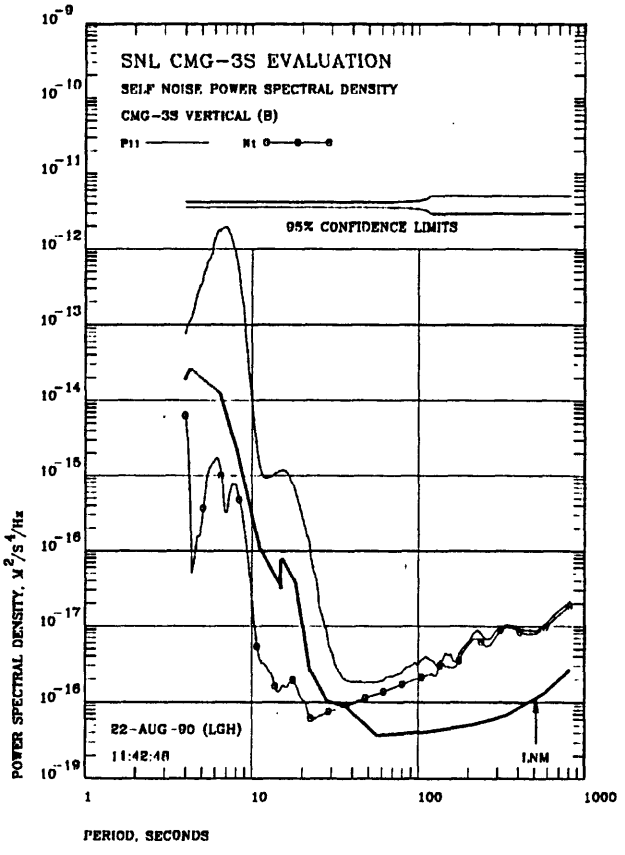

Figure 9.6 Estimated total PSD and self noise PSD of the CMG-3S (B) vertical. The CMG-3S (B) vertical selected the segments.

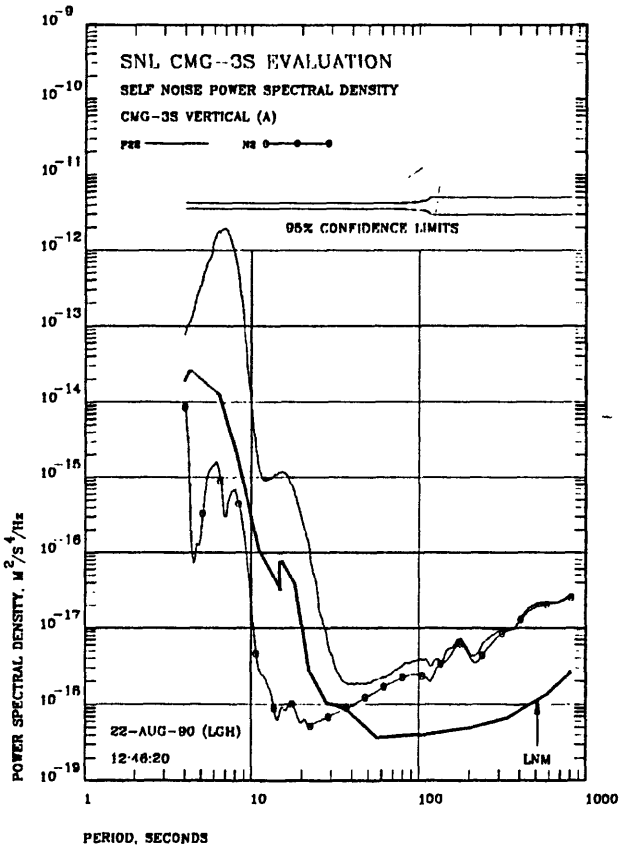

Figure 9.7 Estimated total PSD and self noise PSD of the CMG-3S (A) vertical. The CMG-3S (B) vertical selected the segments.

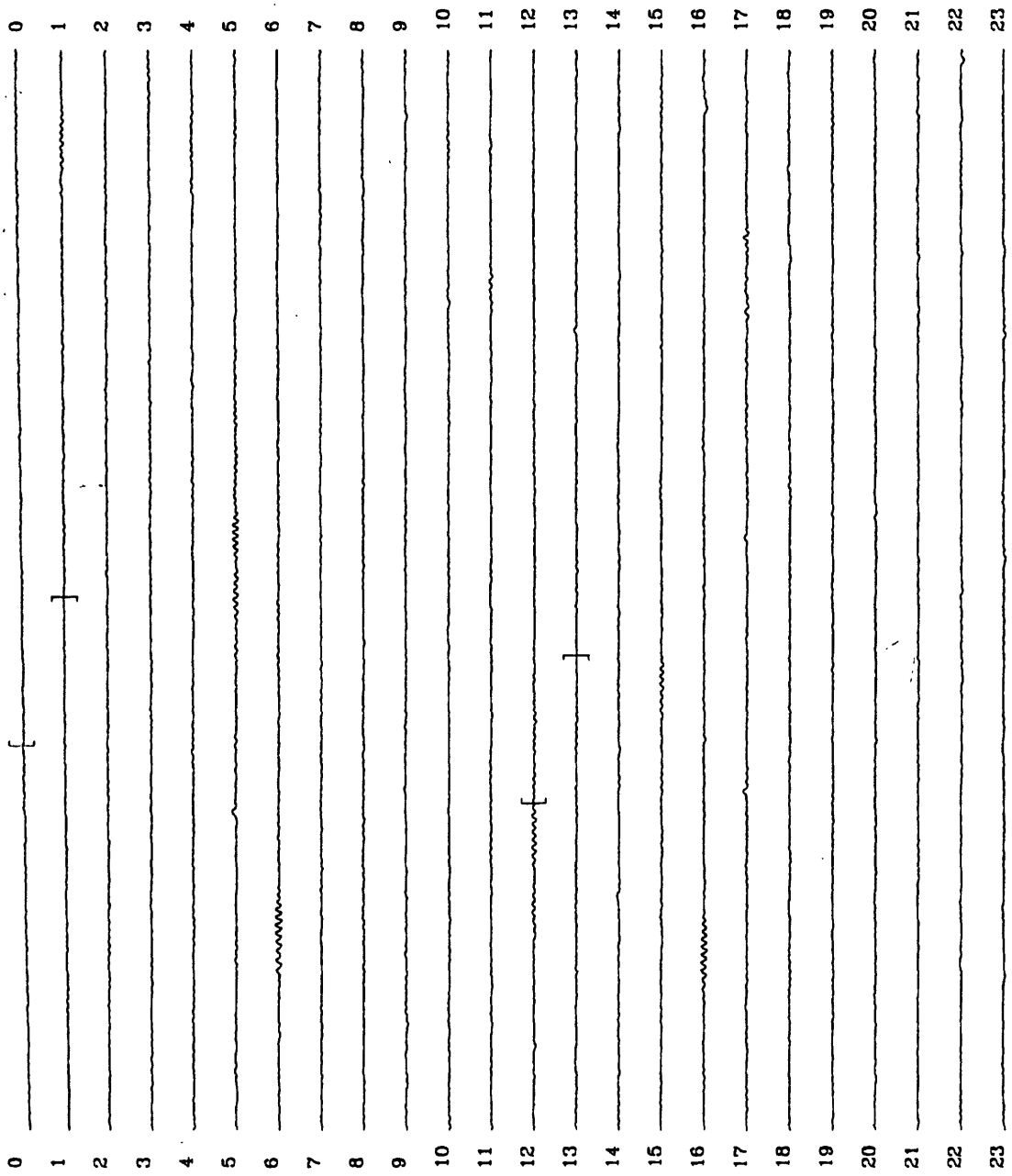

Figure 9.8 Time record for day 363 of the CMG-3S (B) vertical.

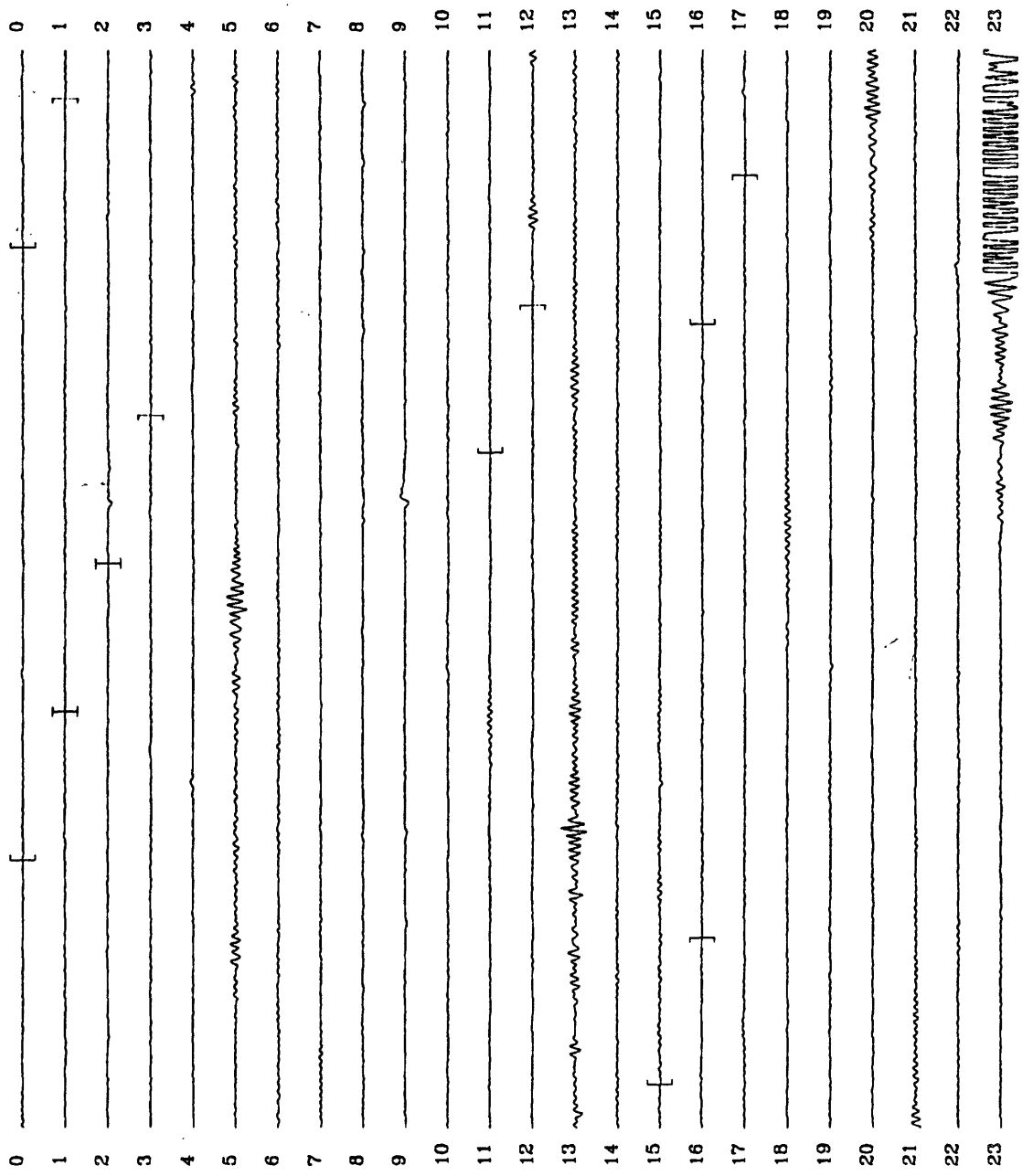

Figure 9.9 Time record for day 364 of the CMG-3S (B) vertical.

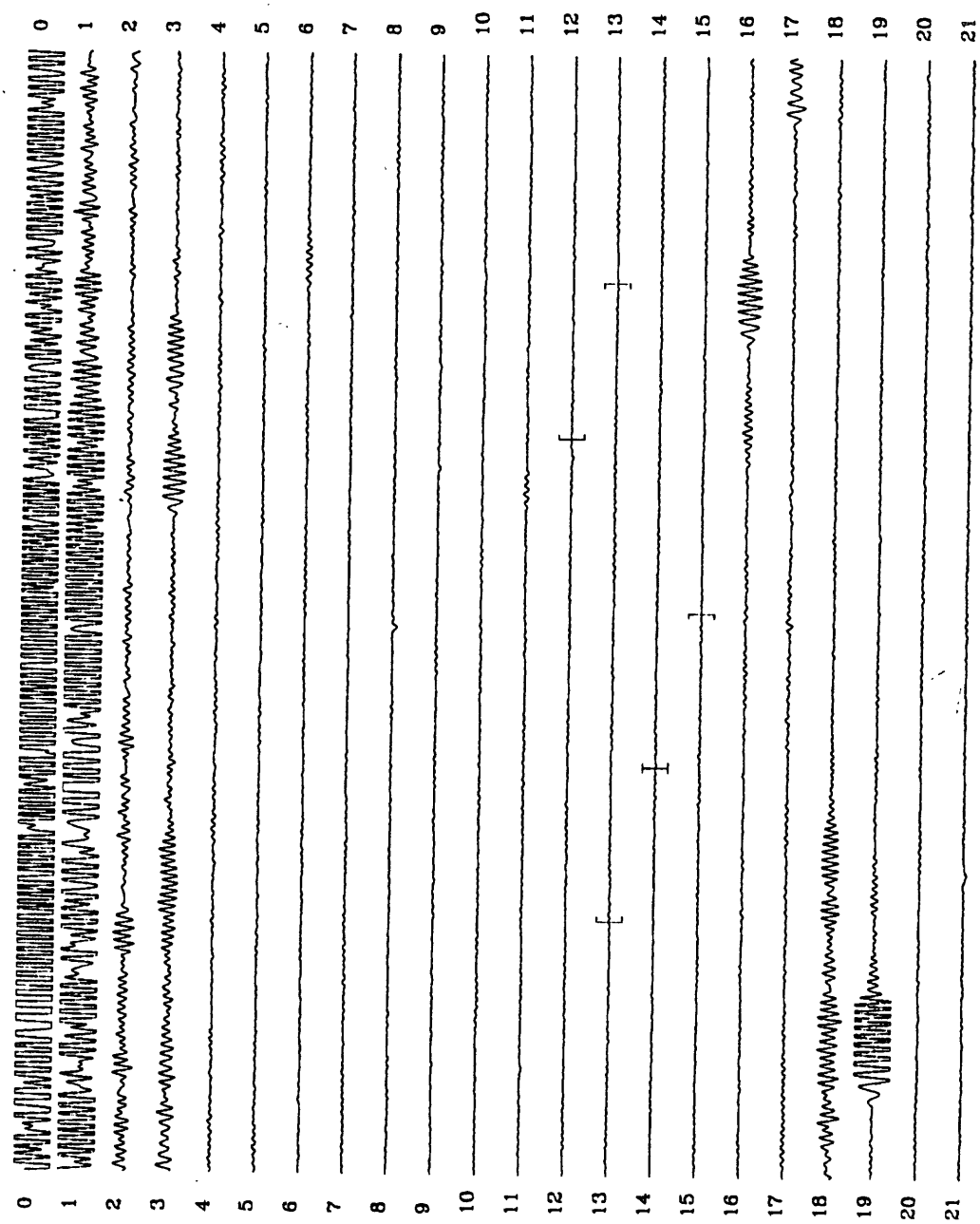

Figure 9.10 Time record for day 365 of the CMG-3S (B) vertical.

Figures 9.6 and 9.7 contain noise PSD estimates for the two CMG-3S verticals in which the roles have been reversed; sensor (B) selected the segments to be included in the analysis. The segments actually included in these figures are depicted in Figures 9.8 through 9.10. Once again the noise estimates in Figures 9.6 and 9.7 from 4 to 10 seconds appear to be dominated by misalignment noise. Above 10 seconds, both noise estimates are approximately equal to one another.

Inspection of the vertical time domain data for sensor (B) shown in Figures 9.8 through 9.10 reveals that this channel was burping more than the corresponding channel for sensor (A). For instance, significant burps are evident on day 363 at approximately 05:15, 09:55, 13:45, 17:18 and 22:59. With careful study of Figure 9.8, the reader should be able to identify more burps on day 363. On day 364 (see Figure 9.9), readily identifiable burps occur at approximately 02:35, 09:35, 17:55, and 22:45. On day 365 (see Figure 9.10), a burp occurs at 08:30. The burp at 02:35 on day 364 occurs within a segment which was included in the segments analyzed to obtain the noise estimates for the CMG-3S (B) vertical shown in Figure 9.6. The authors can not identify any more burps within included segments, but more may be present; they may be too small to be visually identified in the plots.

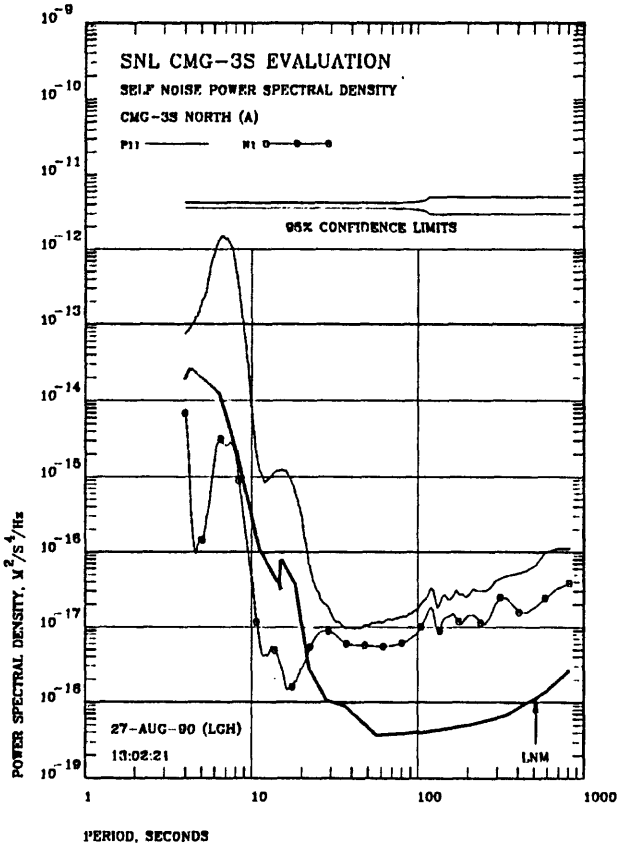

Figure 9.11 Estimated total PSD and self noise PSD of the CMG-3S (A) north. The CMG-3S (A) north selected the segments.

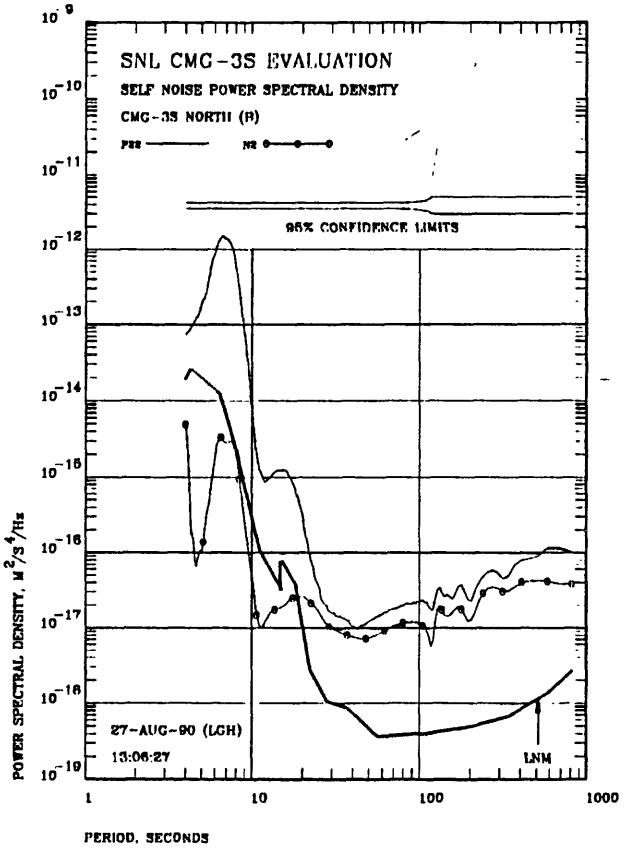

Figure 9.12 Estimated total PSD and self noise PSD of the CMG-3S (B) north. The CMG-3S (A) north selected the segments.

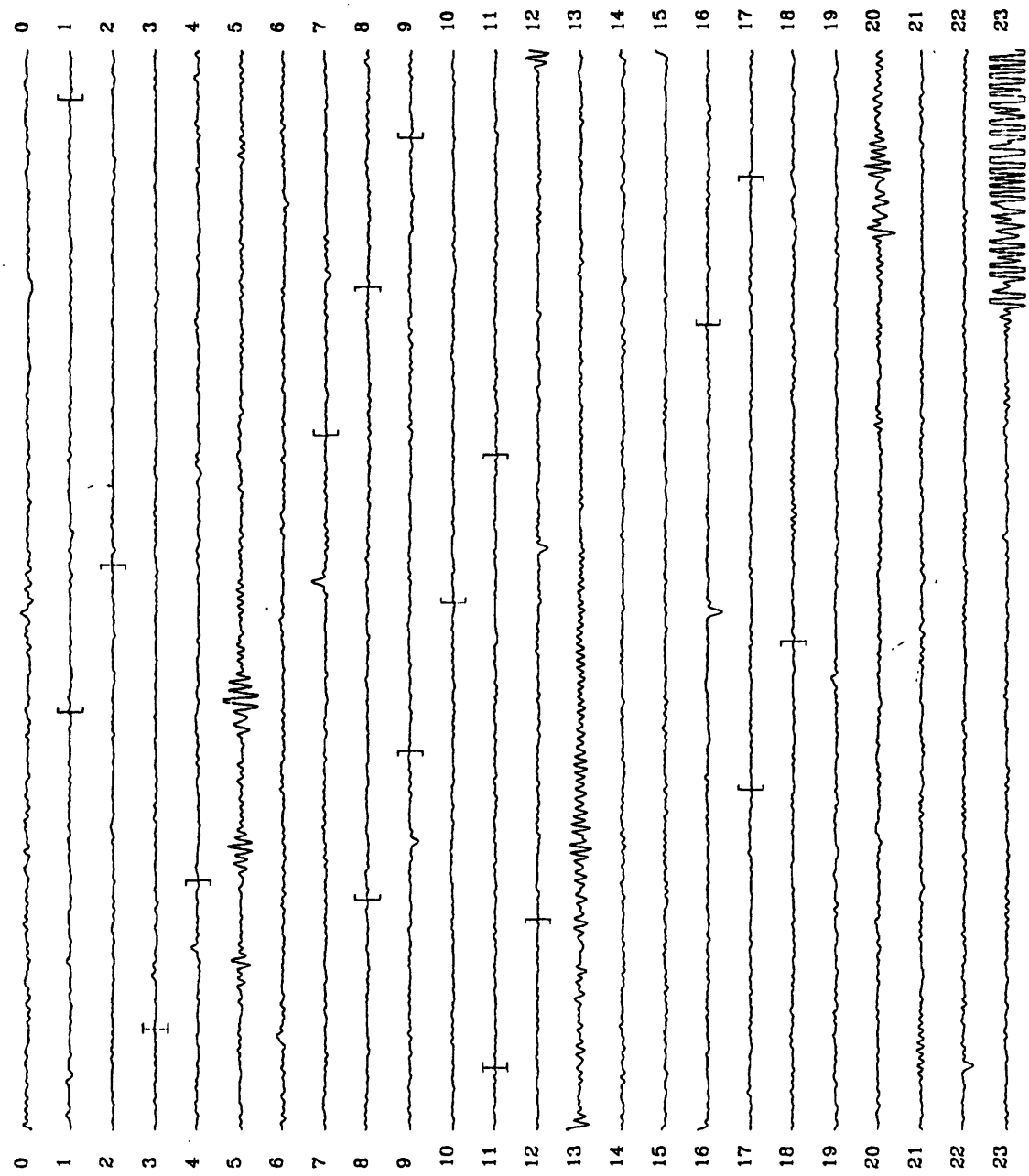

Figure 9.13 Time record for day 364 of the CMG-3S (A) north.

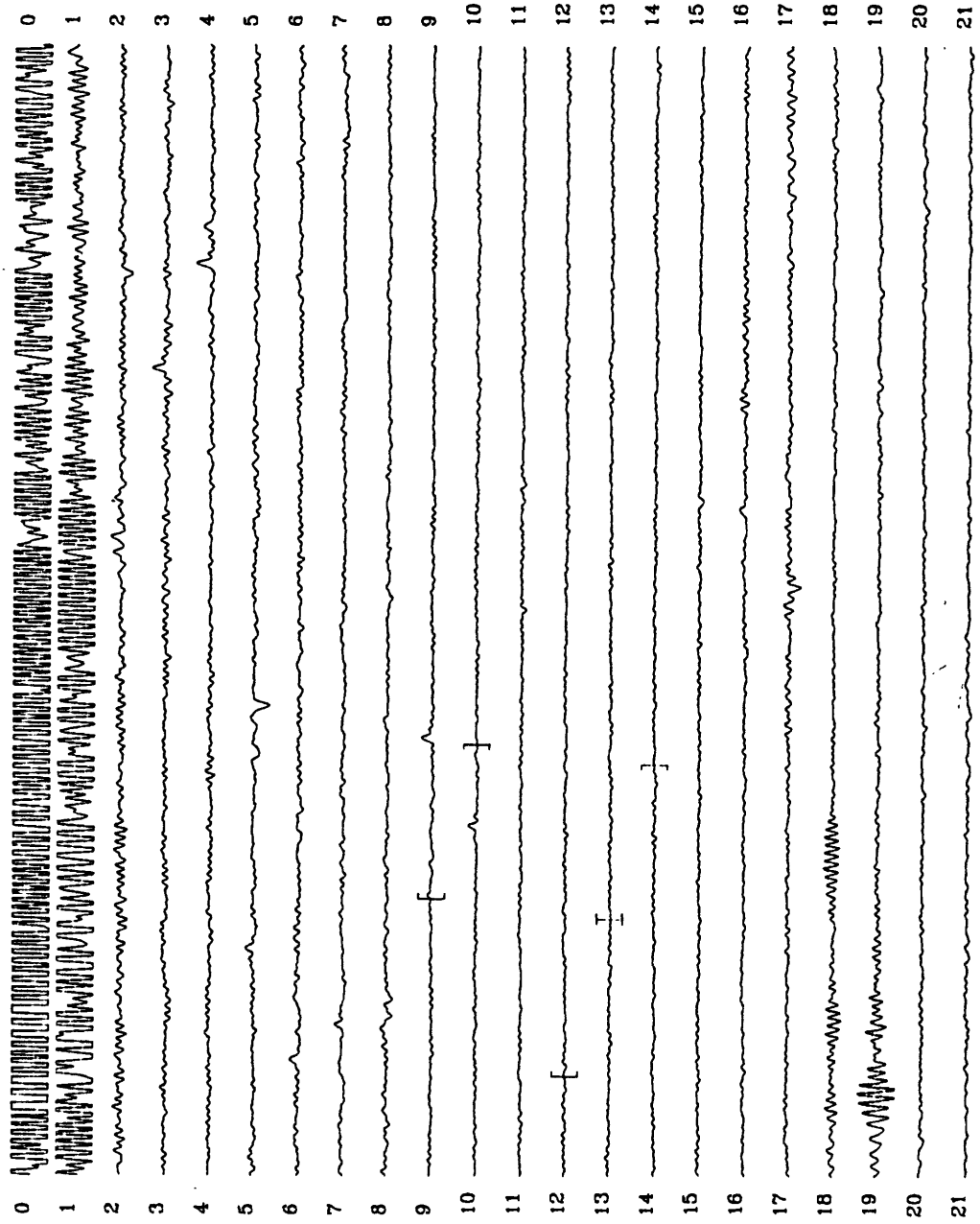

Figure 9.14 Time record for day 365 of the CMG-3S (A) north.

The fact that CMG-3S (B) vertical was burping more severely than was the (A) vertical probably explains why the estimated noise levels for the (B) vertical between 10 and 100 seconds in Figure 9.2 are higher than the corresponding estimates for the (A) vertical in Figure 9.1. The (A) vertical selected the segments for both figures; therefore, burps in the (B) vertical were probably included in the segments included in the data used to create Figure 9.2. Although a comparison of Figures 9.3 through 9.5 with Figures 9.8 through 9.10 reveals that only one of the burps identified above (the burp occurring at 09:55 on day 363) was included in data used to create Figure 9.2, additional unidentified burps may have been included in that figure.

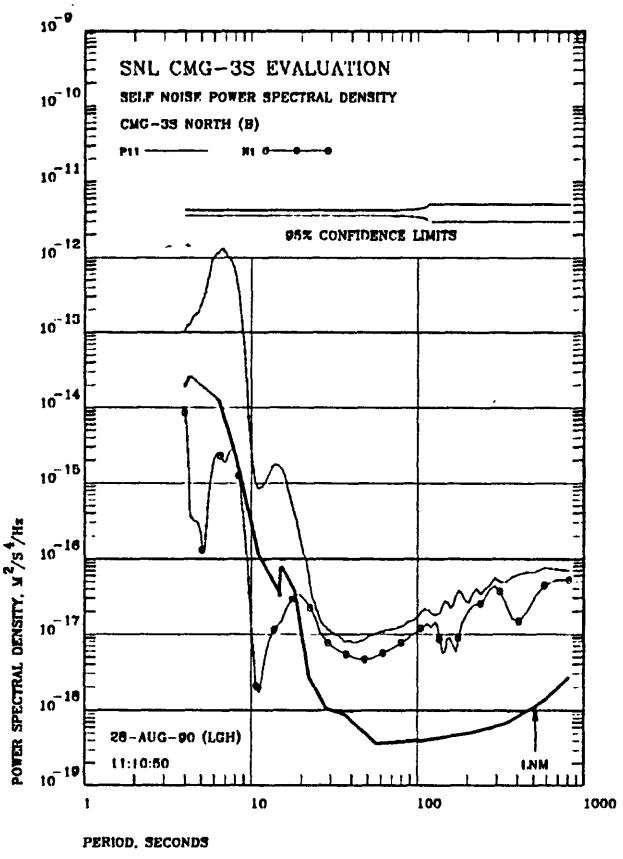

Figure 9.15 Estimated total PSD and self noise PSD of the CMG-3S (B) north. The CMG-3S (B) north selected the segments.

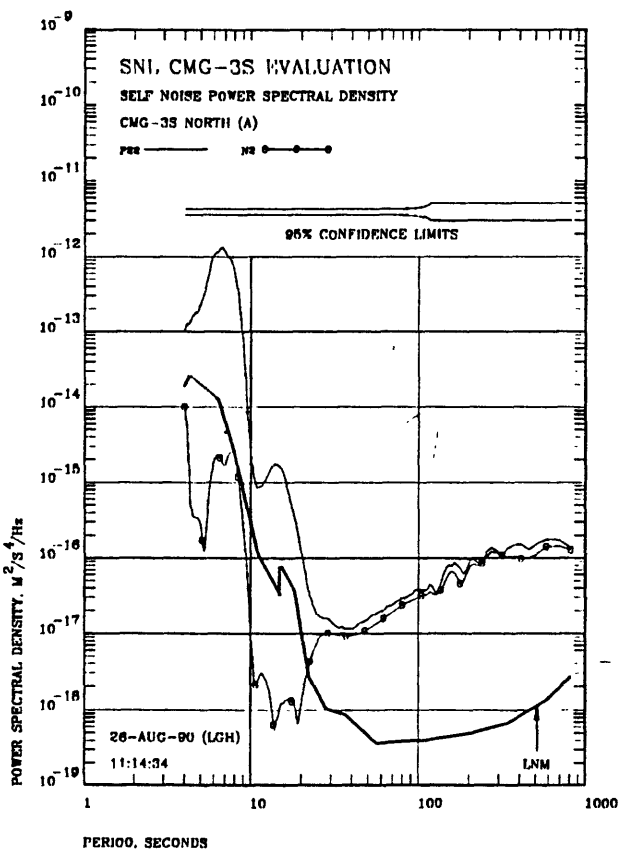

Figure 9.16 Estimated total PSD and self noise PSD of the CMG-3S (A) north. The CMG-3S (B) north selected the segments.

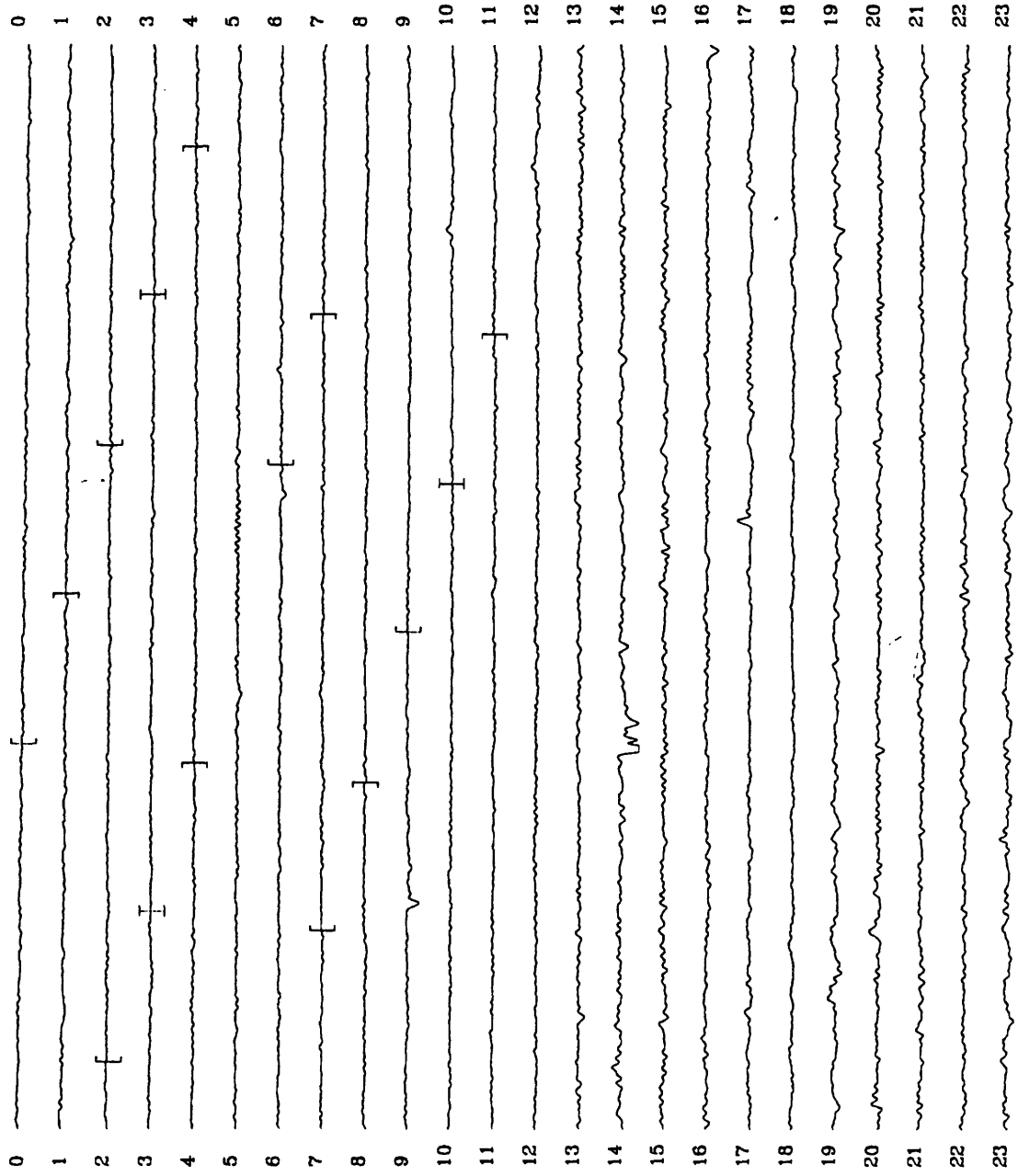

Figure 9.17 Time record for day 363 of the CMG-3S (B) north.

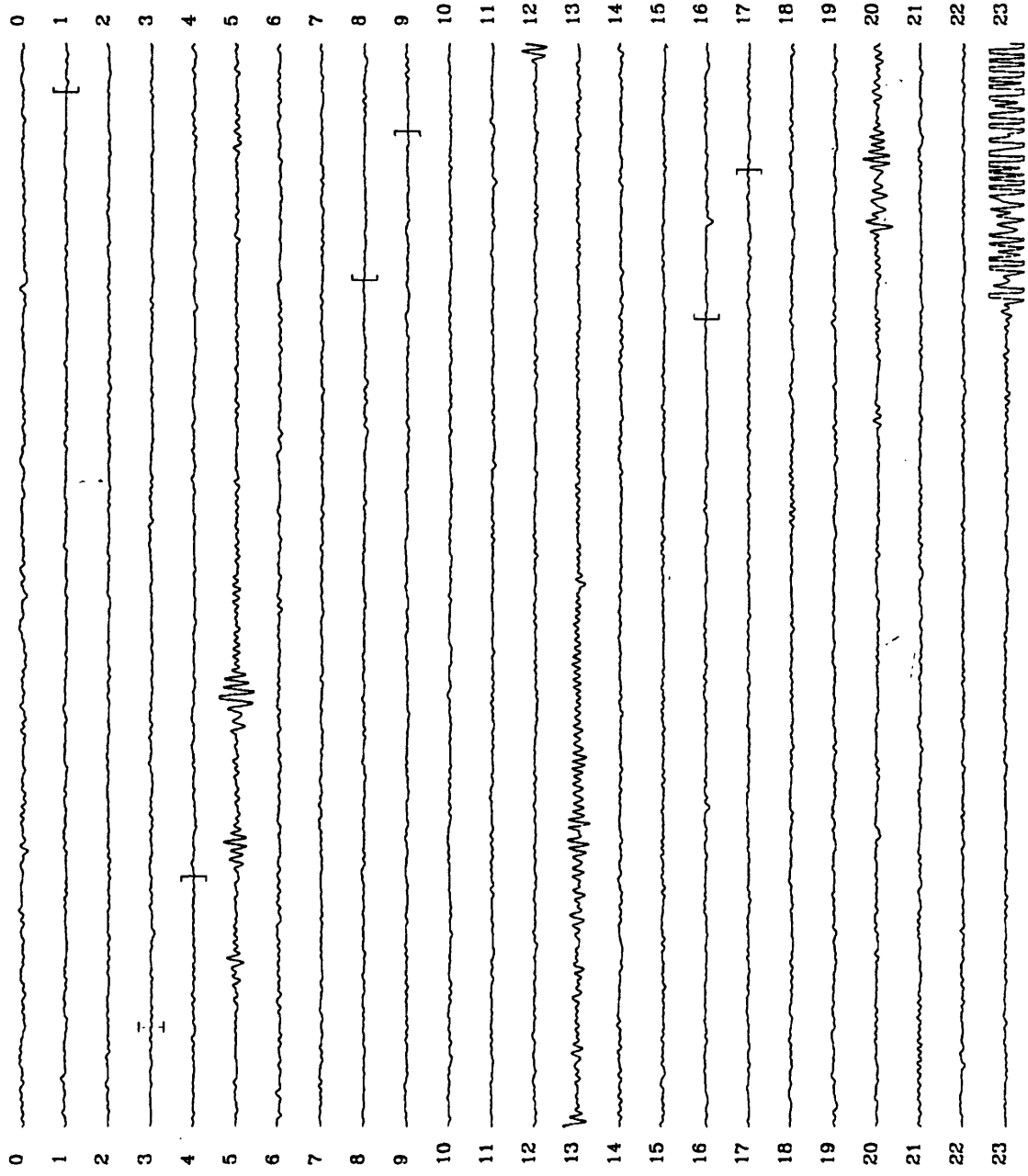

Figure 9.18 Time record for day 364 of the CMG-3S (B) north.

Figures 9.11 and 9.12 contain noise PSD estimates for the CMG-3S (A) and the CMG-3S (B) north components. The time segments as selected for these estimates by the CMG-3S (A) north are shown in Figures 9.13 and 9.14. Note that no time segments were selected by the (A) north component from the first day of the recording period (363), therefore, the time domain data for that day has not been included as a figure. It is readily evident that the north components were considerably noisier than the vertical components. From 4 to about 12 seconds, the noise estimates for the north components of the two instruments are virtually identical; once again the noise estimates in this part of the spectrum appear to be dominated by misalignment noise. From 12 to about 30 seconds, sensor (B) is considerably noisier than (A) whereas above 30 seconds, sensor (B) is slightly noisier than (A).

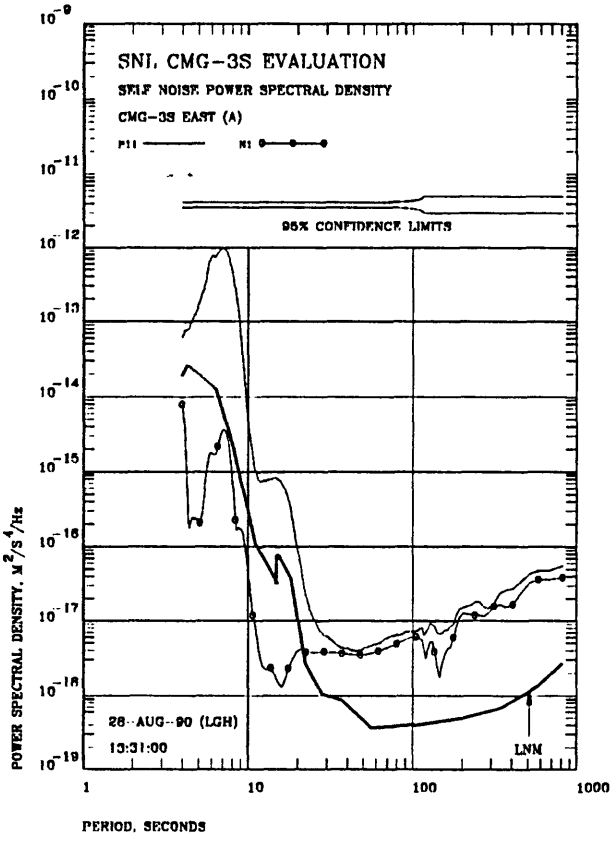

Figure 9.19 Estimated total PSD and self noise PSD of the CMG-3S (A) east. The CMG-3S (A) east selected the segments.

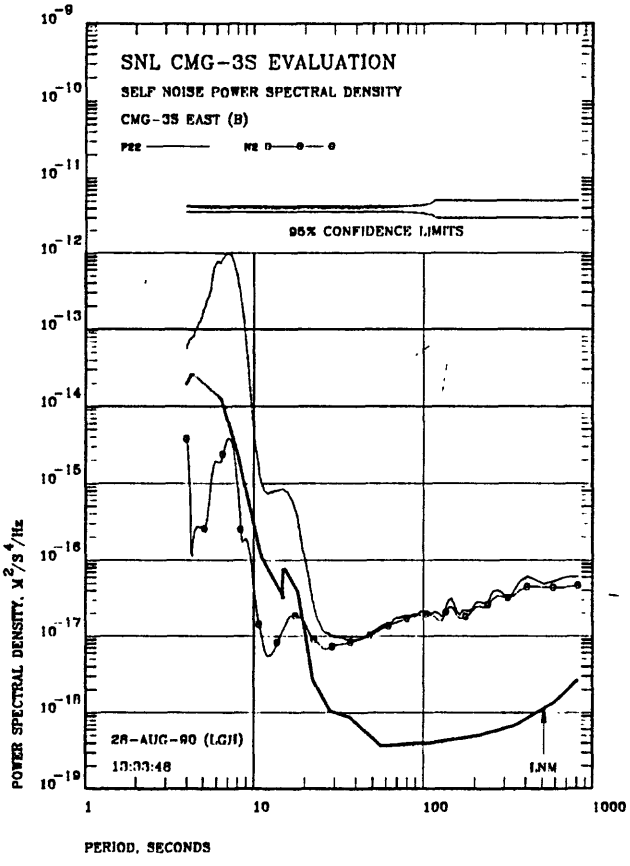

Figure 9.20 Estimated total PSD and self noise PSD of the CMG-3S (B) east. The CMG-3S (A) east selected the segments.

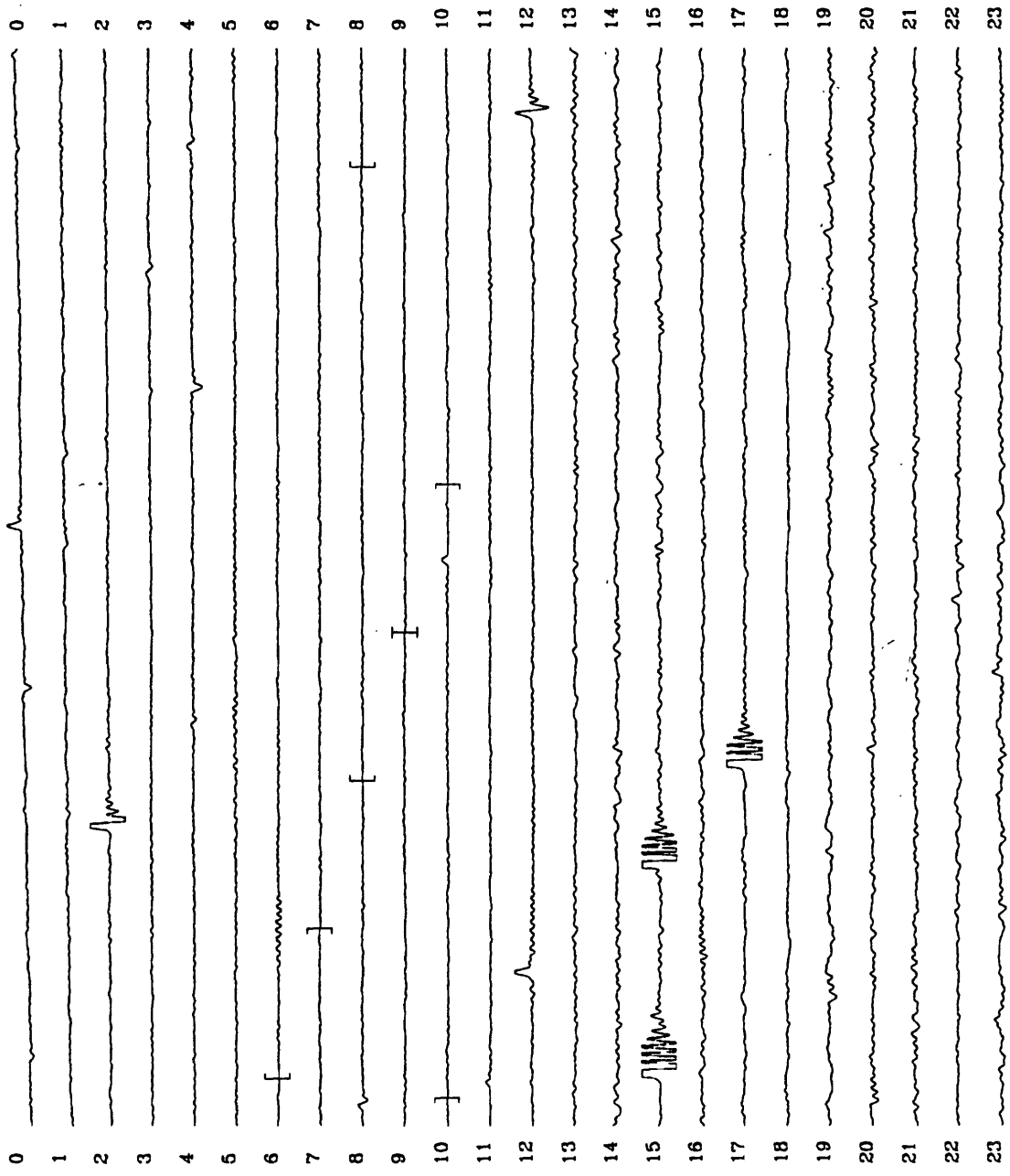

Figure 9.21 Time record for day 363 of the CMG-3S (A) east.

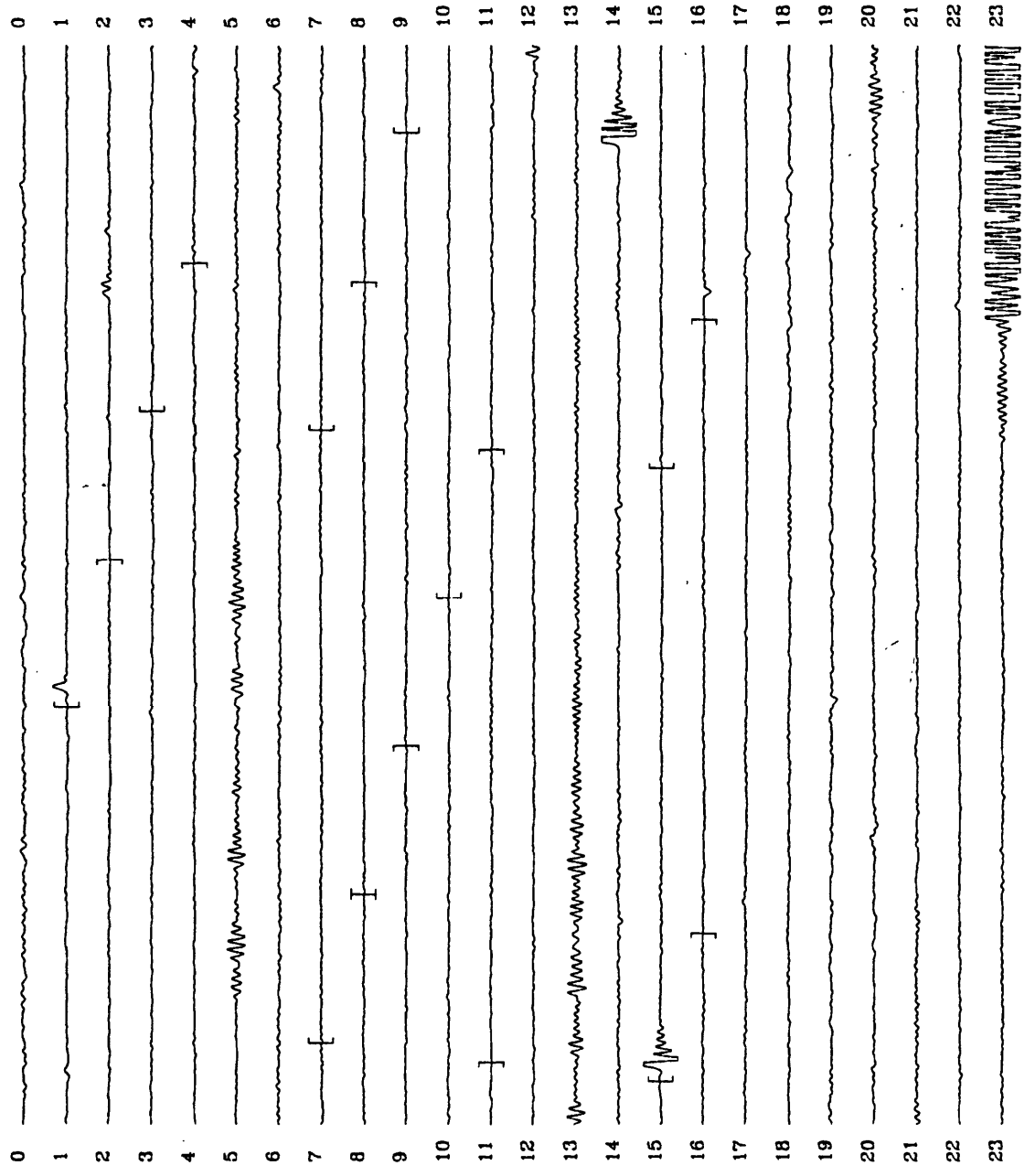

Figure 9.22 Time record for day 364 of the CMG-3S (A) east.

The north time domain data for sensor (A) in Figures 9.13 and 9.14 contains many more burps than did the vertical data in the figures above. Relatively large burps are present in day 364 (see Figure 9.13) at about 07:30, 09:18, 12:35, 16:00, 16:30, and 22:05. On day 365 (see Figure 9.14) burps occur at approximately 04:45, 05:25, 09:25, 10:20, 15:35, and 16:35. Careful study of the figures will probably reveal several additional burps not listed above. Inspection of the figures indicates that the burp at 09:18 on day 364 and the burps at 09:25 and 10:20 on day 365 were included in the data used to estimate the CMG-3S (A) north noise levels contained in Figure 9.11.

Figures 9.15 and 9.16 contain noise PSD estimates for the two CMG-3S north components in which the roles have been reversed; sensor (B) selected the segments to be included in the analysis. The time segments actually included in these figures are depicted in Figures 9.17 and 9.18. Note that no time segments were selected from the last day of recording (365) by the (B) north component, therefore, the time domain data for that day has not been included as a figure. From 4 to about 10 seconds, the noise estimates for the two channels are very similar and are probably dominated by misalignment noise. From 12 to about 30 seconds sensor (A) is quieter than sensor (B) whereas sensor (B) is quieter above 30 seconds.

The data in Figures 9.17 and 9.18 indicates that the CMG-3S (B) north component was also burping significantly during the recording period. On day 363, burps occur at 09:15, 10:45, and at numerous time during the time interval extending from 13:00 to the end of the day. The data for the second half of day 363 (12:00 to the end) is also noisier in general which may indicate that wind generated tilt is present during that time period. On day 364, burps probably occur during hour 01 and at 16:48. Other burps probably exist on both day 363 and day 364 but they are difficult to identify because of the nature of the background. Of the burps listed above, the one at 10:45 on day 363 and the one at 16:48 on day 364 occurred in segments which were included in the noise PSD estimate shown in Figure 9.15

Figures 9.19 and 9.20 contain noise PSD estimates for the CMG-3S (A) and the CMG-3S (B) east components. The time segments as selected for these estimates by the CMG-3S (A) east are shown in Figures 9.21 and 9.22. Note that no time segments were selected by the (A) east component from the last day of the recording period (365), therefore, the time domain data for that day has not been included as a figure. Figures 9.19 and 9.20 indicate that the east components are just as noisy as the north components. From 4 to about 12 seconds the noise estimates for the two sensors are very similar as they should be if misalignment is dominating the noise estimate. Above 12 seconds, the noise estimate for sensor (A) is significantly lower than that for sensor (B). This may be due to the fact that sensor (A) selected the data to be included in the noise analysis.

The east time domain data for sensor (A) shown in Figures 9.21 and 9.22 indicates that this component was burping quite badly at times. On day 363, burps occur at 00:25, 00:35, 03:45, 03:40, 03:55, 08:03, 10:33, 12:10, 12:55, 15:05, 15:15, and 17:20. The burps at 12:55, 15:05, 15:15, and 17:20 are especially large; they represent major perturbation to this sensor. The data for the second half of day 363 is also noisier in general which may indicate that wind generated tilt is present during that time period. This (A) east time data is very similar to the (B) north data during the same time period in Figure 9.17. On day 364, burps occur at 01:25, 14:50, 15:05, and 16:45. Of the burps listed explicitly above, those occurring at 10:33 on day 363 and at 01:25 and 15:05 on day 364 lie in time segments selected to be analyzed.

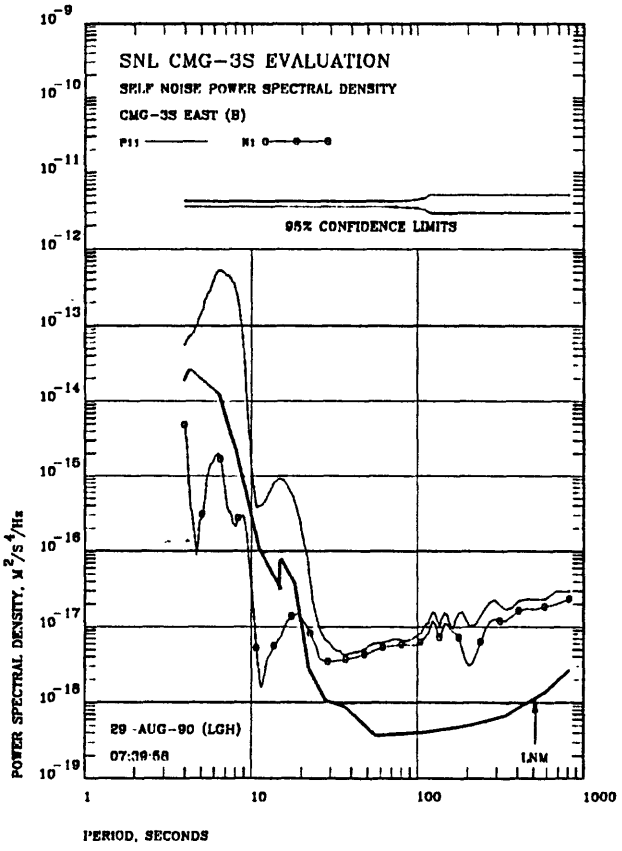

Figure 9.23 Estimated total PSD and self noise PSD of the CMG-3S (B) east. The CMG-3S (B) east selected the segments.

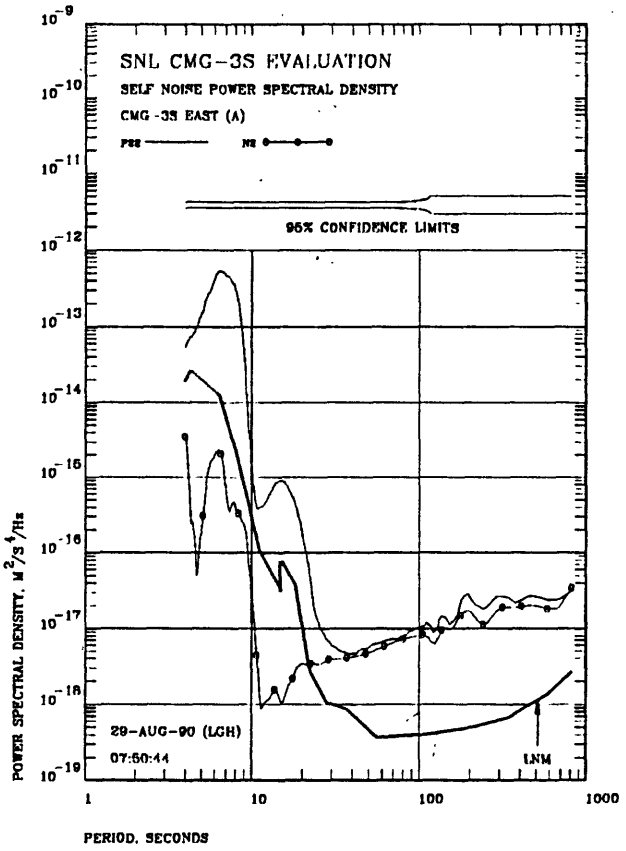

Figure 9.24 Estimated total PSD and self noise PSD of the CMG-3S (A) east. The CMG-3S (B) east selected the segments.

Figures 9.23 and 9.24 contain noise PSD estimates for the two CMG-3S east components in which the roles have been reversed; sensor (B) selected the segments to be included in the analysis. The time segments actually included in these figures are depicted in Figures 9.25 through 9.27. From 4 to about 12 seconds, the noise estimates for the two channels are very similar and are probably dominated by misalignment noise. From 12 to about 30 seconds sensor (B) is noisier than sensor (A). Above 30 seconds, the calculated sensor noise levels are very nearly the same.

The data in Figures 9.25 through 9.27 indicates that the CMG-3S (B) east component was burping significantly. On day 363, burps are found at approximately 01:23, 09:27, 14:20, 14:55, 15:05, 15:15, and probably 21:15. On day 364, burps occurred at 03:35, 07:50, 08:40, 20:40, 22:50, and 23:05. On day 365, burps can be found at approximately 06:50, 09:45, 10:58, 12:40, 14:45, 15:08, 18:25, and 19:35. Numerous smaller burps can probably be identified on all three days by closer inspection. Inspection of the figures shows that the segments selected by the CMG-3S (B) east component contained several identifiable burps.

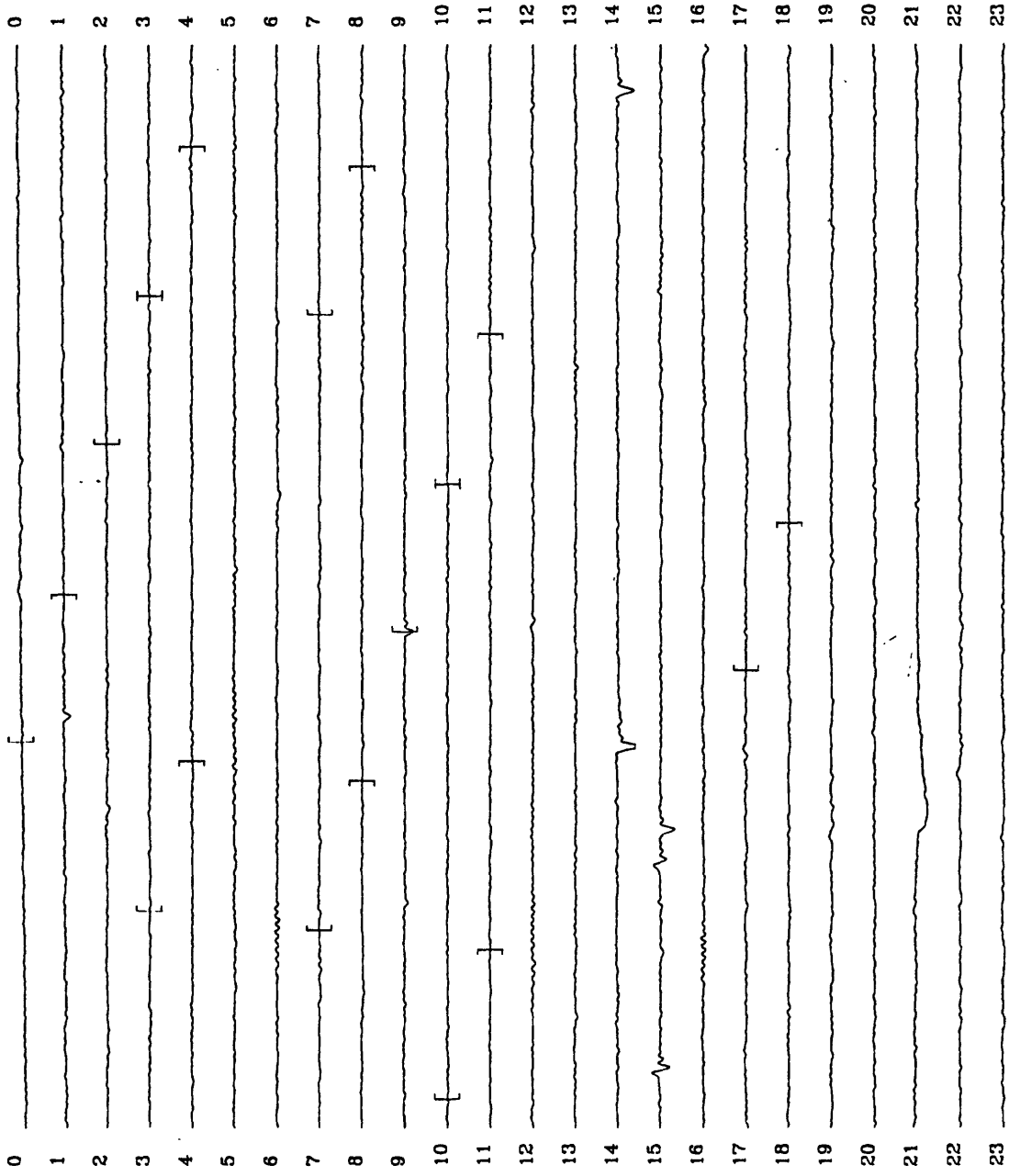

Figure 9.25 Time record for day 363 of the CMG-3S (B) east.

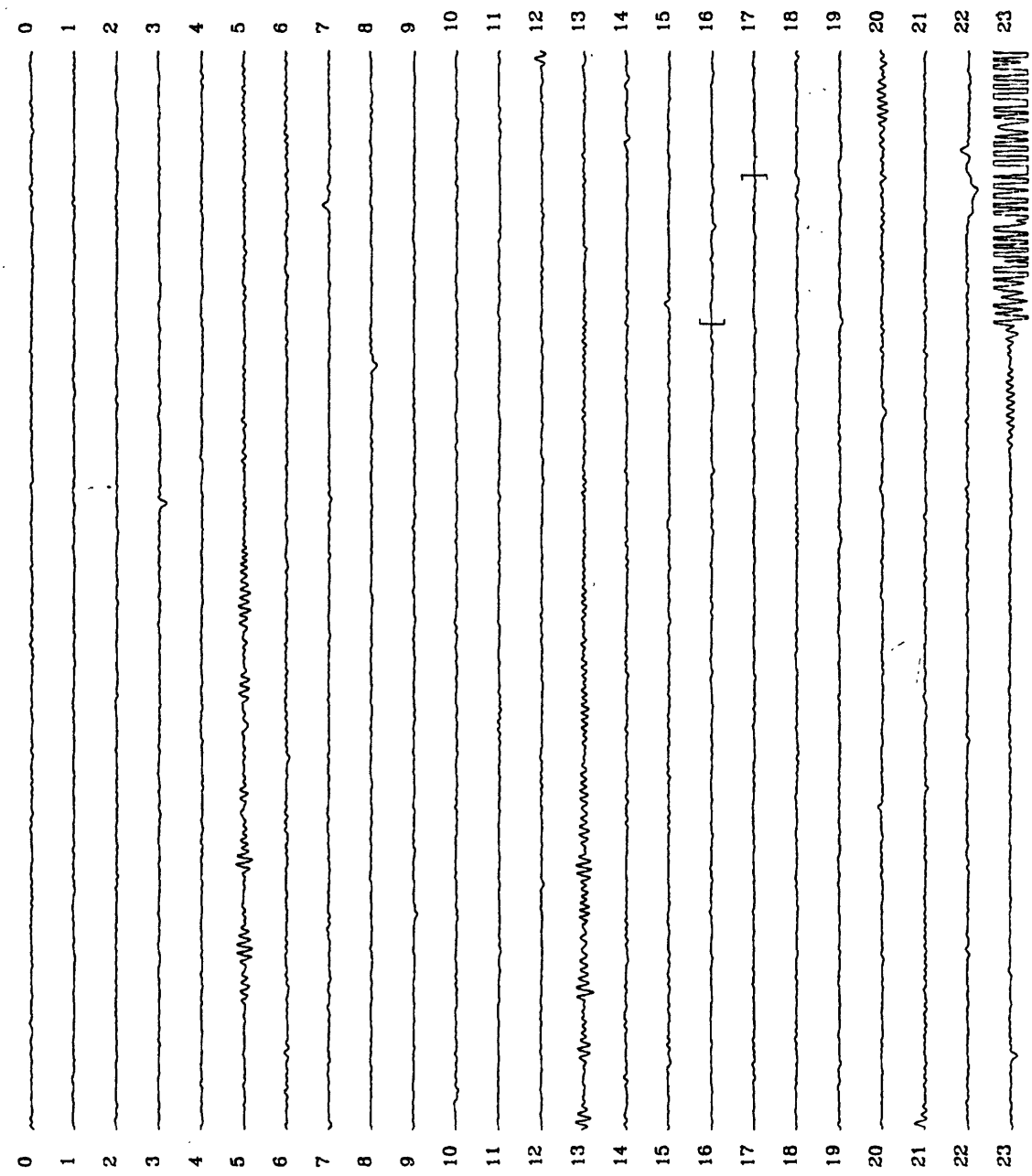

Figure 9.26 Time record for day 364 of the CMG-3S (B) east.

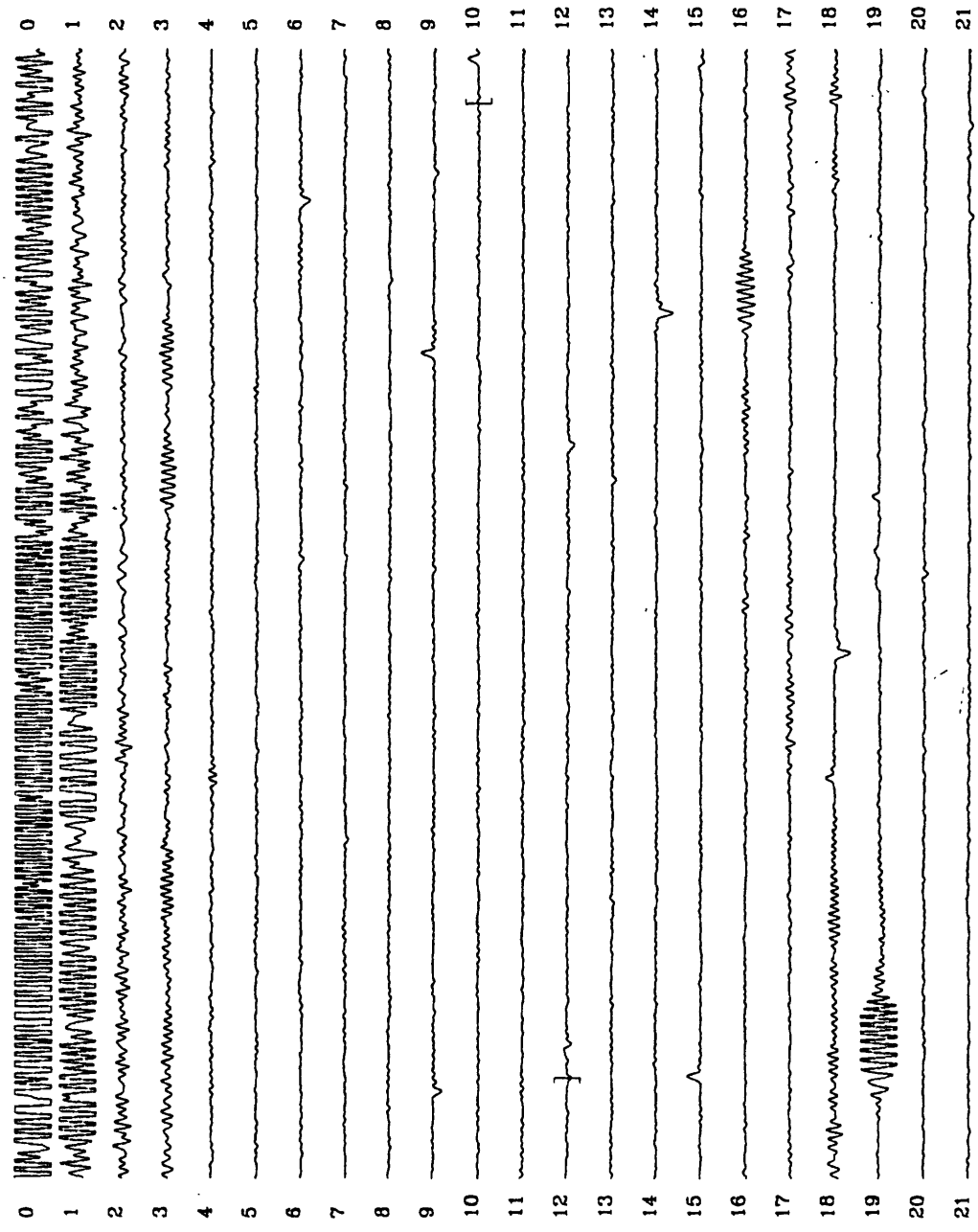

Figure 9.27 Time record for day 365 of the CMG-3S (B) east.

10 CONCLUSIONS

This report presented the results of the evaluation of the performance of the CMG-3S sensor system in several test configurations. In general, the system performed quite well at long periods. However, "burping" was found to be a problem in several of the tests and time constraints did not permit sufficient time to evaluate whether or not the "burps" would die out with time.

The sensor system was tested for its sensitivity to atmospheric pressure changes by installing it in a HGLP tank to isolate it from those changes. No atmospheric pressure change sensitivity was found.

A new installation technique, which utilized plaster of paris as a potting medium, was tested with positive results at high frequencies. The use of plaster of paris as a potting medium improved the reproducibility of the recorded PSD estimates in the high frequency portion of the spectrum (above about 20 Hz) eliminating abnormal "humps" in the PSD estimates which are believed to be due to extraneous resonances in the sensors mechanical structure. At long periods the use of the plaster of paris potting installation technique produced mixed results. When potted, the vertical components of the CMG-3S sensors performed quite well; however, the horizontal components were incredibly noisy. The source of the horizontal noise may have been the plaster of paris curing process; a longer duration investigation is needed to evaluate this possibility.

The effects of operating the sensors with their cases roughed down to create a partial vacuum were evaluated with limited success. Pumping the cases down significantly increased the severity of sensor "burping" of both the vertical and horizontal components. The "burping" might have died off with time, but once again a longer duration investigation is needed to evaluate this possibility.

Finally, the two CMG-3S sensor systems were operated in a configuration which was as near to a borehole configuration as could be reasonably be simulated in a vault. The long period performance of the vertical component was improved with the system noise level remaining below the low noise model up to at least 40 seconds. The long period performance of the horizontal components was reduced with the system noise level remaining below the low noise model up to about 20 seconds. Significantly more "burping" was present in the horizontal components; this problem may die out with time but once again a longer duration investigation is needed to evaluate this possibility.

The authors emphasize that time is the essential ingredient in conducting truly quantitative evaluations of long period seismic instrumentation. Rushing the evaluation process results in measuring the effects of the installation process, not the characteristics of the instrument. Once the instrument is installed in a particular configuration, the effects of the installation must be allowed to dissipate to quite low levels before the instrument system noise can be qualitatively measured. Patience!!!

11 CREDITS AND ACKNOWLEDGMENTS

Several people were involved in this effort and contributed in varying degrees to its successful conclusion. Sean Keane (Bendix) helped with the plaster of paris potting operation and assisted with solving communications interface problems with the CMG-3S sensors. Alvin Garcia (ASL) assisted with the design and fabrication of several mechanical assemblies.

Finally one of the authors (Holcomb) would like to take this opportunity to apologize to Jim Durham (SNL retired) for failing to reference (in Holcomb, 1990) Jim's early work on misalignment noise (see Durham, 1982). Holcomb also extends thanks to Jim for calling attention to this omission. The omission was certainly not intentional; it was a result of a poor memory on the part of the author.

12 REFERENCES

Bendat, Julius S., Piersol, Allan G., (1971),"Random Data: Analysis and Measurement Procedures: *John Wiley & Sons, Inc.*

Durham, H. B., (1982), "Incoherence of Seismic Signals from Closely Spaced KS-36000 Seismometers": *Sandia National Laboratories Systems Research Report*

Halbert, Scott E., Buland, Ray, Hutt, Charles R., 1988. Standard for the Exchange of Earthquake Data (SEED), Version V2.0, USGS

Holcomb, L. Gary, (1989),"A Direct Method for Calculating Instrument Noise Levels in Side-by-Side Seismometer Evaluations": *U.S. Geological Survey Open-File Report 89-214, 35 p.*

Holcomb, L. Gary, (1990),"A Numerical Study of Some Potential Sources of Error in Side-by-Side Seismometer Evaluations": *U.S. Geological Survey Open-File Report 90-406, 40 p.*

Peterson, J., Hutt, Charles R., Holcomb, L. Gary, (1980)."Test and Calibration of the Seismic Research Observatory" *U. S. Geological Survey Open-File Report 80-187, 86 p.*

Stearns, Samuel D., (1975),"Digital Signal Analysis" *Hayden Book Company, Inc., Rochelle Park, New Jersey*

CMG-3S Z's

FLOAT

NOT POTTED

10/13/89
10:14 M

CMG-3S Z's - not potted

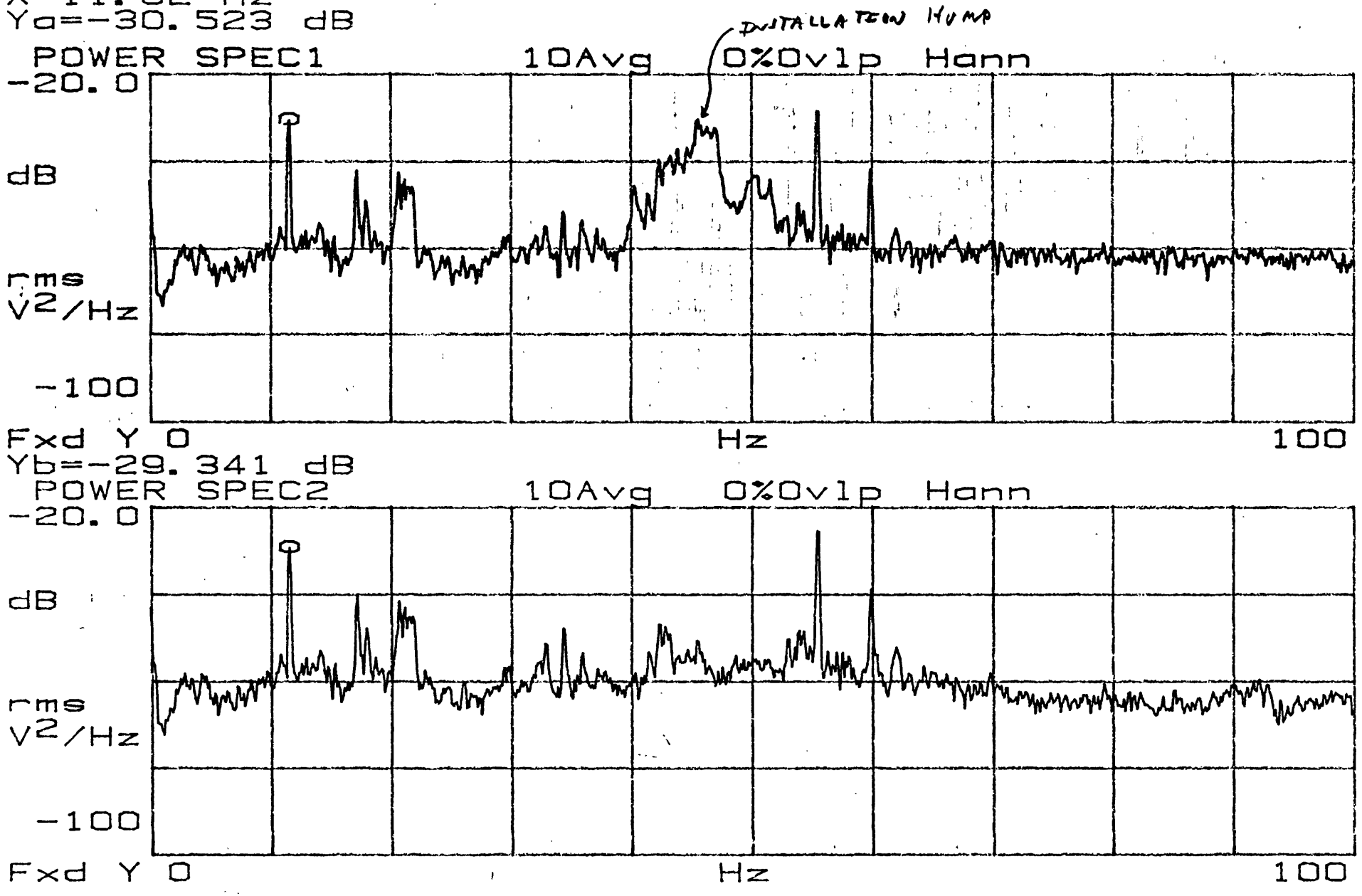

Z's

Figure A.1

CMG-3 NS's NOT POTTED

10/13/89
9:50 MDT

Float

CMG-3S NS's – not potted

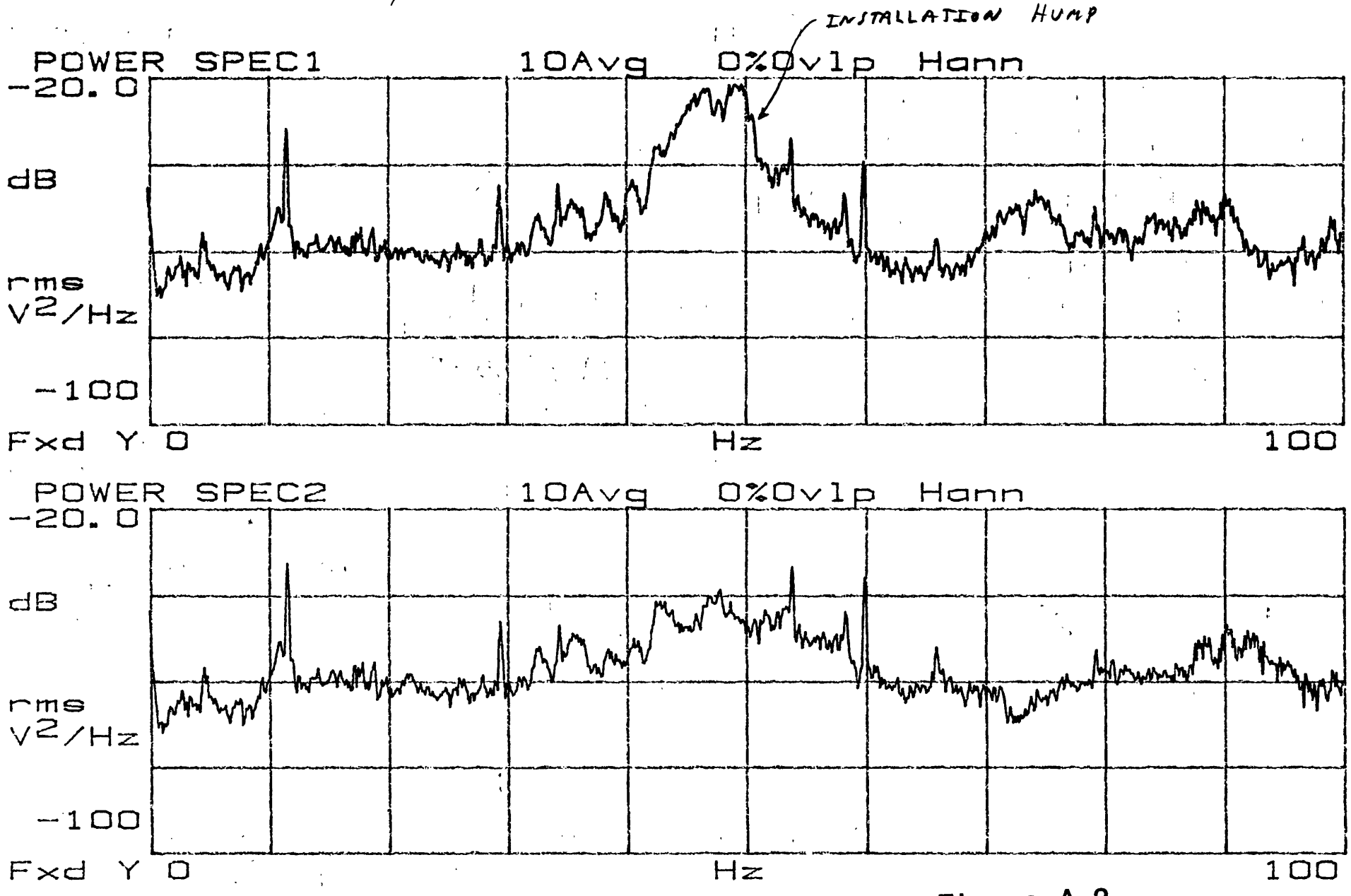

Figure A.2

Range = 632 mV

N-S's

FLOAT NOT POTTED 16:20 MIT

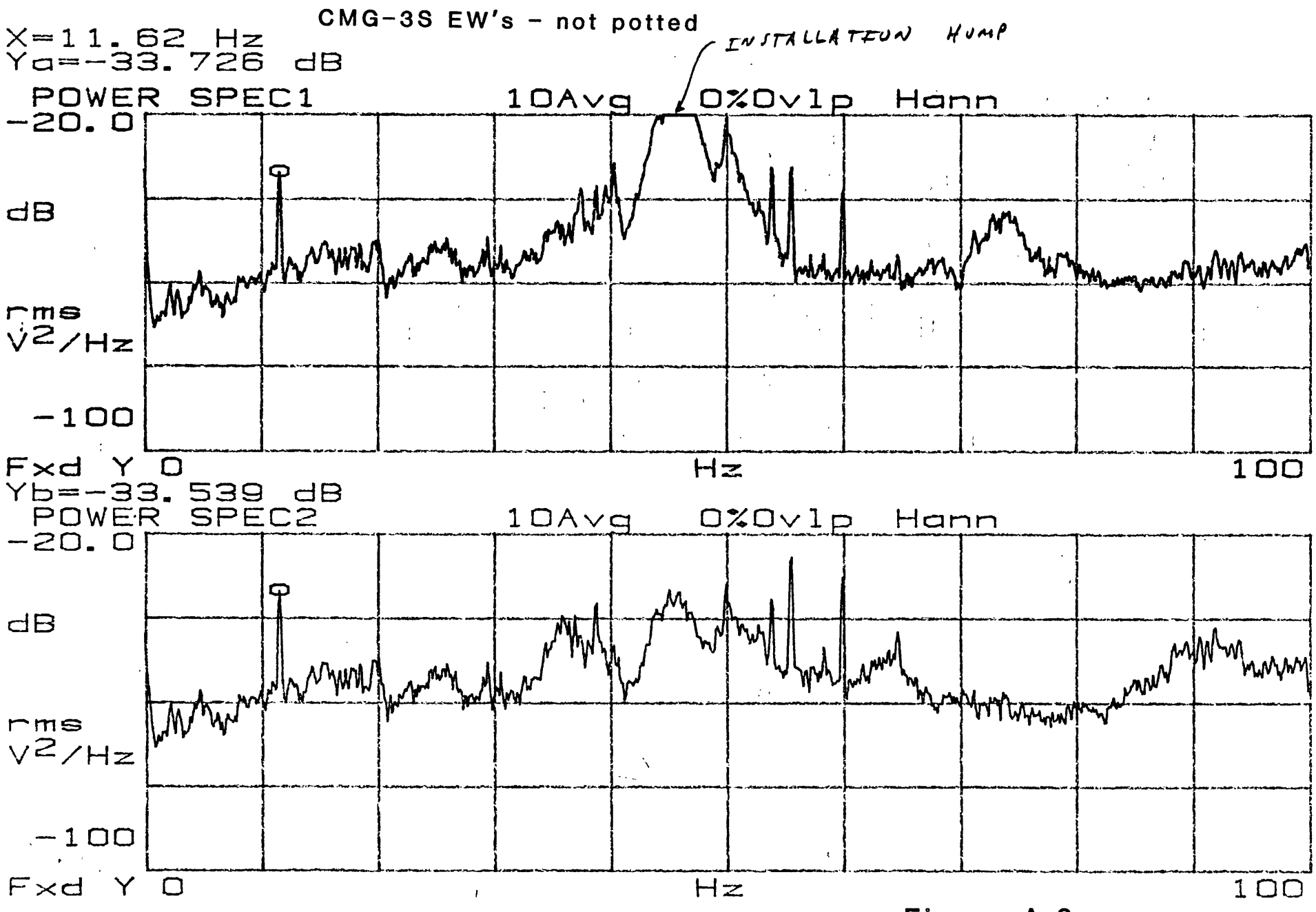

Figure A.3

E-W'J

CMG-3S Z's
FLOAT

Z's

10/13/89
10:14 MDT

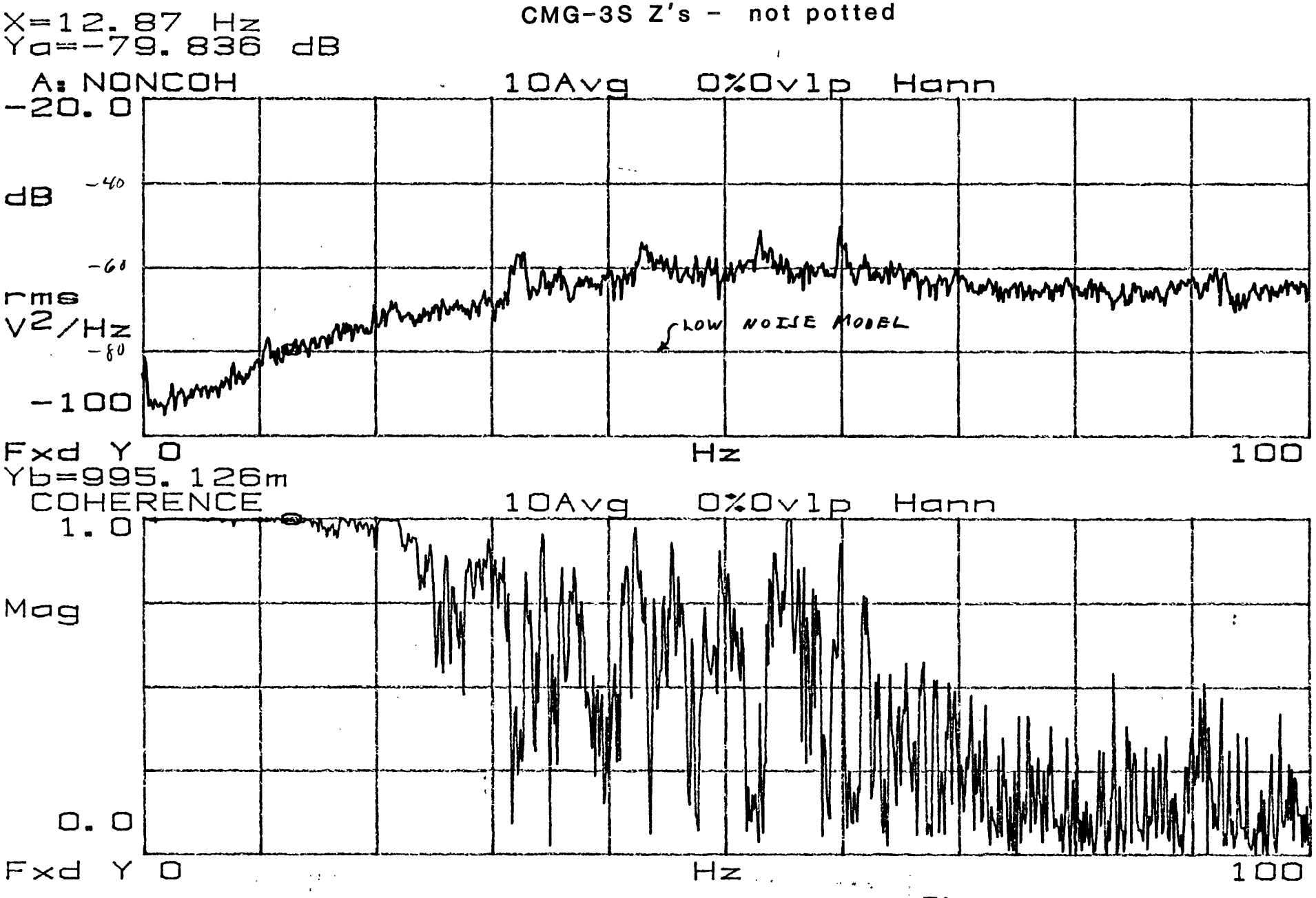

Figure A.4

CMG-3S NS's
FLOAT

10/13/91
9:15 MDT

CMG-3S NS's - not potted

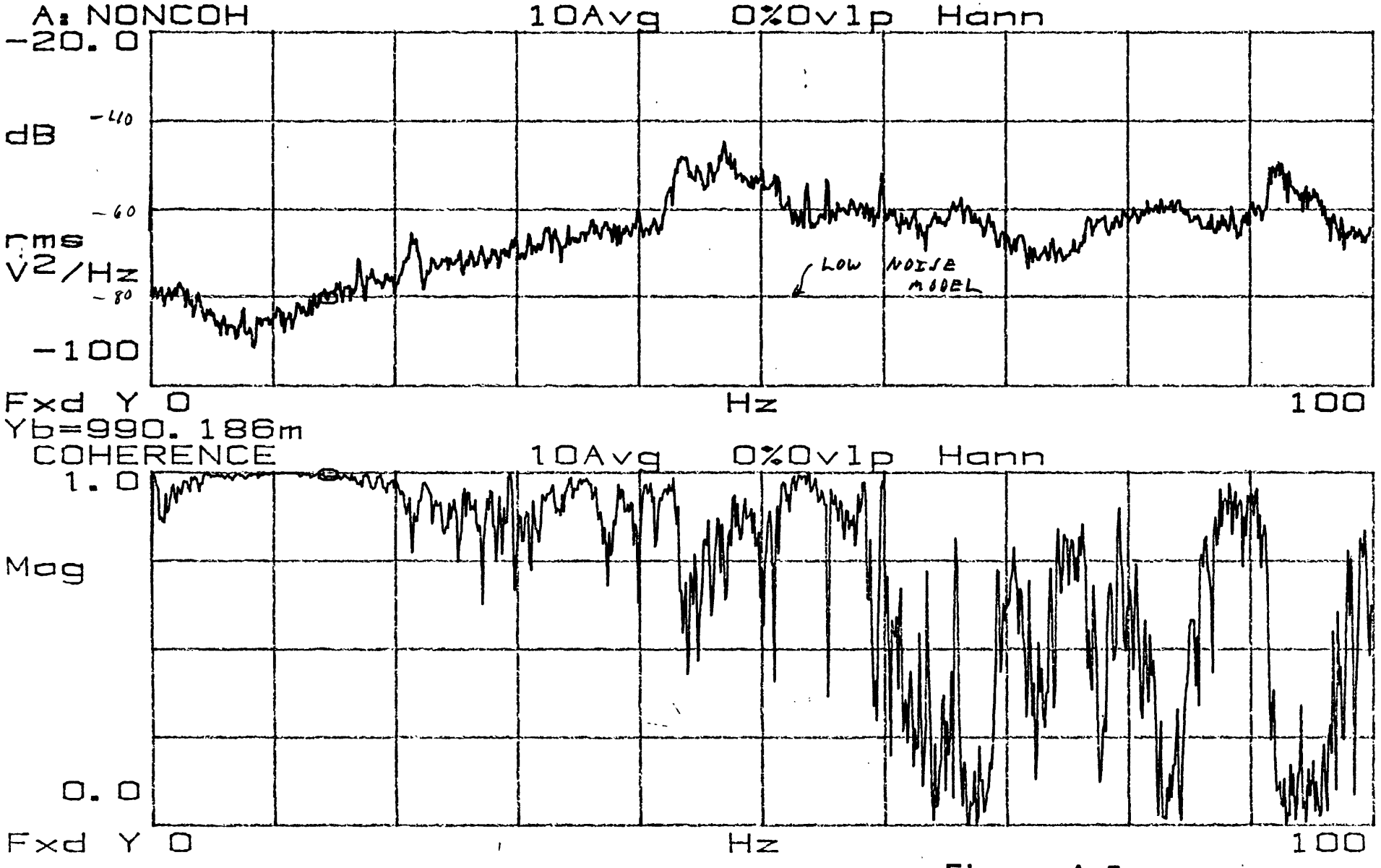

Figure A.5

CMG-3S E-W's

FLOAT

10/13/89
10:20 MST

CMG-3S EW's - not potted

Y=-87.902 dB

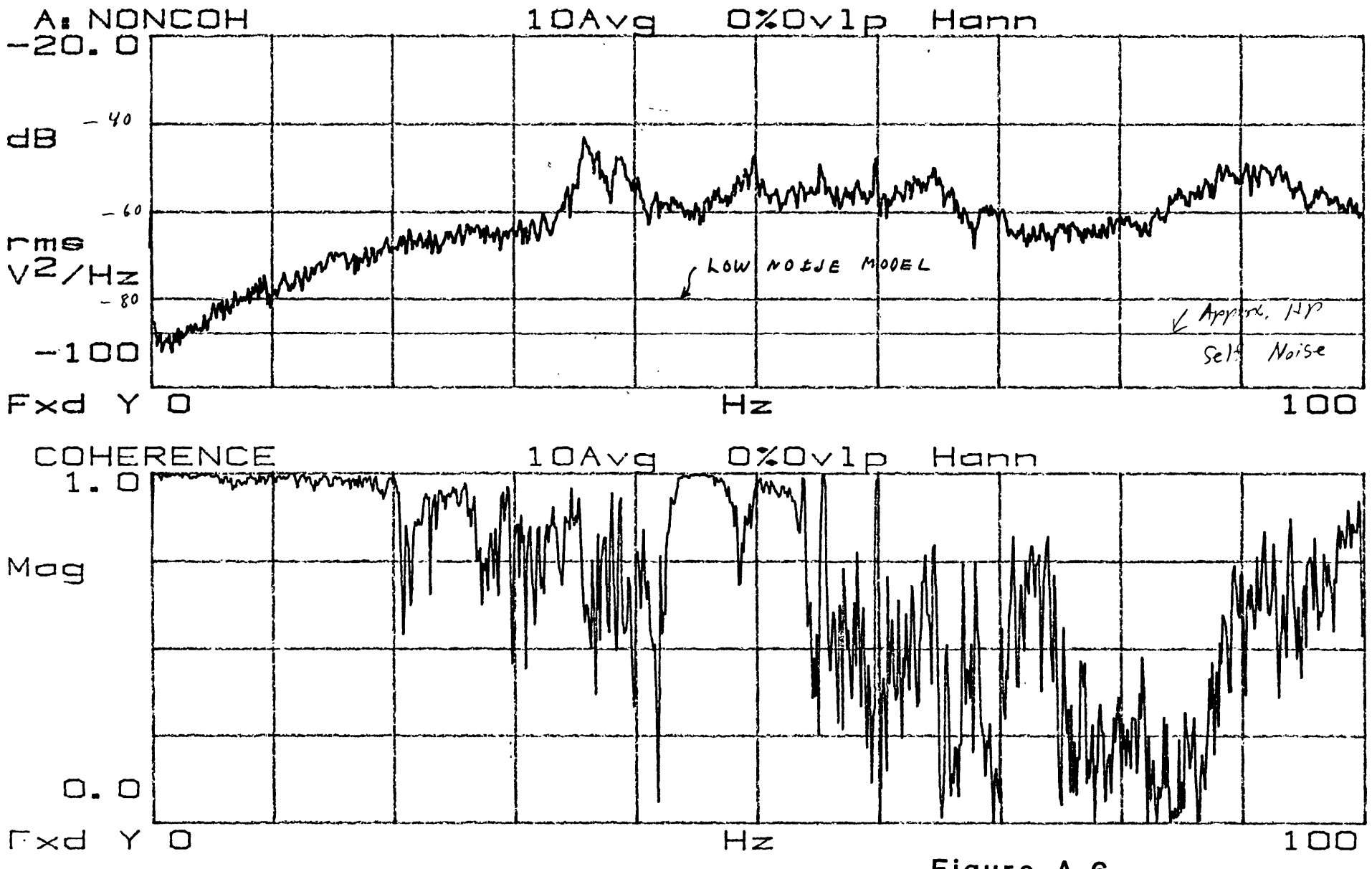

Figure A.6

Range = 1.59V peak

CMG-3S Z's
POTTED
RANGE = 399 mv-pk

CMG-3S Z's – potted

Windy

09:51 MDT

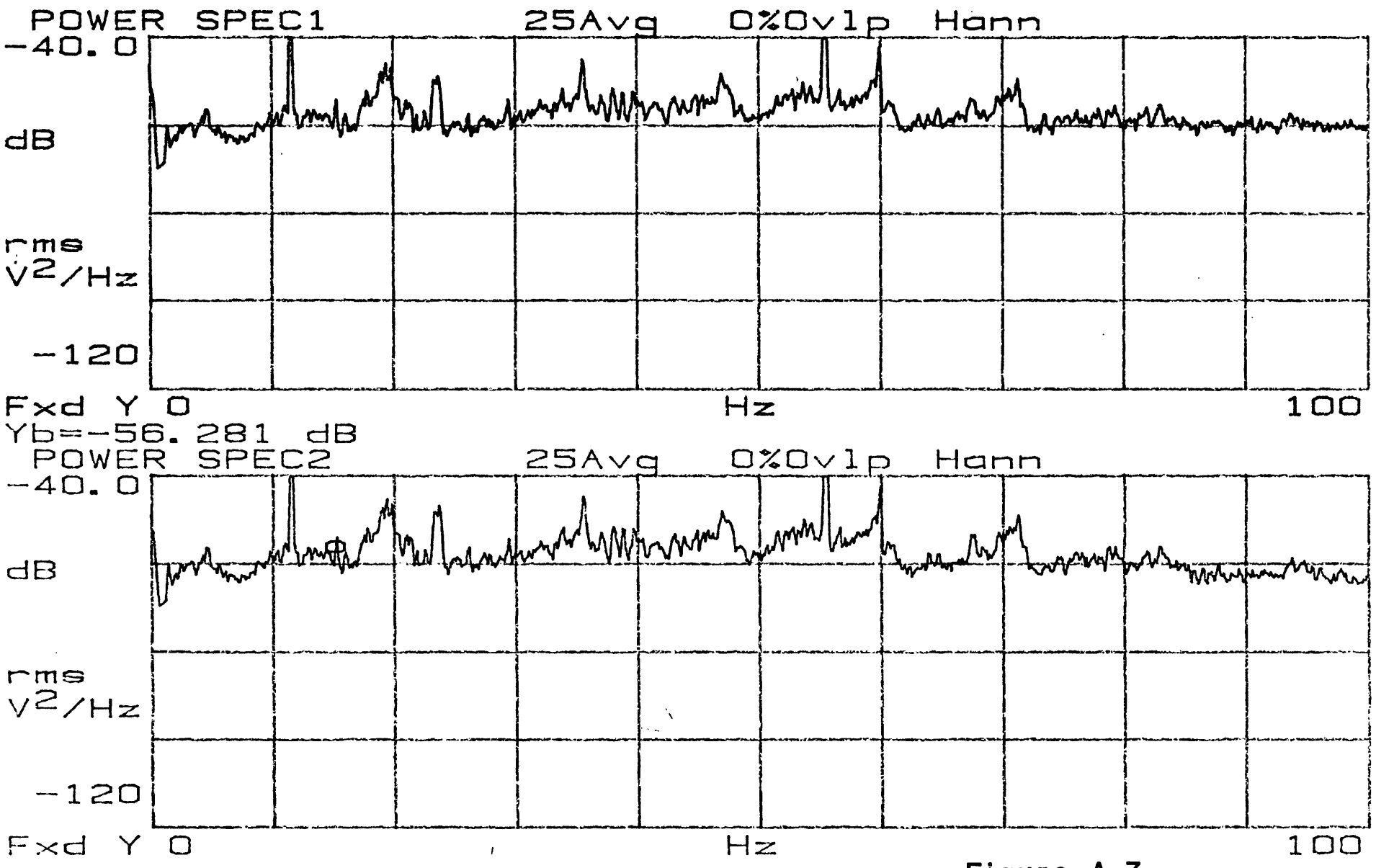

Figure A.7

Z's

CMG-3S N-S's
POTTED
≈ 502 mvpb

WINDY

10/17/89
08:32 MDT

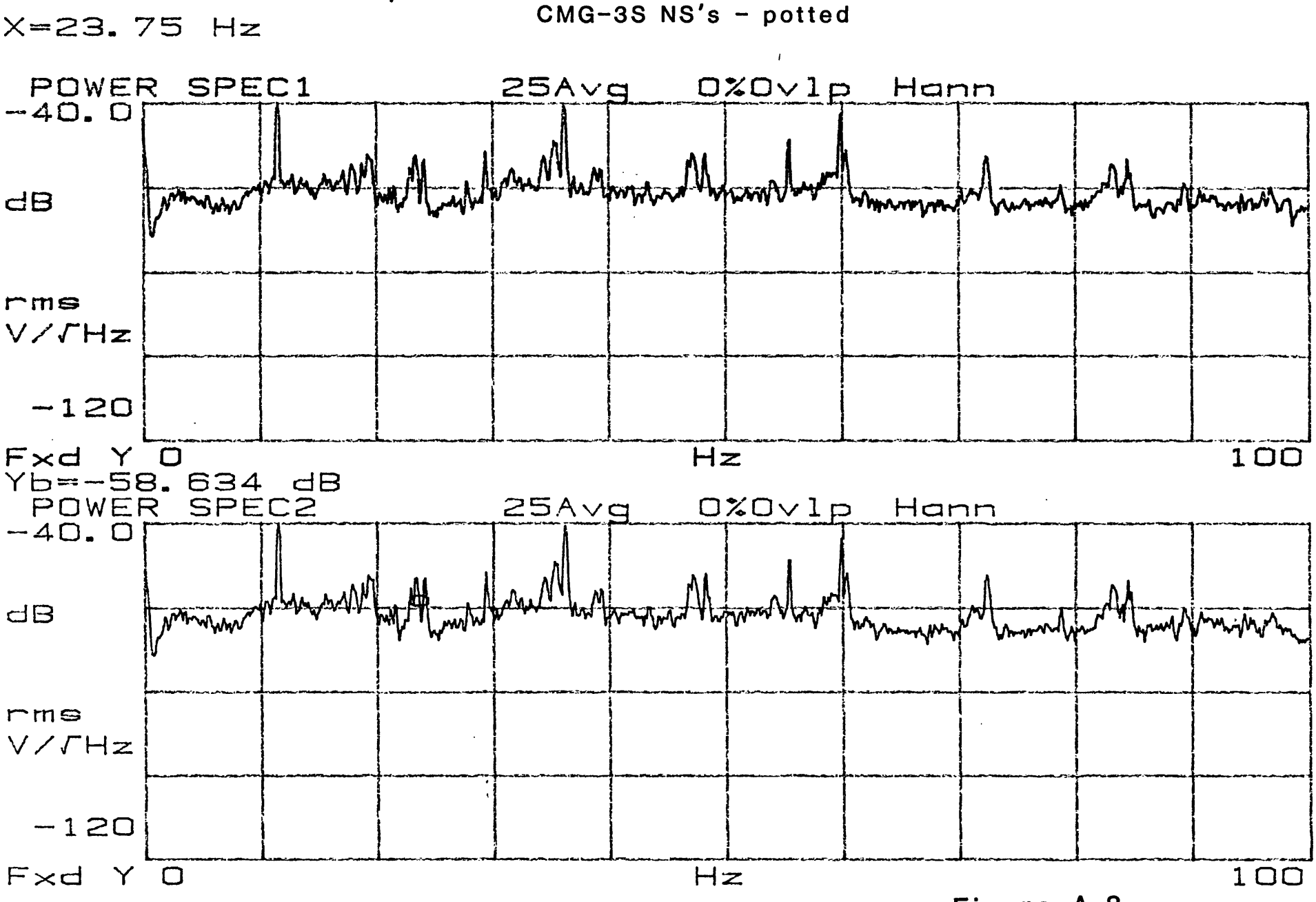

Figure A.8

CMG-3S
POTTED
≈ 512 mV/pb

WIN1X

08:17 M

CMG-3S EW's - potted

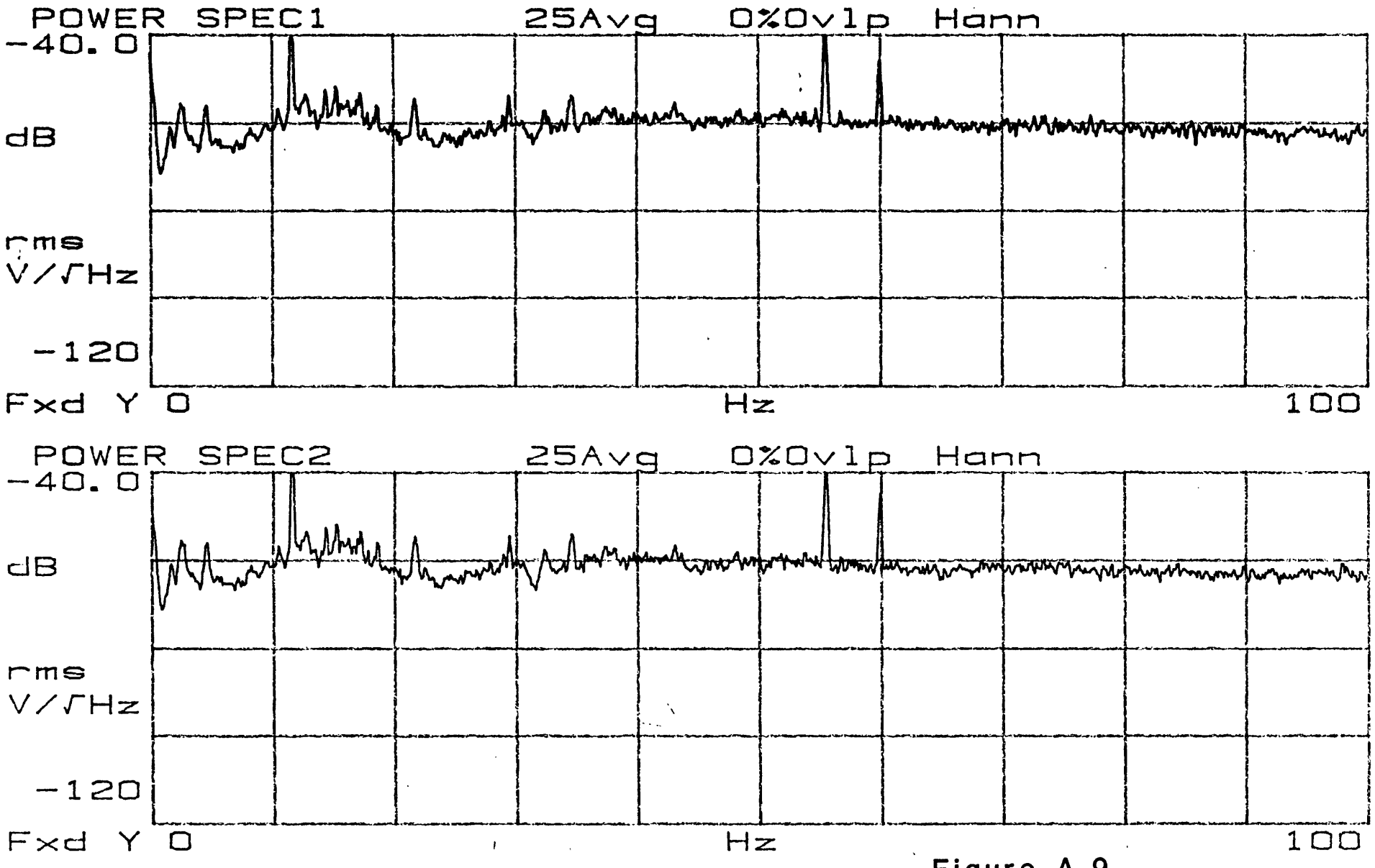

Figure A.9

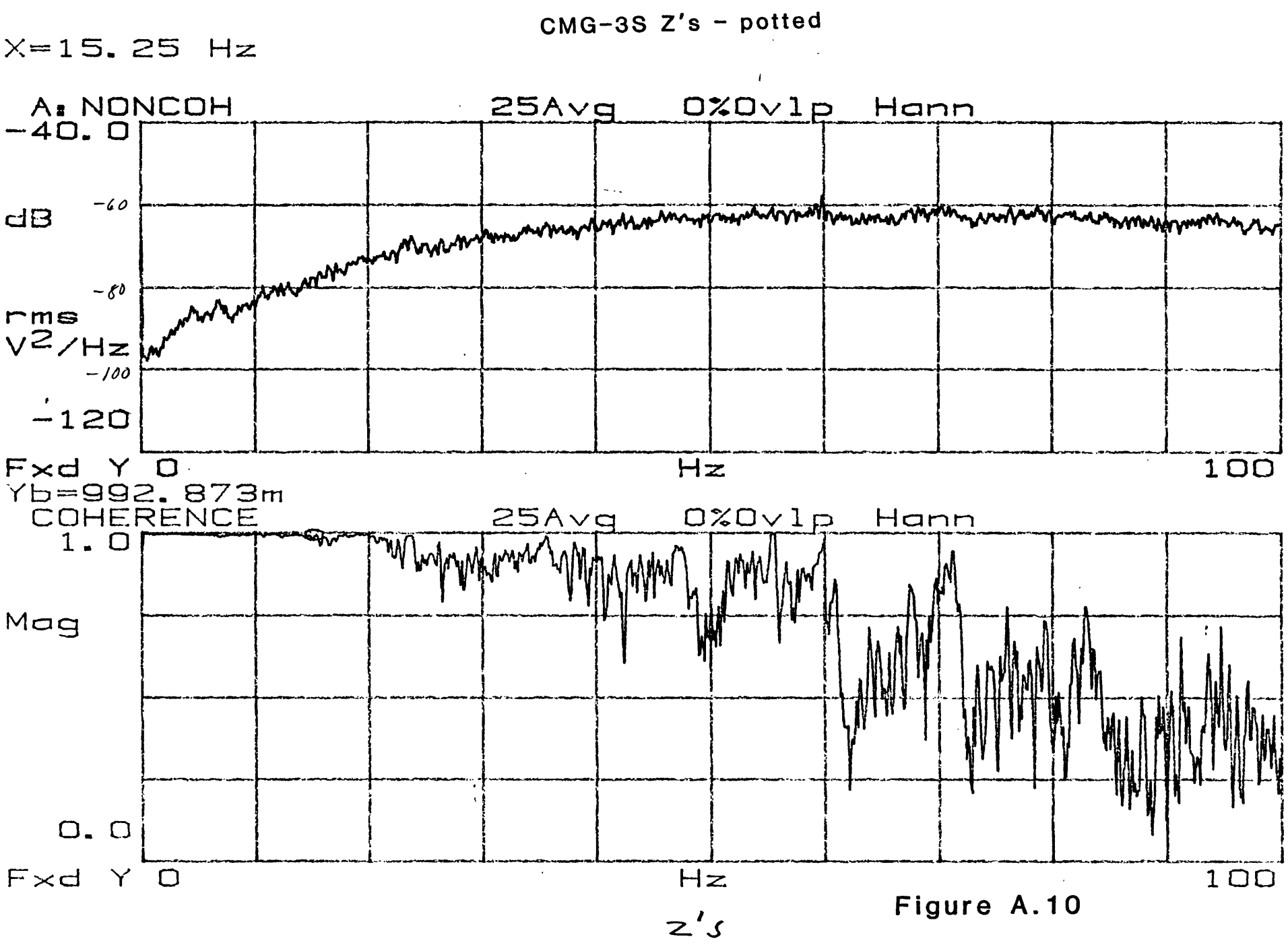
CMG-3S Z's - potted
X=15.25 Hz
A: NONCOH
25Avg
0%Ovlp
Hann
-40.0
dB
-60
-80
rms
V2/Hz
-100
-120
Fxd Y 0
Hz
100
Yb=992.873m
COHERENCE
25Avg
0%Ovlp
Hann
1.0
Mag
0.0
Fxd Y 0
Hz
100
Z's

Figure A.10

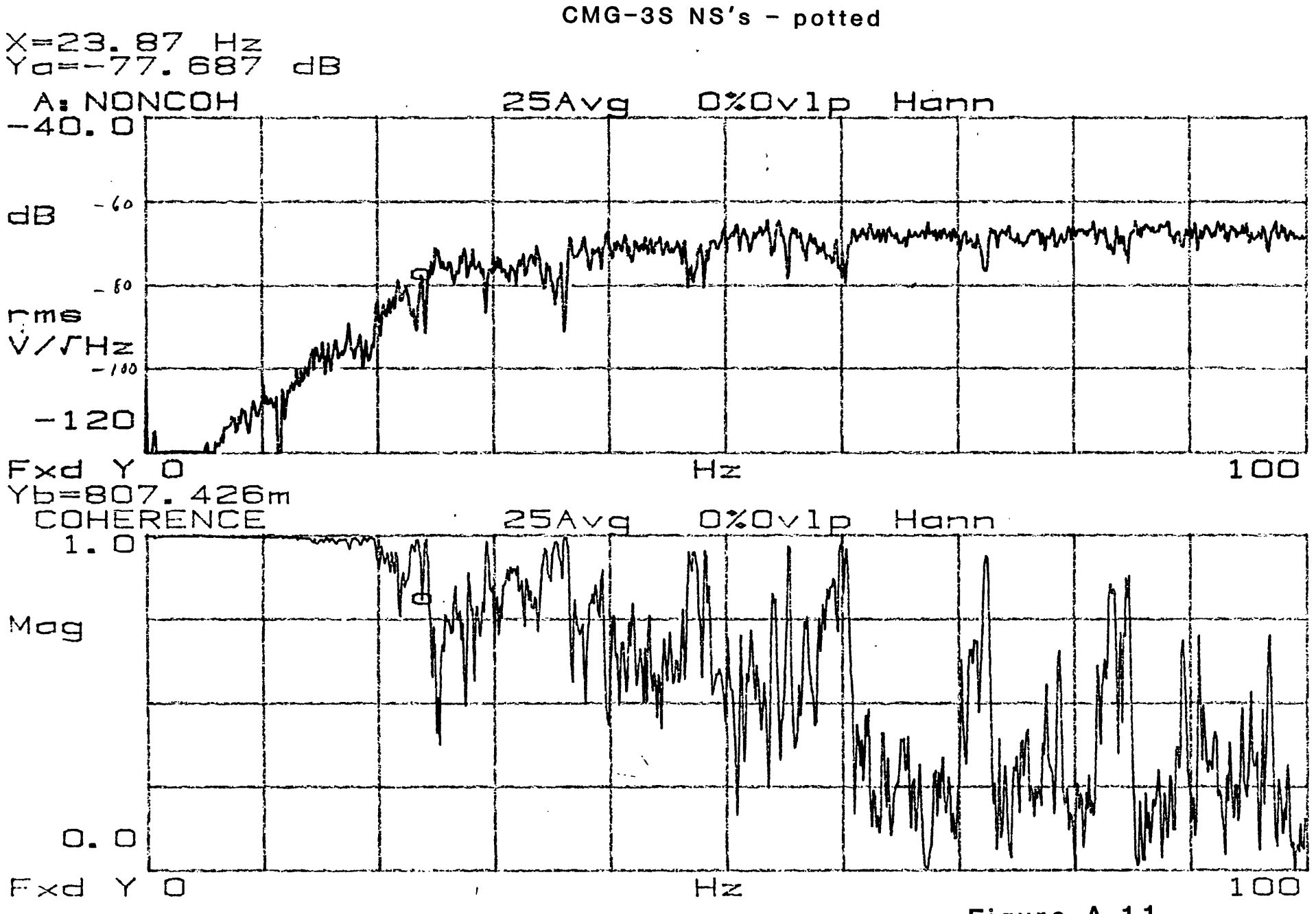
CMG-3S NS's - potted
X=23.87 Hz
Ya=-77.687 dB
A: NONCOH
25Avg
0%Ovlp
Hann
-40.0
dB
-60
-80
rms
V/√Hz
-100
-120
Fxd Y 0
Hz
100
Yb=807.426m
COHERENCE
25Avg
0%Ovlp
Hann
1.0
Mag
0.0
Fxd Y 0
Hz
100

Figure A.11

CMG-3S EW's - potted

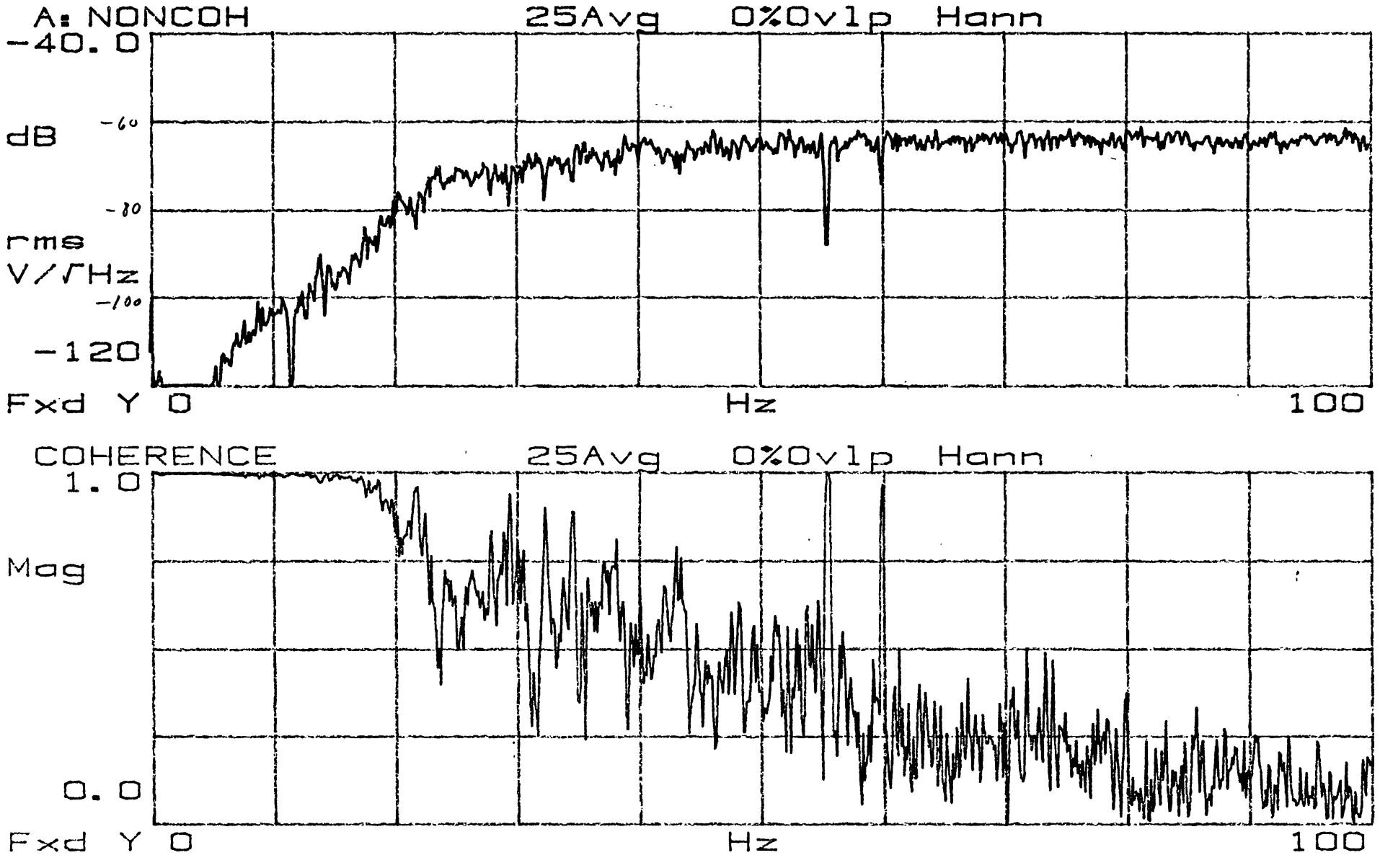

Figure A.12